SPECTROSCOPIC STUDIES OF CALCIUM AND MAGNESIUM PHOSPHATE SOIL MINERALS

A Thesis Submitted to the College of Graduate and Postdoctoral Studies
in Partial Fulfillment of the Requirements
for the Degree of Master of Science
in the Department of Soil Science
University of Saskatchewan
Saskatoon

by

David Michael Hilger

PERMISSION TO USE

In presenting this thesis in partial fulfillment of the requirements for a Postgraduate degree from the University of Saskatchewan, I agree that the Libraries of this University may make it freely available for inspection. I further agree that permission for copying of this thesis in any manner, in whole or in part, for scholarly purposes may be granted by the professor or professors who supervised my thesis work or, in their absence, by the Head of the Department of Soil Science or the Dean of the College of Agriculture and Bioresources. It is understood that any copying or publication or use of this thesis or parts thereof for financial gain shall not be allowed without my written permission. It is also understood that due recognition shall be given to me and to the University of Saskatchewan in any scholarly use that may be made of any material in my thesis. Requests for permission to copy or to make other uses of materials in this thesis, in whole or part, should be addressed to:

Head, Department of Soil Science

University of Saskatchewan

Saskatoon, Saskatchewan

Canada, S7N 5A8

DISCLAIMER

Reference in this thesis to any specific commercial products, process, or service by trade name, trademark, manufacturer, or otherwise, does not constitute or imply its endorsement, recommendation, or favouring by the University of Saskatchewan. The views and opinions of the author expressed herein do not state or reflect those of the University of Saskatchewan, and shall not be used for advertising or product endorsement purposes.

ABSTRACT

Phosphorus (P) is widely recognized as an element of vital importance as it is essential to life. Availability in natural systems is strongly influenced by the chemical form of P present; however, there are difficulties in measuring these forms *in situ* due to a combination of low concentrations and matrix effects. This research improves the applicability and confidence of using P K-edge X-ray Absorption Near Edge Structure (XANES) for P speciation in calcareous soils. Calcium (Ca) and magnesium (Mg) phosphate minerals were synthesized with varying Ca:Mg ratios to replicate conditions found in calcareous soils. The synthesized minerals were characterized with a number of techniques: Attenuated Total Reflectance Infrared (ATR-FTIR) and P K-edge XANES to determine local bonding environment, Transmission Electron Microscopy (TEM) to determine macro-structure and shape, Synchrotron Powder X-ray Diffraction (SP-XRD) to determine the precise crystal structure. It was found that in a wide range of Ca:Mg ratio solutions, mineral formation favoured poorly or less crystalline phases such as amorphous calcium phosphate (ACP)/short order hydroxyapatite (HAP) or Mg-bearing brushite, dependent on pH and (Ca+Mg)/P ratios. These phases have not been traditionally been considered important in prior soil P speciation studies, but this research strongly implies they are likely to be major components in soil systems. Next, the limits of P XANES semi-quantitative analysis in examining Ca/Mg phosphate minerals was tested by Linear Combination Fitting (LCF) of constructed mixtures of known proportions. It was determined that P XANES LCF analysis of calcium and magnesium phosphates is highly accurate in binary mixtures with an average

deviation of 3.2%. A maximum deviation of 24% in a ternary mixture was found. In summary, this study has expanded the knowledge of Ca-Mg interactions in phosphate mineral formation, improved the ability to speciate these minerals within soil, and determined a confidence level in which to do so.

ACKNOWLEDGEMENTS

The foremost acknowledgement belongs to my supervisor, Dr. Derek Peak, who has been instrumental in aiding myself through the research and writing process. His knowledge of environmental soil chemistry and spectroscopy was an immense resource. I would also like to thank by name, Jordan Hamilton, for teaching myself a number of different analytical techniques. I would also like to thank my advisory committee Dr. Matt Lindsay, Dr. Jeff Schoenau, and Dr. Steven Siciliano. I am appreciative of the Canadian Light Source beamline staff (CMCF and SXRMB) and the University of Saskatchewan Biology Imaging Lab in their aid for their respective facilities. A special thanks is warranted to my mother and family for the support they have provided me throughout my education.

TABLE OF CONTENTS

LIST OF FIGURES

LIST OF TABLES

LIST OF ABBREVIATIONS

ACP	amorphous calcium phosphate
ATR-FTIR	attenuated total reflectance fourier transformed infrared
BOB	bobierrite
CDHA	calcium-deficient hydroxyapatite
CLS	canadian light source
DCPD	brushite
HAP	hydroxyapatite
LCF	linear combination fitting
NBTE	newberyite
OCP	octacalcium phosphate
PFY	partial fluorescence yield
SP-XRD	synchrotron powder X-ray diffraction
STVE	struvite
SXRMB	soft X-ray microcharacterization beamline
TCP	tricalcium phosphate
TEM	transmission electron microscope
TEY	total electron yield
XANES	X-ray absorption near edge structure
XAS	X-ray absorption spectroscopy
XRD	X-ray diffraction

1. GENERAL INTRODUCTION

1.1 Phosphorus, macronutrient of importance

Phosphorous (P) is a macronutrient essential for plant and microbial growth, and is integral to all life. Phosphorus is utilized in cellular energy transfer in the form of ATP, constitutes the backbone of DNA/RNA, is a major component of cell walls, and provides structural integrity to bones and teeth (Toor et al. 2006, Ben-Nissan 2014) Phosphorus is a finite resource that often limits crop production, which pressures a high demand on its efficient usage and makes P nutrient efficiency tightly coupled to global food demands (Cordell et al., 2009, Van Vuuren et al., 2010, Cooper et al. 2011). When there is an abundance of P from anthropogenic sources, such as fertilizer over-application, it promotes rapid growth of microbial and plant life, producing eutrophication of water bodies due to algae blooms that are detrimental to the environment (Ryther 1971, Carpenter et al., 1998, Elser et al., 2007). Phosphorus is often a limiting nutrient for microbial hydrocarbon degraders, which has important implications for bioremediation projects (Mills and Frankenberger 1994, Xiong, et al., 2012, Siciliano et al., 2016). For these reasons, there is a need to fully understand the chemical fate of phosphorus mineral phases in the environment to optimize bioaccessibility.

Calcium phosphates are a major phosphorus phase in calcareous soils and are widely studied in soil and geochemical systems (Lindsay 1979, Dixon, 1982, Toor et al., 2006). In contrast, magnesium (Mg), an abundant Group 2 element like Ca, has not widely been studied by soil scientists with regard to phosphate chemistry. Magnesium is abundant in

soils systems which contain a large amount of dolomitic parent material or inputs from Mg rich manure (Razc and Soper, 1967, Cao et al., 2007, Wadu et al., 2012). In biomaterial studies (Salimi et al., 1985, Darr et al. 2008, Lee and Kumta, 2010a.) and more recently in soil chemistry (Cao et al., 2007, Wadu et al., 2012), Mg has been shown to limit the precipitation of calcium phosphates and inhibit the formation of insoluble crystalline calcium phosphate phases such as hydroxyapatite (Diallo-Garcia et al., 2011). The application of this knowledge towards soil P is a potential method to increase P bioavailability for plant uptake and microbial accessibility for hydrocarbon remediation by increasing the solubility of inorganic P minerals.

For most spectroscopic techniques, solid-state P speciation is not trivial due to low total P concentrations and matrix issues/interferences within the soil (Hesterberg, 2010). Within the last 15 years, P K-edge X-ray Absorption Near Edge Structure (XANES) spectroscopy has matured as the primary technique for soil P speciation as the accessibility of suitable synchrotron radiation sources and appropriate tender X-ray beamlines have increased. This technique is capable of semi-quantitatively determining phosphorus speciation at natural soil concentrations. However, P K-edge XANES spectroscopy necessitates the need for a robust and accessible XANES library to deconvolute spectra for semi-quantitative analysis. There is an absence in the "library" of calcium and magnesium phosphate and co-substituted/precipitated minerals that are likely to occur in soil environments. Previous research has focused on crystalline minerals and/or measured with slightly different methods (ie: Total Electron Yield - TEY) that are not perfectly applicable for soils (Hesterberg 1999, Ingall et al., 2011). The need is to have these spectra in one library, freely/openly accessible, and measured in partial fluorescence yield (PFY) which is more representative of the bulk sample and mineral. Furthermore, estimates of the

suitability of Linear Combination Fitting (LCF) approaches to deconvolution of P K-edge XANES where similar phases are present also needs careful evaluation beyond what has been previously studied (Werner and Preitzel, 2015, Abjiboye et al., 2007).

1.2 Organization of thesis and overall objectives

The thesis was written with two hypothesis and corresponding objectives in mind:

(1) Changes in calcium phosphate crystal structure upon magnesium substitution will result in identifiable changes to P K-edge XANES spectra. This was tested through synthesizing and characterizing calcium and magnesium phosphate minerals associated with soils over a range of Ca:Mg ratios and pH.

(2) Linear Combination Fitting is capable of high accuracy in semi-quantitative fitting calcium and magnesium phosphates. This hypothesis was challenged by testing the capabilities of LCF for P K-XANES calcium and magnesium phosphates with constructed mixtures.

This thesis has been written in manuscript format. Chapter 1 is a short introduction to the research topic followed by Chapter 2, a literature review of the concepts incorporated into the thesis. There are two main research projects contained in Chapters 3 and 4. The focus of the research in Chapter 3 is to challenge the first hypothesis through formation of calcium and magnesium phosphate minerals with varying Ca:Mg ratios and the building of a XANES library based on these mixed cation minerals. Chapter 4 addresses the second hypothesis by an examination of the abilities of Linear Combination Fitting of P K-edge XANES through constructed mixtures of calcium and magnesium phosphates. In addition, Appendices A-F contain the spectra library referred to in Chapters 3 and 4. Chapter 5, is a

summary of the conclusions drawn in the previous chapters, ad discussion of the implications of the results, and proposals for future areas of study in this field.

2. LITERATURE REVIEW

2.1 Phosphate mineralogy and magnesium inhibition of calcium phosphate formation in soils

The work by Hesterberg (2010) in "Developments in Soil Science, Volume 34" does an excellent job of summarizing phosphorus in the environment. In summary, there are two major (organic and inorganic) and two minor (biomass and porewater) pools of P within soil. The major pools, organic and inorganic phosphate, comprise greater than 99% of the total phosphorus with much of the remainder falling in living plant biomass pool. Organic P encompasses microbial biomass (~0.4-7.5%) and P found in organic matter (30-65%). Inorganic phosphate makes up 35-60% of total phosphate and is split between inorganic P minerals (Al/Fe/Ca-P) and P sorbed to Fe and Al oxides. Porewater P comprises only 0.002% of total soil phosphorus but is nonetheless extremely important as porewater is the fraction responsible for dissolution, precipitation, transport, and plant uptake.

The identity and relative proportions of inorganic pools are determined by pedagogical factors such as parent material and weathering which control concentrations and pH of the soil solution (Khasawneh et al., 1980). Soils which are low in pH (~3.5-5.5) due to high organic acid input and chemical and physical weathering are typically low in basic cations (Ca and Mg) as they are readily leached out of the system (Lindsay, 1979). Iron and aluminum are ubiquitous in any soil system, and at low pH these cations strongly complex with orthophosphate (Lindsay, 1979, Dixon, 1982, Sato et al., 2005). At neutral to

high pH (~6.0-9.5) , Fe and Al form hydroxide mineral phases, onto which phosphate has a high affinity to form inner-sphere surface complexes (Ler and Stanforth, 2003, Khare et al. 2005, Makris et al., 2005). However, in alkaline systems phosphate interactions with calcium is considered more important due to the low solubilities and high abundance of calcium phosphate minerals (Khasawneh et al., 1980).

The works by Driessens and Verbeeck (1990), Dorzohkin (2011 and 2012), and Ben-Nissan (2014) form the basis for calcium phosphate mineralogical applications in the biomedical field (primarily covering dental and bone cement) but are also modern and expansive studies on calcium orthophosphate formation and solubility in general. The formation of calcium orthophosphate minerals are largely determined by a factor of Ca/P ratio and pH. The solution pH controls the relative abundance of orthophosphate protonation states ($H_2PO_4^-/HPO_4^{2-}/PO_4^{3-}$). For example, solutions pH 9 or higher will be dominated by PO_4^{3-} and thereby the majority of minerals formed at high pH will also incorporate this oxyanion. The different protonation states of orthophosphate require a different number of divalent Ca^{2+} cations to satisfy their ionic charge. In the same basic solution example, the -3 charge of the PO_4^{3-} oxyanion requires a minimum of 1.5 Ca^{2+} cations to satisfy this charge. The general trend of calcium phosphate minerals is that the greater the Ca/P ratio and higher the pH, the less soluble the mineral that is formed. The solubility product (Ksp) of the mineral increases with pH and the number of ionic bonds.

Magnesium phosphate precipitation has not widely been considered due to its high solubility relative to pure calcium phosphates, but there has been some research indicating that Mg can inhibit both the precipitation and crystallization of calcium phosphates in calcareous soils (Razc and Soper, 1967, Cao et al., 2007, Wadu et al., 2012). This effect is more pronounced on the precipitation of stable Ca-P end mineral such as octacalcium

phosphate ($Ca_8H_2(PO_4)_6 \bullet 2H_2O$ – OCP) and hydroxyapatite ($Ca_5(PO_4)_3OH$ – HAP), whereas the effect is minimal on neutral-acidic phases such as brushite ($CaHPO_4 \bullet 2H_2O$ – DCDP) (Salimi et al., 1985, Wang and Nancollas 2008). Brushite that has incorporated Mg does not thermodynamically transform to apatite despite pH conditions dictating it would do so (Lee and Kumta, 2010). Magnesium, like Ca, is divalent, but the smaller atomic radius of Mg induces strain to the crystal lattice of HAP (Salimi et al., 1985). In mineral formation, it has been observed that Mg^{2+} poisons crystal growth by adsorbing to active seed crystal sites and preventing propagation (Salimi et al., 1985, Wang and Nancollas, 2008).

At high Mg concentrations relative to Ca, HAP precipitation is inhibited and dominant phases that form are (a) amorphous calcium phosphate (ACP) with incorporated Mg and (b) whitlockite, the Mg polymorph of β-tricalcium phosphate (Ca_3PO_4 –TCP) (Cao et al., 2007, Wandu et al., 2013). Generally, β-TCP requires high temperature and/or pressure for stable formation and is not readily precipitated in aqueous systems (Driessens and Verbeeck, 1990, Dorozhkin, 2011). However, β-TCP contains ion vacancies that are too small for Ca^{2+} but are the correct size for Mg^{2+}. In contrast with HAP-OCP, Mg^{2+} stabilizes the structure and makes the formation of the mineral possible (Wang and Nancollas, 2008). Amorphous calcium phosphate is a short-range order apatite-like mineral that is defined by having an amorphous XRD pattern i.e. lacks a long range repeating crystal lattice (Elliot, 1994). The formation of ACP can be the result of inhibited HAP crystal growth and maturation (Wang and Nancollas, 2008). It has been proposed that ACP produced in the presence of Mg^{2+} is, in fact, Mg-whitlockite nanoparticles (Driessens and Verbeeck, 1990). The small size of proposed Mg-whitlockite particles makes differentiating these phases from a truly amorphous phase difficult since both will appear amorphous in XRD patterns. Chemical fractionation between these minerals would

similarly be difficult as smaller precipitates are more prone to dissolution and have a higher solubility than larger phases (Peak et al., 2012).

In aqueous systems below 200 ^{o}C, the dominant HAP crystal structure is a monoclinic polymorph and Mg substitution is minimal. However, in some specific geochemical conditions, it is possible for Mg substitution to occur in HAP. For example, a high temperature hexagonal polymorph associated with macro-crystals is found in geological formations. The hexagonal structure has a greater disorder in the Ca^{2+}-OH^{-} columns which connect the parallel Ca-PO_4 tetrahedron sheets that can accommodate the strain of isomorphic substitution (Wang and Nancollas, 2008).

All the P forms discussed above are in dynamic equilibrium with the soil solution, and can readily form and dissolve in soil in response to leaching, plant uptake, or inputs of P. The form of P in soils is known to have a strong influence on plant availability and environmental risk. Chemical analysis of soil P has focused on three primary approaches: agronomic soil tests to estimate the "available P", sequential chemical analysis to fractionate P into pools based on "lability", and direct chemical speciation using spectroscopic techniques.

2.2 Conventional P analysis: P speciation within soils using chemical extractions

2.2.1 Agronomic soil tests for "plant available P"

There are a number of agronomic methods for analyzing P known as "soil test phosphorus" (STP) that have been developed and consistently modified for specific soil conditions (Khasawneh et al., 1980). The goal of these tests is not to speciate P but to determine what fraction of the total P is bioavailable for agriculture and whether applied fertilizers will be effective (Khasawneh et al., 1980, Kumaragamage et al., 2007). Agronomic STP methods operate by one of four mechanisms: (i) acid dissolution, (ii) anion

replacement, (iii) cation complexation, (iv) hydrolysis (Khasawneh et al., 1980). Common agronomic STP deriving from these mechanisms are Olsen, Melhich-3, Kelowna, Bray (Kumaragamage et al., 2007). The Olsen test is a "catch all" method utilizing a bicarbonate solution of pH 8.5 which is suitable for both calcareous and mildly acidic soils (Olsen, 1954, Khasawneh et al., 1980). The Kelowna-3 test uses an ammonium acetate and acetic acid extraction solution and is suitable for neutral and basic soils that may be calcareous or non-calcareous (Kumaragamage et al., 2007). Melhich-3 and Bray tests have been developed primarily for non-calcareous soils, utilizing a strong inorganic acid extraction solution such as NH_4F and HCl (Kumaragamage et al., 2007). The tests, regardless of their chemical composition, are correlated to a specific plant's response to P and seek to accurately determine the plant available P within the soil. It is known and indeed is by design that these extractions remove varying proportions of mineral, organic, and absorbed P rather than any single species.

2.2.2 Sequential chemical extractions

The conventional method of P speciation is via sequential chemical extraction, where a series of increasingly strong solvents remove decreasingly soluble P species. The most common sequential extraction method for P is the Hedley fractionation (Hedley et al. 1982). The method differentiates between organic and inorganic P and labile vs. non-labile P (Tiessen and Moir, 1993). Hedley sequential extractions are limited in speciation and should only be used in differentiating between readily bioaccessible and insoluble. (Hunger et al., 2005, Toor et al., 2006, Kar et al., 2011, Beauchemin et al., 2013). Most studies recommend a combination of sequential extractions and a spectroscopic solid-state speciation technique, typically NMR or XANES (Liu et al., 2014). Hedley extractions are *mostly* good at differentiating between and inorganic/organic P but are unable to determine

specific species such as phytic acid or ATP (Beauchemin et al., 2013). Speciation within the inorganic fraction is poor (Hunger et al., 2005, Kar et al., 2011, Wu et al., 2014); Associated extractions are *mostly* associated with the phase they are thought to extract, for example, *most* Al-P forms are extracted by NaOH and *most* Ca-P phases are extracted by HCl but there is spill over (Hunger et al., 2005). As an example, some Ca-P minerals are extracted by the NaOH fraction instead of the HCl extraction (Kar et al., 2011).

2.3 Direct Solid State Spectroscopy and Imaging Techniques

2.3.1 Phosphorus K-edge XANES theory and qualitative analysis

X-ray absorption spectroscopy (XAS) is an atomic spectroscopy that utilizes the phenomena that core electron excitation and ejection are element specific. Primarily, the XAS in this study will be P K-edge XANES. In this technique, a 1s electron is ejected from the P atom when the incident photon energy is equal to the binding energy of the 1s electron; this energy is also known as the absorption "edge" as it is a very abrupt transition (Toor et al., 2006). The core hole vacancy that is produced from this ejection has lower energy requirements than the higher orbital electrons and is rapidly filled to return the excited atom to its ground state. An electron from the 2p orbital decomposes and fills the 1s core hole vacancy. The excess energy is emitted as a photon of fluorescence equal to the energy differences of the shells (Toor et al., 2006).

X-ray absorption near edge structure spectroscopy concerns itself with the spectral region immediately surrounding the absorption edge. The strength of XANES is qualitative fingerprinting of samples, especially in differentiating changes in coordination environment and oxidation state (Fendorf et al., 1994). Variations in the local chemistry environment, i.e. crystal structure, associated cations, etc., have a minor contribution to the spectrum relative to coordination and oxidation state but are still discernable. Common spectral

changes include shifts in the energy threshold of the absorption edge, presence and absence of pre-edge features, and oscillations/resonance features located after the edge (Toor et al., 2006).

Speciation with P K-edge XANES in soil samples is typically constrained by the quality of the data (often due to low concentration) and how well the standards for the system are chosen (Beauchemin et al., 2003). There are many potential P species within soils, but typically adsorption and mineral precipitates with Ca (and possibly Mg), Al, Fe and organic phosphates are the major species present. Pure phosphate minerals are easily distinguishable from one another by pre-edge features (Figure 2.1–1), white line energy shifts (Figure 2.1-2), and post-edge shoulders (Figure 2.1-3) and oscillations (Figure 2.1-4, 2.1-5). For the P K-edge, pre-edge features generally arise due to bonding with 3d transition metals, which can have sp^3 to 3d transitions at lower energy than the absorption edge (Okude et al., 1999). For a phase to significantly contribute to the P K-edge XANES spectra of a mixture, the component needs to be 10-15% of the total P concentration. Even prominent spectral features will not be visible if the concentration is below this threshold (Beauchemin et al., 2003).

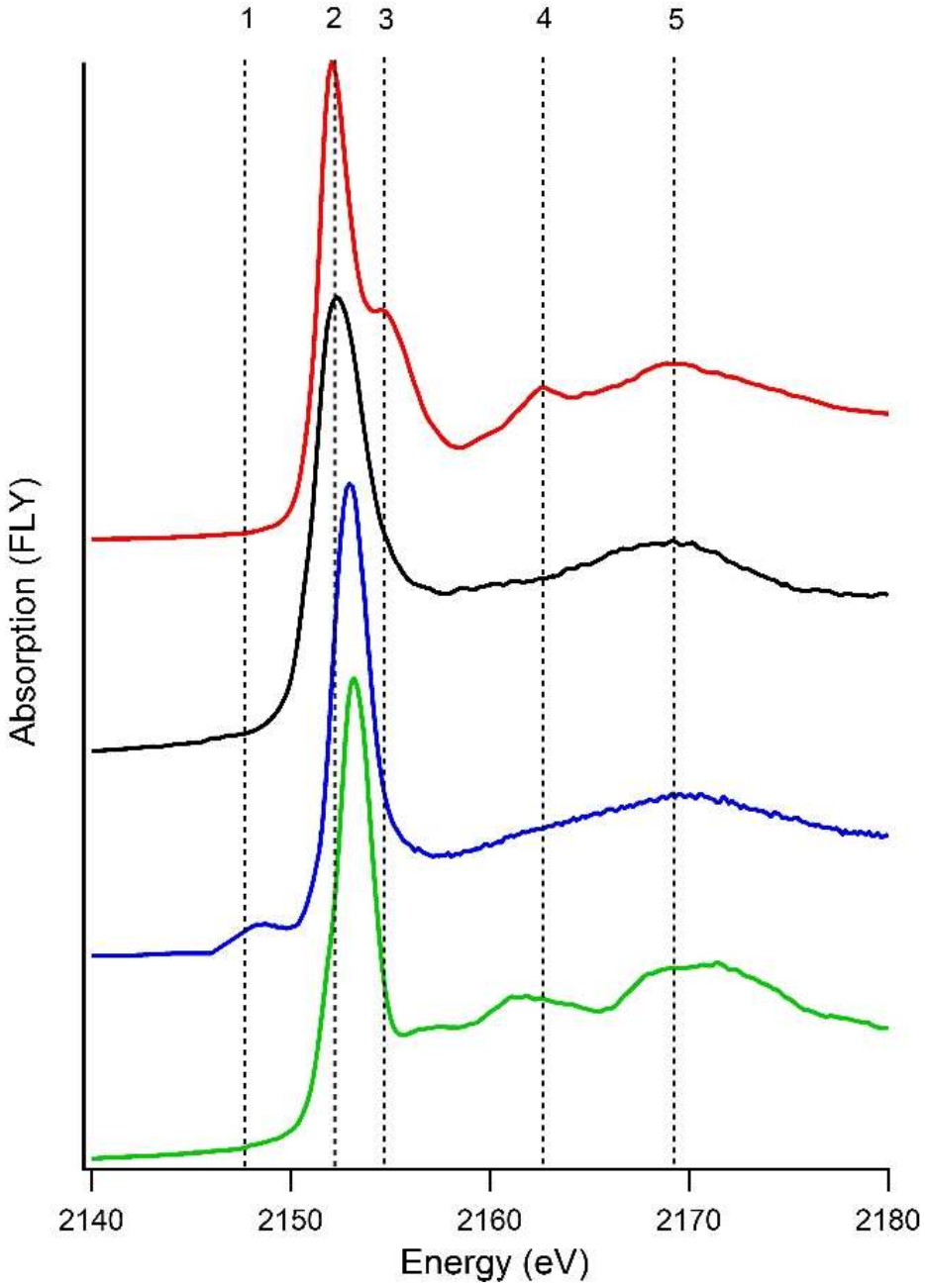

Figure 2.1: P K-edge XANES of 4 common P species: hydroxyapatite in red, phytic acid in black, ferric phosphate in blue, and aluminum phosphate in green. Vertical dashed lines indicate diagnostic spectral features: 1 – pre-edge, 2 – white line/absorption edge, 3 - post-edge shoulder, 4,5 – oxygen oscillations.

Speciation of organic phosphates within soils is not well suited to P K-edge XANES. Organic P species are complex and contain many different P bond environments. The P XANES spectra are an average of all P within the sample, the spectra is ambiguous and relatively featureless. (Hunger et al., 2005). (Figure 2.1 – black) Phytic acid has no pre- or post-edge structure, and the only feature of adenosine 5' triphosphate (ATP) is a minor inflection (Hesterberg et al., 1999). As these species are difficult to identify and often occur in below detectable levels in calcareous soils (Kar et al., 2012), there will be a focus instead on inorganic phosphate minerals for this project.

Both Fe-P and P adsorbed onto Fe hydroxides are perhaps the most unique P species within soil from a XANES spectroscopic standpoint (Figure 2.1 – blue). Both crystalline and non-crystalline Fe-P possess a pre-edge peak which is located 3 to 5 eV before the white line absorption edge (Hesterberg et al., 1999, Ingall et al., 2010). This feature is also weakly present in P absorbed to Fe hydroxides. XANES spectra are unable to distinguish between P absorbed on ferrihydrite and goethite (Beauchemin et al., 2003), but there is an additional structure in the post-edge region that can be used to differentiate between different Fe-P minerals such as phosphosiderite and strengite (Ingall et al., 2010). The diagnostic feature in Al-P mineral phases, in addition to a unique white line energy, is a pre-edge "inflection" located ~1 eV before the adsorption edge (Figure 2.1 – green). This inflection is not present in P sorbed on Al oxides, making identification difficult (Hesterberg et al., 1999, Kizewski et al., 2011). Fe-P and Al-P minerals are present in calcareous soils but are more dominant in well-weathered soils. These minerals are not a focus of this study as they have been previously well studied and are readily identified when present in soil XANES.

The speciation of calcium phosphate minerals by P K-edge XANES is not as straightforward, necessitating the need for a robust spectral standard library to draw upon for fitting within soils. Calcium phosphate minerals have a common set of spectral features that vary in intensity from mineral to mineral (Hesterberg et al., 1999, Ingall et al., 2010). All Ca-P K-edge XANES spectra do not contain a pre-edge feature and have post-edge features at ~ 2-4, 12, and 18 eV past the white line energy (Figure 2.1 – red). There are slight variations in the relative intensity of the 12 and 18 eV which may be used diagnostically. The distinguishing feature of Ca-Ps from other minerals is the feature at 2-4 eV which is a distinct "shoulder" of the absorption edge. This shoulder increases in intensity with increasing crystallinity of the mineral (Hesterberg et al., 1999).

The number of magnesium phosphate P K-edge XANES studies is limited compared to Ca phosphates, but some spectra of these compounds are available (Gungor et al.,2007, Ingall et al., 2010). Magnesium phosphates, newberyite ($MgHPO_4 \bullet 3H_2O$ - NBTE) and struvite ($MgNH_4PO_4 \bullet 6H_2O$), lack sharp spectral features and provide a challenge in identification in bulk soils. There is a slight shift in the white line energy compared to other orthophosphate species and an extra broad oscillation at ~ 2160 eV (Gungor et al., 2007). The XANES spectra of the more crystalline magnesium phosphate, bobierrite ($Mg_3(PO_4)_2 \bullet 8H_2O$ - BOB) are relatively structure-rich which makes identification relatively easy; there are sharp post edge peaks at 2158, 2165, and 2170 eV (Ingall et al., 2010).

2.3.2 Linear Combination Fitting and semi-quantitative analysis of P K-edge XANES

The information that can be inferred from the usage of P XANES as a "fingerprinting" tool is limited as it is not semi-quanitative. There has been a drive from

the beginnings of soil P XANES analysis to use the technique to perform semi-quantitative analysis via Linear Combination Fitting (LCF). The LCF approach has had great success in XAS, for a number of elements in both the EXAFS and XANES region (Ressler et al., 2000, Manceau et al., 2000, Catalano et al., 2006). The LCF approach is time intensive when studying a new system due to the need to collect large libraries of reference spectra and necessitates the usage of specialized software, such as the ATHENA package (Ravel and Newville, 2005). A simplified explanation of how XANES LCF works is the following. The program is given a "sample" spectra to reproduce given a number of "standard" spectra. The program runs combinations of these standards to reproduce the closest average fit to the sample spectra using a partial least squares algorithm (Beauchamin et al., 2002) and assesses the relative percent contribution of those standards. In an example LCF of a low concentration soil sample, proportions of absorbed orthophosphate and brushite are summed together to produce the "Fit" spectra to reproduce the data spectrum (Figure 2.2). Evidence can been seen in the summation of brushite and absorbed orthophosphate spectral features located at Line 1, adsorption edge energy shift, and Line 2, the intensity of the 2164 eV post-edge feature.

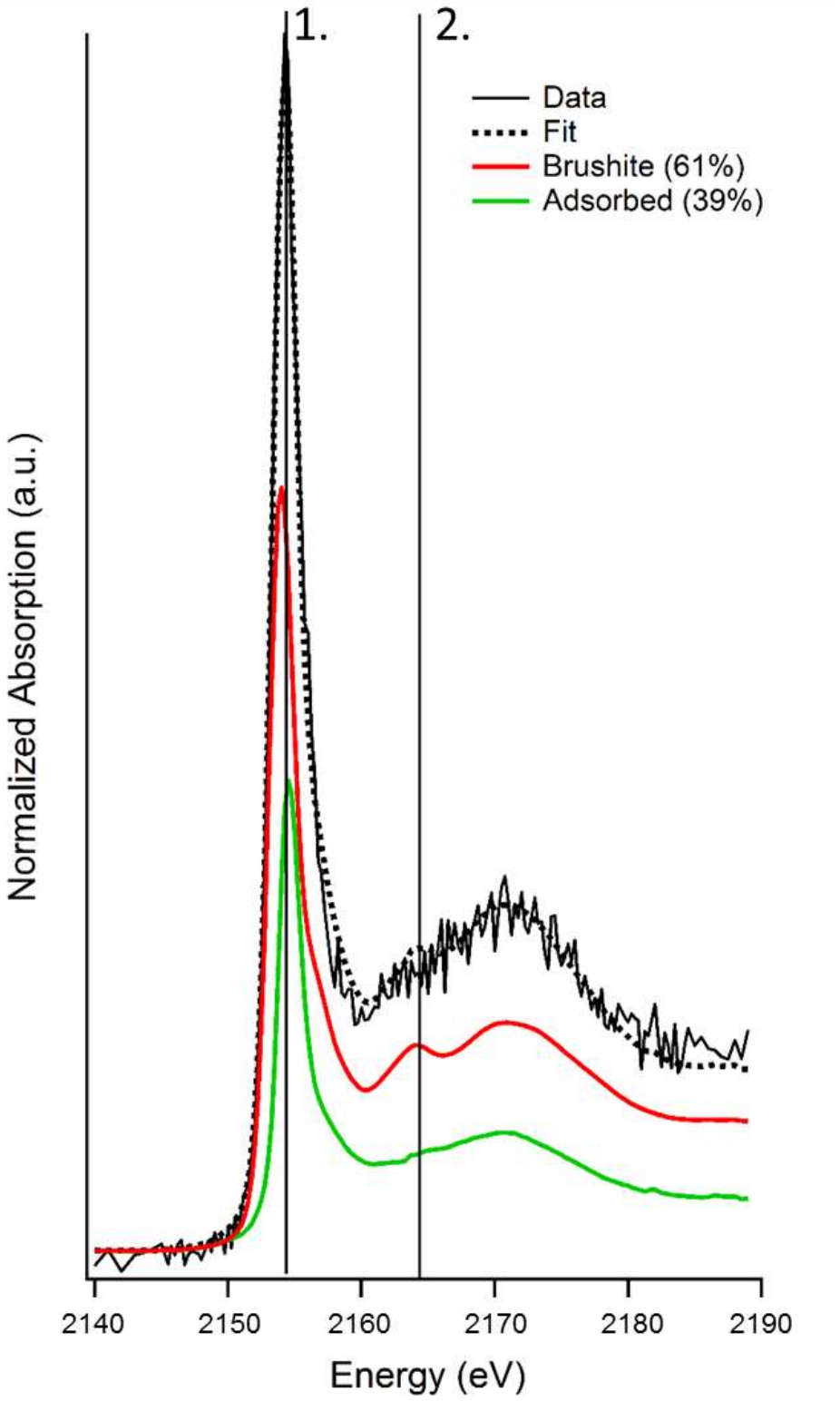

Figure 2.2: P XANES LCF analysis of a soil with a low P concentration adapted from Kar et al., 2017, where Line 1 is the absorption edge and Line 2 is a post-edge oscillation.

The primary limitation of LCF is the assumption that all possible components of the sample are contained in the reference library. Another concern is that statistical analysis of LCF is limited to a comparison of the effectiveness of different models to reproduce a single sample, rather than in the overall quality of an LCF model in describing/explaining a set of samples. Finally, many potential fitting parameters (edge position, standards sum to 100% of sample, etc.) can affect the goodness of fit without being grounded in reality (Manceau et al. 2002).

2.3.3 X-Ray Diffraction theory and application

X-Ray Diffraction (XRD) theory is thoroughly explained in the texts by Waseda et al., (2011), and Percharsky and Zavalij (2009), which can be summarized as follows. X-Ray Diffraction is a powerful technique able to identify mineral phases, relative abundances in heterogeneous samples, and provide insights into the crystal structure based not upon absorption but instead on the diffraction of energy. At what angle photons diffract off the material and the resulting constructive/ destructive interference pattern is specific to how the material is structured, i.e., crystal group and the elements that compose the sample.

A simplified explanation of X-ray diffraction is that a stream of photons is directed at a material and these photons diffracted and spread from the sample in a cone. As the incident photons interact with the atom, the electrons of the sample are oscillated and generate spherical waves of the same wavelength as the incident X-rays, which form areas of constructive and destructive interference. The waves from the "layers" of the sample are in phase but differ due to changes in amplitude and the path length (zero or a multiple of the wavelength). This specific relationship is known as Bragg Diffraction and is dependent on fulfilling Bragg's Law, $2d \sin \theta = n \lambda$, where λ is the X-ray wavelength, n is an integer based on path length, d is the interplanar spacing, and θ is the incident (and reflecting)

angle. This relationship is experimentally exploitable as the wavelength is known (as it is emitted) and the θ angle is controlled via sample geometry and positioning and thereby d, the interplanar spacing of the mineral can be calculated.

The intensity and strength of diffraction is based on the extended order crystallinity, the symmetry, and the elemental composition. A crystal needs to be composed of a unit cell (that can be of varying degrees of symmetry) that repeats across the structure known as a crystal lattice. A unit cell is composed of three lengths (a, b, c), three angles (α, β, γ), and planes are denoted by h, k, l. As the unit cell requires some degree of symmetry, this limits the number of crystals that are possible. There are 8 symmetry elements, 32 point groups, 7 crystal systems, and 14 bravais lattices, which produce 230 possible space groups. The study of these factors is very complex and encompasses the field of crystallography and its application of mineralogy. X-ray diffraction is used for mineral phase identification by techniques such as the Hanawalt method. If the elemental composition is known, the crystal structure and mineral identity can be determined from a list using the d spacing and relative intensities of the strongest peaks. This is not entirely straightforward as d-values and relative intensities can be shifted/altered due to water or impurities, preferred orientation of the crystals, or issues with the crystallite size. The purpose of software is to vastly improve speed, increase the number of peaks matched to improve accuracy and to account for factors which may alter the peak location. After the mineralogical phases are identified, a secondary technique known as Rietveld Refinement is then typically performed which can quantify phase abundance and refine the lattice parameters of that phase.

2.3.4 Attenuated Total Reflectance Infrared spectroscopy theory and application

The text of Stuart (2004) provides a good working knowledge of ATR-FTIR that is summarized below. When a molecule interacts with radiation of the same frequency as its vibration (10^{x}-10^{y} Hz), the atoms of the molecule will resonate and absorb a portion of the incident radiation; the required radiation is in the mid infrared (IR) wavelength. This phenomenon is only distinguishable via absorption of IR energy when the dipole moment of a bond is changed. The magnitude of the resonance and absorption of incident IR radiation is proportional to the size the dipole moment; greater differences in electronegativity will absorb a larger amount of incident radiation and thereby are more strongly IR active. The electric dipole moment manifests in vibrations of the bond between atoms that can be categorized as a "stretch" or a "bend." A stretch is where the bond length is altered either within the phase of the bond, known as a symmetrical stretch, or stretched out of phase, known as an asymmetrical stretch. Alternatively, the bonding angle between the resonating atoms may be "bent" in or out of phase. In this instance, the intermolecular distance is not changed, but the bond angle of the constituent atoms within the molecule are: this may be as deformation (or scissoring), rocking, wagging, or twisting. The specific wavelength at which at a molecule interacts with IR radiation is based on the identity of the constituent atoms and the intermolecular forces that bind them. The "molecular" resonance encompasses all the possible vibrations between the atoms of the molecule; there are multiple diagnostic bands for each molecule, facilitating identification and providing insight on the bonding environment of a sample.

Attenuated Total Reflectance (ATR) is an infrared method in which the studied sample is placed in contact with a crystal of high refractive index for measurement. Attenuated total reflectance is based on the phenomena of total internal reflection where an

incident beam is at such an angle (critical angle) that it reflects entirely within the crystal at the phase boundary. "Total" is a slight misnomer as the beam travels a minute distance outside of the crystal at the phase boundary, on the order of 10^{-6} m. When the beam travels outside of the crystal, it contacts the sample and a small amount of radiation is absorbed.

The technique of ATR-FTIR is generally not applicable in soil P characterization. The diagnostic bands of ortho-P are located in the same wave regions as C=O, C-O, Si-O. In a soil matrix, these bands overwhelm P absorption as they are associated with organic carbon and silca, which are orders of magnitude more abundant. Infrared radiation spectroscopy is an established technique for P, with an extensive spectra library available (Farmer, 1974). Common applications of FTIR spectroscopy in respect to P are characterizing calcium phosphate precipitates in biomineral studies (Lee and Kumta, 2010, Kolmas et al. 2011, Ben-Nissan, 2014) and P absorption on mineral surfaces such as iron (hydr)oxides (Arai and Sparks, 2001, Elzinga and Sparks, 2007).

2.3.5 Transmission Electron Microscopy theory and application

Transmission electron microscopy is a well-established technique that is adequately described in the text by Carter and Williams (2016). Imaging with a Transmission Electron Microscope (TEM) is conceptually similar to a conventional visible light microscope. However, instead of ambient or lamp-generated light, the "light source" is accelerated electrons. Electrons are used because their wavelength is five orders of magnitude smaller than visible light; the wavelength of the light limits the resolving power of microscopy. The generated electrons are focused into a tight, coherent beam with an electromagnetic "lens" which is then transmitted through the sample. A portion of the beam interacts with the sample and is scattered or diffracted. The electrons that pass through the sample hit a plate that fluoresce where contact is made. This creates a greyscale graduated image based on

the local mass of the sample. Areas of the image that are "darker," where fewer electrons have been transmitted through the sample, indicate an area that is either more dense or thicker than the surrounding sample.

Transmission Electron Microscopy is a technique that is not often used in soil science because bulk soils are much too thick to permit meaningful electron transmission. For soil components, such as crystallites, TEM is a useful technique in which general morphology and particle size can be determined. The usage of TEM in P research is limited to supporting evidence in crystallographic studies, often in the biomedical or material research fields (Abonna and Baronnet, 1996, Lu and Leng, 2003).

2.4 Summary

The literature review has established several key facts that support the need for the research of this thesis. (1) Conventional chemical analysis, while applicable for testing for bioavailability, is not a suitable method for precise P speciation. (2) The presence of Mg can be a significant factor in calcium phosphate formation. This has been tentatively shown to alter solubility of P within soil, but this has not been directly measured with spectroscopy. (3) P XANES has a proven track record, but confidence limits in LCF for Ca and Mg phosphates needs to be affirmed. (4) TEM, ATR-FTIR, and XRD are well established techniques capable of characterization when used in conjunction with XANES.

3. XANES INVESTIGATION OF THE INFLUENCE OF MAGNESIUM IN THE FORMATION OF CALCIUM PHOSPHATE MINERALS

3.1 Preface

The work found in the third chapter is original work undertaken by the author, D.M. Hilger in conjunction with the principal investigator Dr. Derek Peak. Aid was provided by J.G. Hamilton in the form of XAS/XRD data collection and in the editing process. As was discussed in the literature review, the role of Mg in the formation of phosphate minerals has been not largely studied. Accordingly, this research chapter seeks to examine what minerals are formed as Mg concentrations are varied to mimic possible Ca:Mg ratios within soil environments. The work detailed in this chapter is *in-preparation* for journal submission as "D.M. Hilger, J.G. Hamilton, D. Peak, XANES Investigation of the Influence of Magnesium in the Formation of Calcium Phosphate Minerals".

3.2 Abstract

Calcium phosphate minerals are typically the solubility-limiting phase for phosphate in calcareous soils. Despite the possibility of a high concentration of magnesium (Mg) in calcareous soils (Razc and Soper, 1967, Wadu et al., 2012), its role in the formation and stability of these minerals has been largely ignored. A series of two common calcium phosphate minerals, hydroxyapatite ($Ca_5(PO_4)_3(OH)$ – (HAP)) and brushite ($CaHPO_4 \bullet 2H_2O$ – (DCPD)) were synthesized in the presence of Mg and analyzed with a range of spectroscopic techniques to examine the effect Mg substitution has upon the local

bonding environment and overall structure. Phosphorus K-edge X-Ray Absorption Near Edge Structure (XANES) and Attenuated Total Reflectance Fourier Transformed Infrared (ATR-FTIR) provide insight into the local structure while SP-XRD (Synchrotron Powder X-Ray Diffraction), and Transmission Electron Microscopy (TEM) were used for macrostructure. In acidic to neutral pH systems, Mg-bearing brushite phases were the dominant mineral forming over a wide range of Ca:Mg ratios. In neutral to high pH systems, a short-range order amorphous calcium phosphate (ACP) with a local structure analogous with hydroxyapatite precipitated for a wide range of Ca to Mg ratios. It can be inferred that the presence of Mg in soils leads to stabilization of the metastable brushite phase via cation substitution at neutral pH. At higher pH, Mg inhibits hydroxyapatite formation via poisoning of crystal growth propagation and leads to ACP metastability.

3.3 Introduction

Phosphorous (P) is a macronutrient for plant and microbial growth, and is integral to all life. Phosphorus is of concern as it is a finite resource that often limits crop production, which pressures a higher efficiency usage and is tightly coupled to global food demands. There is a need to fully understand the chemical fate of P minerals in the environment to facilitate or limit bioaccessibility. The goal of this study is to improve the ability to speciate inorganic P species within bulk soil through a greater understanding of magnesium-calcium phosphates and improving the P-K edge X-Ray Absorption Near Edge Structure (XANES) library of these minerals.

Magnesium is a potentially significant cation within soils that has largely been omitted from the P species balance due to assumptions that pure Mg phases are more soluble than Ca-P minerals (Razc and Soper, 1967, Wadu et al., 2012). In biomaterial

studies, and more recently in soil chemistry, Mg has been shown to limit the precipitation of calcium phosphates and inhibit the formation of insoluble crystalline minerals such as hydroxyapatite, HAP ($Ca_5(PO_4)_3OH$) (Diallo-Garcia et al 2011, Wang and Nancollas 2008, Salimi et al 1984, Cao et al 2008, Wadu et al., 2012), whereas acidic phases and precursors such as brushite, DCPD, ($CaHPO_4 \bullet H_2O$) are minimally affected (Wang and Nancollas, 2008, Salimi et al., 1984). In basic solutions containing ~10% of cations as Mg, it has been observed that HAP precipitation is inhibited with reaction products instead being (a) amorphous calcium phosphate, ACP, with incorporated Mg or (b) whitlockite, the Mg polymorph of β-TCP, after heat treatment (Driessens and Verbeeck, 1990, Cao et al., 2007, Diallo-Garcia et al, 2011, Wadu et al., 2012). The nanoscale of these particles causes difficulty in differentiating these phases from a truly amorphous phase with many spectroscopic techniques. Chemical fractionation between these phases would similarly be difficult as smaller precipitates are more prone to dissolution (Peak et al., 2012).

It has been established that phosphate is an element of interest and that there are missing components in the story of P fate in soils. One explanation for this knowledge gap is that P is a difficult element to speciate within the soil. Nuclear Magnetic Resonance, X-Ray Diffraction, and infrared techniques all have significant issues due to matrix effects and the low concentration of P within soil (Hesterberg, 2010). Phosphorus K-edge X-ray Absorption Near Edge Spectroscopy (XANES) as a technique for direct solid state P speciation in soils has matured as the accessibility of suitable synchrotron radiation sources and beamlines has increased. However, the utility of P XANES spectroscopy is limited in many cases by the breadth and quality of spectral reference libraries that are used in semi-quantitative analysis. Spectral libraries are available, notably Ingall et al., (2010), but most studies have utilized highly crystalline minerals and focused towards acidic, weathered

systems where Fe and Al phosphates dominate. There is a relative lack of study in calcium phosphates and particularly mixed Ca:Mg systems that are typical in calcareous soils.

This study has created a XANES spectral library of calcium and magnesium phosphates for the use in calcareous soils. The creation and inclusion of a wide range of calcium and Mg-bearing phosphate phases are more representative of what is found in the inorganic phase of soil systems and as a result may lead to more accurate semi-quantitative analysis. The prevalence of the phases is significant as substituent ions in calcium and magnesium phosphate minerals alter crystallinity, resulting in higher dissolution rates and the inhibition of thermodynamic end species formation.

3.4 Materials and Methods

3.4.1 Mineral synthesis

Newberyite ($MgHPO_4 \cdot 3H_2O$). Newberyite was synthesized by the dropwise mixing of $MgCl_2 \cdot 6H_2O$ and H_3PO_4 by a modification of the method of Aramendia et al., (1999). Phosphoric acid was neutralized to pH 7.0 with concentrated NaOH before the reaction to prevent over acidification. Reaction conditions are held at 25°C and between pH 6.0 and 7.4. The reaction is saturated with respect to P, 0.067M $MgCl_2 \cdot 6H_2O$ and 0.1M H_3PO_4. Three additional precipitation reactions with mixed Ca:Mg solutions were performed. Calcium substitution was performed through the replacement of $MgCl_2 \cdot 6H_2O$ with $CaCl_2$ in molar ratios of 12.5:87.5, 25:75, and 50:50 (Ca:Mg). As per the cited source, the precipitate was separated from the supernatant by vacuum filtration with a 40 µm cellulose filter then washed several times with double deionized (DDI) H_2O to remove entrained ions. The sample was then dried at 80 °C. The precipitate was referenced in all measurements by a commercially acquired equivalent (Magnesium hydrogen phosphate trihydrate - Alfa Aesar).

Brushite ($CaHPO_4 \cdot 2H_2O$). Pure brushite was synthesized by the dropwise mixing of equimolar $CaCl_2$ and Na_2HPO_4 (Lee and Kumta, 2010). Briefly, 50 mmoles of $CaCl_2$ were slowly dripped into 50 mmoles of Na_2HPO_4 while stirring at 25 C° with unregulated pH. A series of Mg-bearing brushite was created using the same method but replacing $CaCl_2$ with $MgCl_2 \cdot 6H_2O$ in the proportions of 100:0, 75:25, 68.75:31.25, 62.50:37.50, 56.25:43.75, 50:50, 25:75, and 0:100 (Ca:Mg molar ratio). Samples were vacuum filtered with 40 µm filter paper, washed with DDI H_2O, and dried at 80 C° overnight. The precipitate was referenced in all measurements by a commercially acquired equivalent (Calcium phosphate dibasic dihydrate – Sigma Aldrich).

Hydroxyapatite ($Ca_5(PO_4)_3(OH)$). Hydroxyapatite was synthesized by the methods of Riman et al., (2007). Two solutions, one of 16.7 mM $Ca(CH_3COO)_2 \cdot H_2O$ and the other of 10.0 mM of H_3PO_4, are rapidly mixed then stirred, then mixed for 1hr. Suspension pH was be held at 9.0 using 1.0 M NaOH. Nitrogen gas was bubbled through the system during the reaction to minimize carbonate substitution. Magnesium substitution will occur by replacing a portion of the $Ca(CH_3COO)_2 \cdot H_2O$ with $Mg(CH_3COO)_2 \cdot 4H_2O$ in the proportions (by mole fraction) of 100:0, 95:5, 90:10, and 80:20. This amount of substitution is relatively small compared to the proposed cation substitution in other minerals in this study, as literature indicates Mg substitution into HAP does not readily occur, and instead high Mg concentrations inhibit HAP precipitation (Laurencin et al., 2011, Kolmas et al., 2011). Prepared samples were vacuum filtered through 40 um cellulose filters, washed with DDI H_2O, and dried at 110 C° overnight. The precipitate was referenced in all measurements by a commercially acquired equivalent (Calcium phosphate tribasic – Alfa Aesar).

Bobierrite ($Mg_3(PO_4)_2 \cdot 8H_2O$). The synthesis of bobierrite minerals was based on European Patent method 0 113 153 (Sherif, 1987). The formation of bobierrite by this approach occurs in two stages. The first stage entails the rapid mixing at room temperature of 5.00 mmoles of concentrated H_3PO_4 with 2.50 mmoles of $Mg(OH)_2$ to form a "newberyite like" solution of 100 mL total volume. In the second stage, the acidic newberyite solution was dripped into a $MgOH_2$ slurry with a minimum concentration of 5.00 mM. The second reaction occurs at 50°C over the course of 5hrs. The study sought to form bobierrite with increasing amounts of Ca substitution. Calcium hydroxide ($Ca(OH)_2$) replaced $Mg(OH)_2$ as a reagent in the proportions of 0/100, 12.5:87.5, 25:75, and 50:50 (Ca:Mg molar ratio), with the hope this would result in increasing cation substitution. Precipitates were vacuum filtered, washed with DDI H_2O, and oven dried at 80 C° overnight. The precipitate was referenced in all measurements by a commercially acquired equivalent (Magnesium phosphate tribasic octahydrate – Sigma Aldrich).

3.4.2 Synchrotron Powder X-Ray Diffraction

Synchrotron Powder X-ray Diffraction (SP-XRD) patterns of the Ca and Mg minerals were collected at the Canadian Light Source (CLS) on the Canadian Macromolecular Crystallography Facility 2 beamline CMCF-BM (08B1-1). The incident energy was 18 keV with a wavelength of 0.6888 angstroms and the detector distance set at 250 mm. The precipitates were finely ground and packed into polyamine tubing of 0.215 mm diameter. Collected patterns were calibrated to LaB_6 diffraction patterns, subtracted from the polyamine tubing blank, and integrated from diffraction rings to peak patterns using GSAS II (Toby and Von Dreele, 2013). HIGHSCORE (PANalytical, Almelo, Netherlands) and GSAS I were used in phase identification of the patterns, Rietveld

refinement, and determination of unit cell parameters (Degen et al., 2014, Larson and Von Dreele, 2000).

3.4.3 Attenuated Total Reflectance Fourier Transform Infrared (ATR-FTIR) spectroscopy

All powdered samples were analyzed with ATR-FTIR spectroscopy using a Bruker Equinox 55 FTIR spectrometer with a single bounce accessory equipped with diamond-coated ZnSe optics and a liquid nitrogen cooled Mercury-Cadmium-Tellurium (MCT) detector. Desiccated samples were ground with a mortar and pestle before analysis to ensure a firm pressing on the diamond surface, and measured in the mid-infrared region between 4000 cm^{-1} and 400 cm^{-1} with 4 cm^{-1} resolution.

3.4.4 Elemental Analysis

Samples were dissolved in a solution of 37% HCL and 65% HNO_3 then microwave digested via EPA method 3051. Magnesium and Ca measured with an Agilent Microwave Plasma Atomic Emission Spectrograph 4100 (MP-AES) (Mississauga, Ontario) and P concentrations were determined colourmetrically with a SEAL Analytical Auto Analyzer (AA-1) (Kitchener, Ontario).

3.4.5 Transmission Electron Microscopy (TEM)

The pure and cation substituted phases were suspended in H_2O and deposited on a copper mesh grid with a pipette. Samples were imaged with a Philips CM10 (1990, Philips Electron Optics, Eindhoven, The Netherlands) TEM with an accelerating voltage of 80kV which has a resolution of 0.5 nm at a point and 0.34 nm on the line with a magnification of 20,000-450,000. Images were processed with Adobe Photoshop.

3.4.6 Phosphorus K-edge XANES spectroscopy

All P K-edge XANES spectra were collected in partial fluorescence (PFY) mode at the Canadian Light Source (CLS) at beamline 06B1-1, the Soft X-Ray Microcharacterization Beamline (SXRMB). The storage ring of the facility operates at an energy of 2.96 GeV and a stored current between 225-150 mA. Spectra were collected using an InSb (111) monochromator and a four-element Si-drift fluorescence detector (Bruker). Samples were diluted to 1% wt. P with BN to minimize self-absorption effects associated with PFY. Powders were ground with an agate mortar and pestle, thinly spread on double-sided carbon tape, and mounted on a copper plate. A minimum of two spectra was collected for each mineral sample, which were then averaged. A check of beamline resolution and stability was performed after every storage ring injection by measuring a BN diluted $ZnPO_4$ standard. Samples were scanned from 2120 to 2220 eV.

3.5 Results and Discussion

3.5.1 Brushite/Newberyite mineral series

The series was examined via XAS (Figure 3.1 left), XRD (Figure 3.1 right), ATR-FTIR (Figure 3.2, top row), and TEM (Figure 3.3, top row). Each of these methods was useful in examining different aspects of structural changes due to cationic substitution. The applicability of P K-edge XANES as a speciation tool in whole soils warrants a focus on this method and to relate observations from the other techniques to the XAS spectra. Brushite synthesis occurred at 5.4 pH and newberyite synthesis occurred at pH 6.0-7.0. (Appendix B) Brushite series is available across the entire range with comparable, albeit less crystalline, results to the newberyite series.

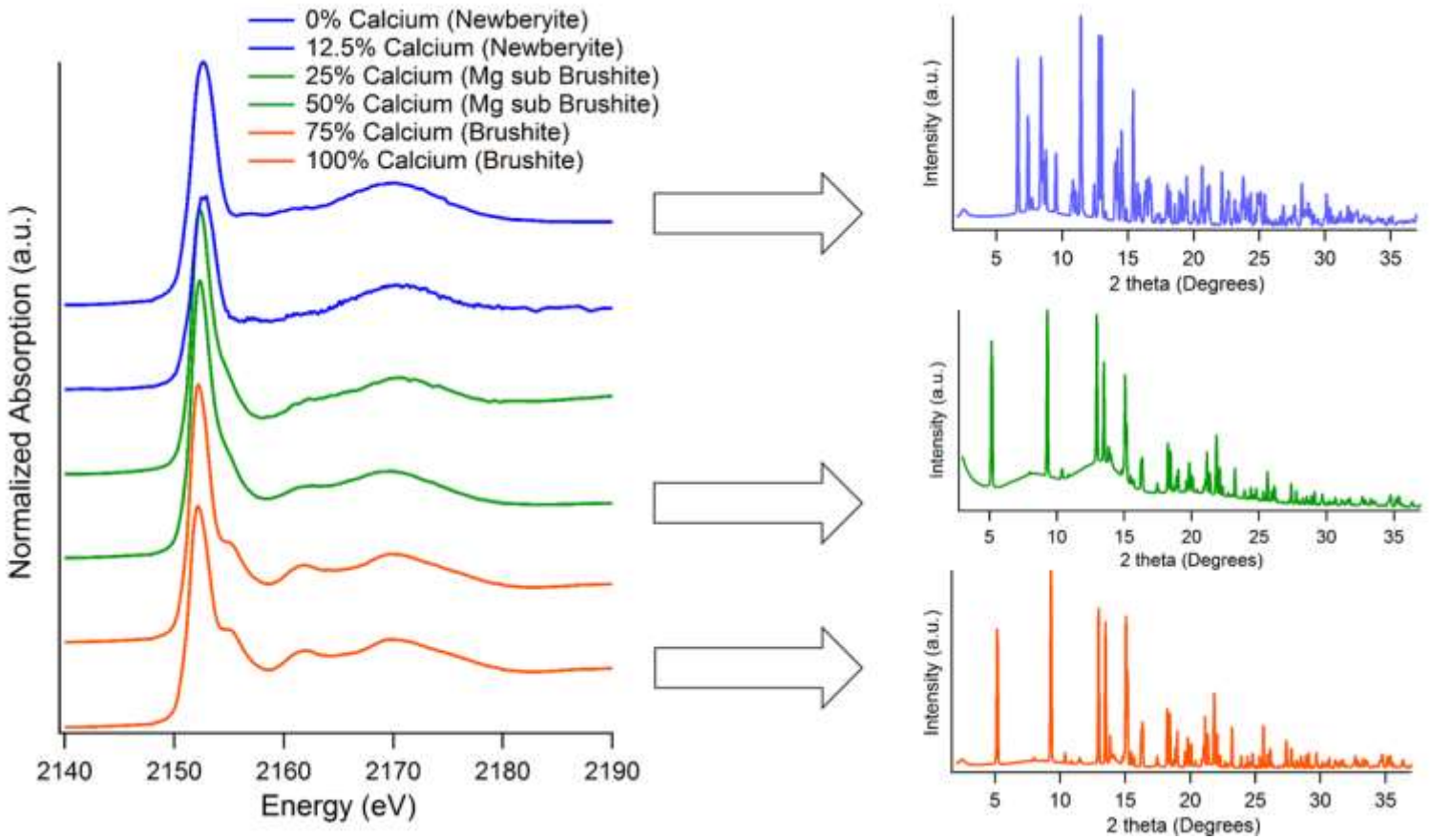

Figure 3.1: XANES and XRD patterns of Acidic/Neutral mineral series. Blue spectra/patterns indicate magnesium phosphates, green spectra indicate minerals formed in mixed cation solutions with unique characteristics, and orange spectra are crystalline calcium phosphates.

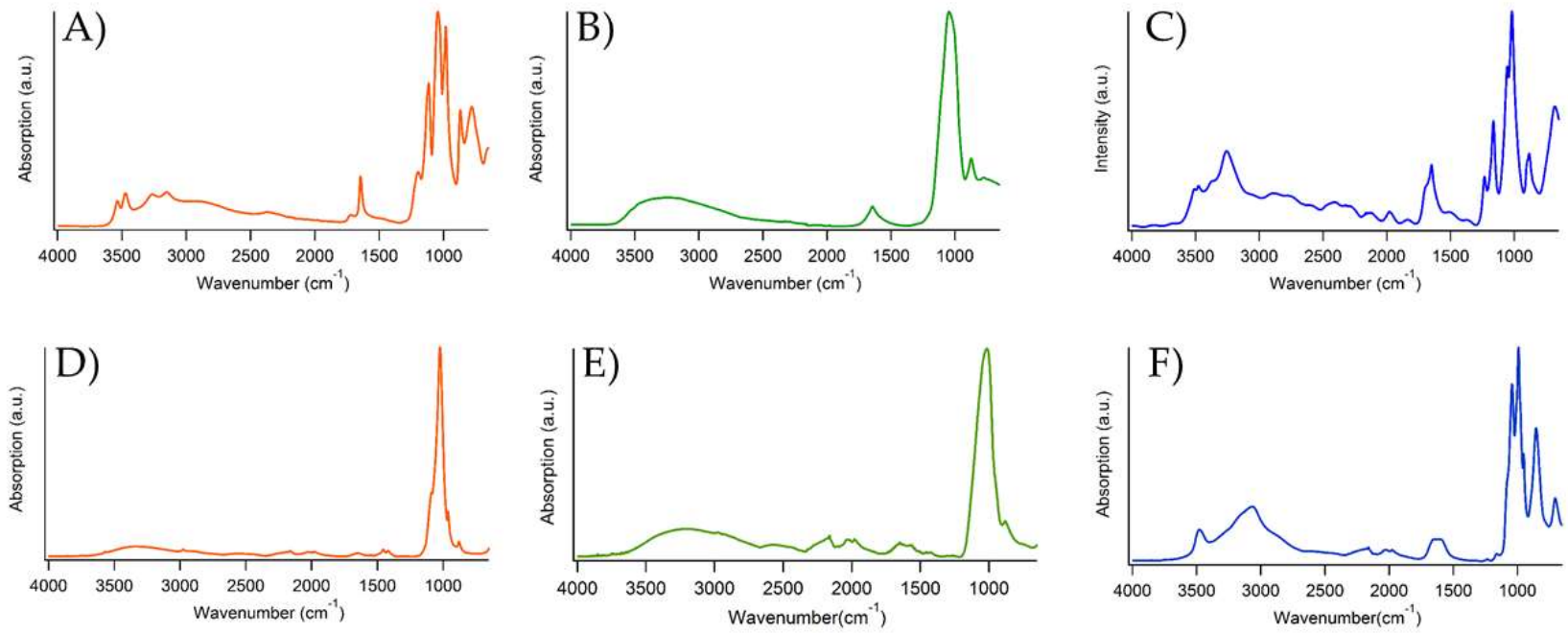

Figure 3.2: ATR-FTIR of hydroxyapatite/ bobierrite and brushite/newberyite series: A) pure brushite, B) 1:1 (Ca:Mg) brushite, C) pure newberyite, D) pure hydroxyapatite, E) 5:1 (Ca:Mg) hydroxyapatite, F) pure bobierrite.

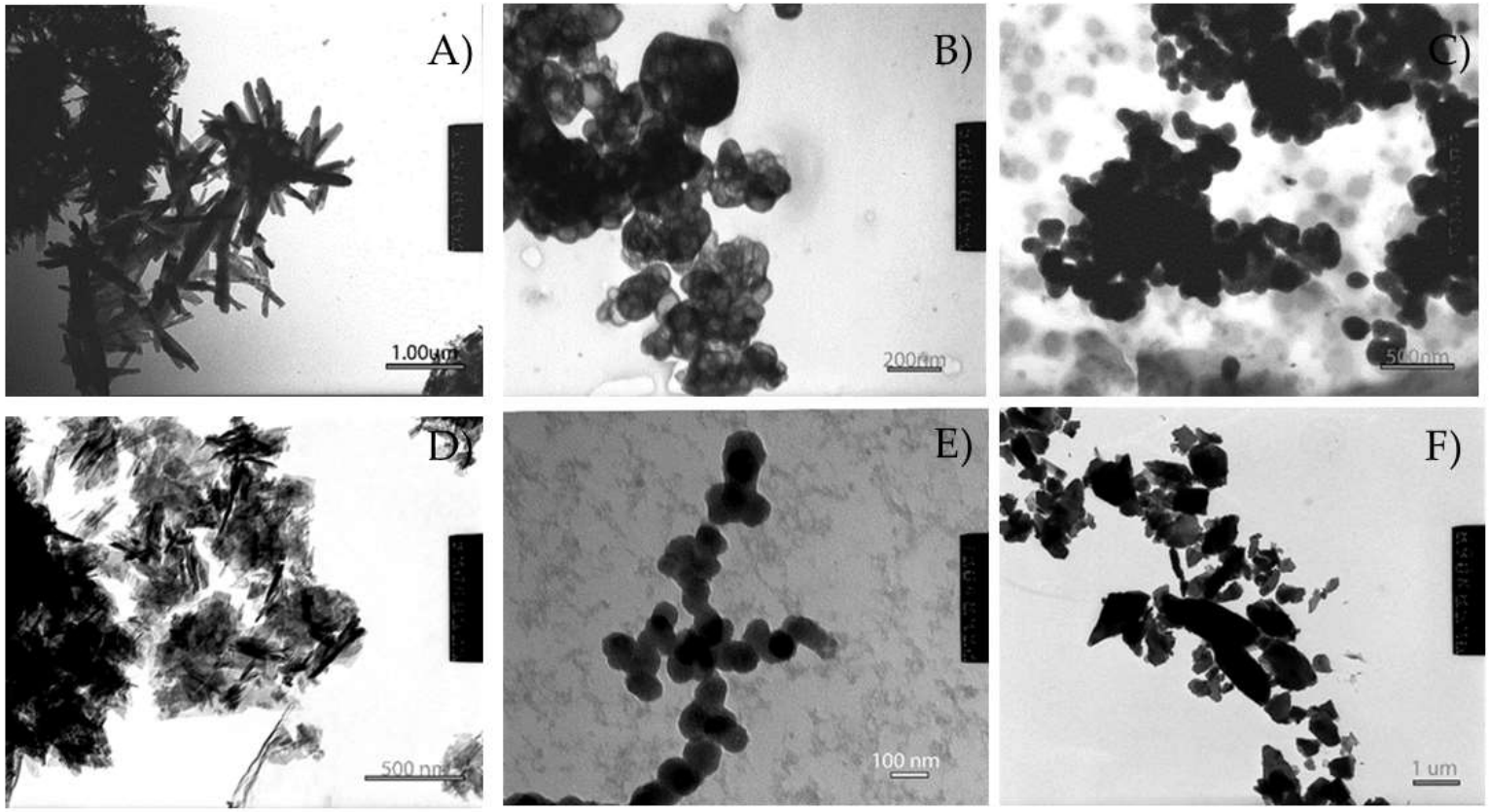

Figure 3.3: Transmission Electron Microscopy images of: A) pure brushite, B) 1:1 (Ca:Mg) brushite, C) newberyite, D) pure hydroxyapatite, E) 5:1 (Ca:Mg) hydroxyapatite/amorphous calcium phosphate, F) pure bobierrite

Brushite is stable in aqueous systems that are acidic to neutral and have a 1:1 Ca to P ratio. The natural occurrence of brushite, or acidic calcium phosphates in general, are limited to slightly acidic soils due to being Ca and phosphate poor. Brushite has been observed in fertilized soils (Kar et al., 2012, Wadu et al., 2012) and there is mounting evidence, chiefly in the biomedical field, that brushite is an important HAP precursor for many different formation conditions (Johnsson and Nancollas, 1992, Valsami-Jones, 2001). In this study, low levels of Mg in solution, < 25%, have little effect on the structure of the mineral formed, brushite. There is a slight discrepancy in XRD patterns as the relative peak intensities of lower d-spacings are skewed relative to published parameters and Miller indices, but are overall consistent with a pure brushite phase (Schofield et al., 2004). The local structure of these minerals, based on P K-edge XANES spectra, are unaffected by Mg incorporation (Figure 3.1, orange). Diagnostic spectral features such as the white line intensity and energy position, post edge shoulder, and oxygen oscillations at 2162 and 2170 eV are consistent with the brushite XANES standard. Corroborating evidence is presented in the ATR-FTIR spectra (Figure 3.2, Appendix B, Figure B2). Infrared spectra of pure and 25% Mg-bearing brushite are consistent with standard spectra from commercially acquired minerals, primarily based on the diagnostic close triplet of peaks around 1000cm^{-1}. These features are located at 983 (ν_1 PO), ($_{\nu 3}$ PO) 1043, and (ν_3 PO) 1115 cm^{-1} associated with PO vibrations (Figure 3.2A). A shift of 5-10 cm^{-1} to higher wavenumber occurs in the ν3 PO vibration with the addition of 25% Mg in solution, (ν_1 PO 983 cm^{-1}, ν_3 PO 1054 cm^{-1}, and ν_3 PO 1120 cm^{-1}). This shift indicates there is a change in the local environment, but there

is no lack of definition or peak broadening to indicate that there are multiple bonding environments or significant strain (Appendix B, Figure B2). In summary, there is a threshold of approximately 3:1 (Ca:Mg) where if there is proportionally less Mg than this value, Mg does not significantly affect the formation of brushite or alter the crystal structure. Magnesium does have some impact on the mineral formation, as the crystallite macrostructure of low Mg brushite differs from pure Ca brushite in TEM (Figure 3.3B). Brushite formed in exclusively Ca solution is aggregated in rod crystals where the length is much greater than the width and where the size is fairly consistent. These crystals are on the order of 1000 nm in length and 100 nm in width. The crystallites of brushite containing low levels of Mg in solution are smaller, spherical or ovoid in shape, and appear to be much less uniform. These minerals are all heavily aggregated which makes identifying specific particle dimensions difficult but are approximately 200 nm × 150 nm. Low levels of Mg substitution does not induce localized structural changes: X-ray absorption near edge spectroscopy, ATR-FTIR, and XRD spectra and patterns are all in agreeance with a structure that is unchanged from a pure Ca brushite mineral. The only obvious change upon low Mg incorporation is a decrease in particle size and morphology, which may have an effect upon solubility.

In solutions that are roughly equimolar in respect to Ca and Mg, and range in pH from 5.4 to 7.0, produce a precipitate that is consistent with brushite that has a strained local structure. The overall crystal lattice is largely the same, but the local bonding environment is altered, chiefly observed via P K-edge XANES spectra that are much more altered from pure brushite than is the XRD pattern (Figure 3.1, green). The crystal lattice of these minerals are largely not different from a pure brushite phase. The chief difference

is a raised background through 4 to 25^{o} that is consistent with increased amorphous content and/or disorder in the structure of the mineral (Waseda et al., 2011). This is plausible, since Mg substitution into the brushite crystal lattice will result in strain due to the smaller atomic radius of Mg (Salimi et al., 1985). The ATR-FTIR and P K-edge XANES spectra are more sensitive to the local structure and show a more dramatic change in spectral features. The most apparent change in the XANES spectra is the loss of definition of the post edge shoulder, which decreases from a 1 eV "ledge" to a medium to small aberration (Figure 3.1). The intensity of the oscillation at 2162 eV is also decreased. As these spectral features are diagnostic of calcium phosphates and have a positive correlation with the crystallinity of these minerals, it can be inferred that these moderate Mg phases are less crystalline than the pure phase but that are still essentially a calcium phosphate mineral with the same basic structure. Similarly, the ATR-FTIR spectra are heavily modified in equimolar cation solutions. In systems with moderate concentrations of Mg relative to Ca (Figure 3.2B), the spectra have very broadened features: the triplet of PO around 1050 cm^{-1} is not present. Instead, there is one broad peak centred at 1049 cm^{-1}, a 1647 cm^{-1} vibration due to H-O-H bending that is present but broadened, and an ν OH^{-} stretch at 3300cm^{-1}. This peak broadening and loss of features are also consistent with the strain that Mg causes on the crystal structure resulting in a range of slightly different bond distances and symmetries all with slightly different IR stretches that appear as a single broad peak. Transmission Electron Microscopy images are not largely different than those of 25% substituted brushite and show precipitates with smaller dimensions, spherical or ovoid in shape, less uniform and heavily aggregated Figure (3.3B). The particle size is smaller with moderate Mg substitution, on the order of 120 nm × 80 nm, rather than 200-150 nm as in

low Mg substitution. In summary, solutions composed of 25:75 to 75:25 (Ca:Mg) produced a modified brushite mineral. The local bonding environment is strongly influenced by the mixed cation solution as the ATR-FTIR spectra and P K-edge XANES of these precipitates is recognizable as a low crystallinity calcium phosphate but are not readily apparent as brushite.

At high Mg concentrations (above 1:8), the solution exclusively forms newberyite, a neutral/acidic magnesium phosphate phase. These phases have little to no Ca inclusion, which produces a XRD newberyite pattern with few irregularities (Figure 1C). This pattern may appear as a mixture, but newberyite is of the low symmetry triclinic space group which produces many diffraction peaks. Phosphorus K-edges XANES spectra of these minerals are not rich with spectral features but are distinct from calcium phosphate phases. The white line intensities of magnesium phosphate phases are shifted slightly to higher energy and have no post edge shoulder or oscillation at 2162 eV. There is a very slight peak at 2155 eV that is more pronounced in some newberyite standard compounds than in the mixed phases produced in this study. The local bonding environment is also (> 1:8 Ca:Mg) consistent with newberyite when measured using ATR-FTIR (Figure 3.2C). The PO stretches are present in a prominent peak located at 1016 cm^{-1}, and lesser peaks located at 1156 cm^{-1} and 883 cm^{-1}. There is also structure at high wavenumber with a relatively strong absorbance band at 3250 cm^{-1}. Solutions with 0% Ca have a wide size distribution, but a rough average of the particle dimensions are 500 × 400 nm (Figure 3.3). The particles of newberyite containing 12.5% Mg in solution are aggregated, roughly ovoid particles with a rough dimension of 150 × 130 nm. In summary, magnesium phosphates do not form in mixed solutions unless the concentration is overwhelmingly in favour of Mg (1:8). As

found with the other minerals in this series, the macro-structure via TEM was changed in the mixed solution. The crystal structure and the local bonding environment are newberyite.

The observation that Mg-bearing brushite has a P K-edge XANES spectra that is distinct from pure Ca brushite, and that this identifiable substituted phase occurs at Ca:Mg ratios less than those commonly found in nature, including soils, may also be important to the metastability of brushite in soils. The diffraction pattern of Mg-bearing brushite is consistent with that of pure brushite indicating the overall crystal structure is unaffected. However, there are extreme morphological changes presented by TEM images as well as broadening of FTIR bands consistent with many slightly different local bonding environments deriving from strains caused by Mg incorporation and/or substitution. This is in agreement with P K-edge XANES spectra that are similar to the pure brushite mineral but with a lower crystallinity/ordered local environment. This may provide insight into why crystalline hydroxyapatite is observed in more weathered agricultural soils rather than brushite, where phosphate and lime (calcium carbonate) have repeatedly been applied yet the natural soil contains very low to non-existent concentrations of Mg due to plant uptake and leaching.

3.5.2 Hydroxyapatite/Bobierrite mineral series

Solutions containing a very high proportion of Ca to Mg, 20:1, produce a precipitate structurally similar to pure hydroxyapatite mineral. There is a decrease in Ca in the mineral (Table 3.1) but no corresponding increase in Mg inclusion. The Mg/P ratio associated with this mineral is less than 0.03, which may be entirely due to surface adsorption. Based on this information, it can speculated that the mineral is a Calcium-deficient hydroxyapatite

(CDHA) (Dorohzkin, 2011). The local bonding environment is not drastically changed relative to pure hydroxyapatite. Phosphorus K-edge XANES and ATR-FTIR spectra exhibit the diagnostic features that are associated with HAP with several differing spectral characteristics (Figures 3.2 and 3.4). The 20:1 mineral features the "wide" post-edge shoulder located at 2155 eV in the P K-edge XANES spectra associated with CaP crystallinity. In the ATR-FTIR spectra, a prominent peak located at (ν_3 PO) 1027 cm^{-1} with slight peaks/shoulders located at (ν_3 PO) 1087 cm^{-1} and (ν_1 PO) 962 cm^{-1} in the ATR-FTIR spectra. It is worthwhile noting that there does not appear to be the inclusion of water in the crystal structure that is associated with amorphous calcium phosphate (ACP) as opposed to CDHA. Water inclusion is exhibited by defined peaks, such as those found in brushite (Figure 3.2A) or bobierrite (Figure 3.2F). The broad, relatively low intensity absorbance band at 3300 cm^{-1} found in the 20:1 minerals corresponds to H_2O, but not inclusion. Full dehydration requires high temperature, which increases crystallinity and forms the β-tricalcium phosphate analog whitlockite if Mg is present (Diallo-Garcia et al., 2011, Stipniece et al., 2013). On the "macro" scale, the mineral (Appendix C, Figure C1) is considerably different than a pure phase HAP. When analyzed with TEM, the mineral was difficult to de-aggregate but is clearly not composed of the thin, platy sheets approximately 200 × 50 nm that were found in pure HAP.

Table 3.1: Elemental composition of synthesized minerals exhibiting proportions of Mg/Ca substitution.

	ACIDIC						BASIC						
	DCPD †			NBTE ‡			HAP §				BOB ¶		
Ca:Mg	1:0	3:1	1:1	1:3	1:8	0:1	1:0	20:1	10:1	5:1	1:3	1:8	0:1
Ca/P	1.12	1.08	0.87	0.54	0.20	0.00	2.31	1.77	1.62	1.48	0.72	0.29	0.00
Mg/P	0	0.06	0.31	0.38	0.57	0	0.00	0.03	0.04	0.09	1.22	1.36	1.20
Ca+Mg/P	1.12	1.14	1.18	0.92	0.78	1.41	2.31	1.59	1.42	1.31	1.85	1.65	1.20

† DCPD = brushite
‡ NBTE = newberyite
§ HAP = hydroxyapatite
¶ BOB = bobierrite

Phosphorus K-edge XANES spectra of pure hydroxyapatite contain the most spectral features of all calcium phosphates (Figure 3.4). For apatite group phosphates, the white line intensity is located at 2151.7 eV, and the most diagnostic feature is the "wide" post-edge shoulder located at 2155 eV that is stronger and sharper relative to other calcium phosphates such as brushite. The two remaining diagnostic features of hydroxyapatite are slight peaks located at 2162 and 2170 eV corresponding to oxygen oscillations. These peaks differ from other calcium phosphates in that the peak at 2162 eV is sharper and the height of these two peaks are somewhat similar compared with more acidic calcium phosphate minerals. P K-edge XANES spectra of bobierrite white line energy is shifted to higher energy, 2152 eV, relative to calcium phosphates. This mineral has a twin set of oxygen oscillations that are similar to calcium phosphates, but shifted to slightly higher energy. The SP-XRD patterns for these minerals are both consistent with crystalline pure phases or very low levels of cationic substitution. From 10% to 75% Mg in solution, the phases are amorphous to XRD, with no distinct peaks in the pattern and only two broad low intensity features located at 14 2θ and 22 2θ. The P K-edge XANES of these "amorphous" substituted phases are consistent with slightly altered hydroxyapatite spectra, where the post edge shoulder is less defined as is the 2162 eV oscillation but otherwise typical of pure hydroxyapatite.

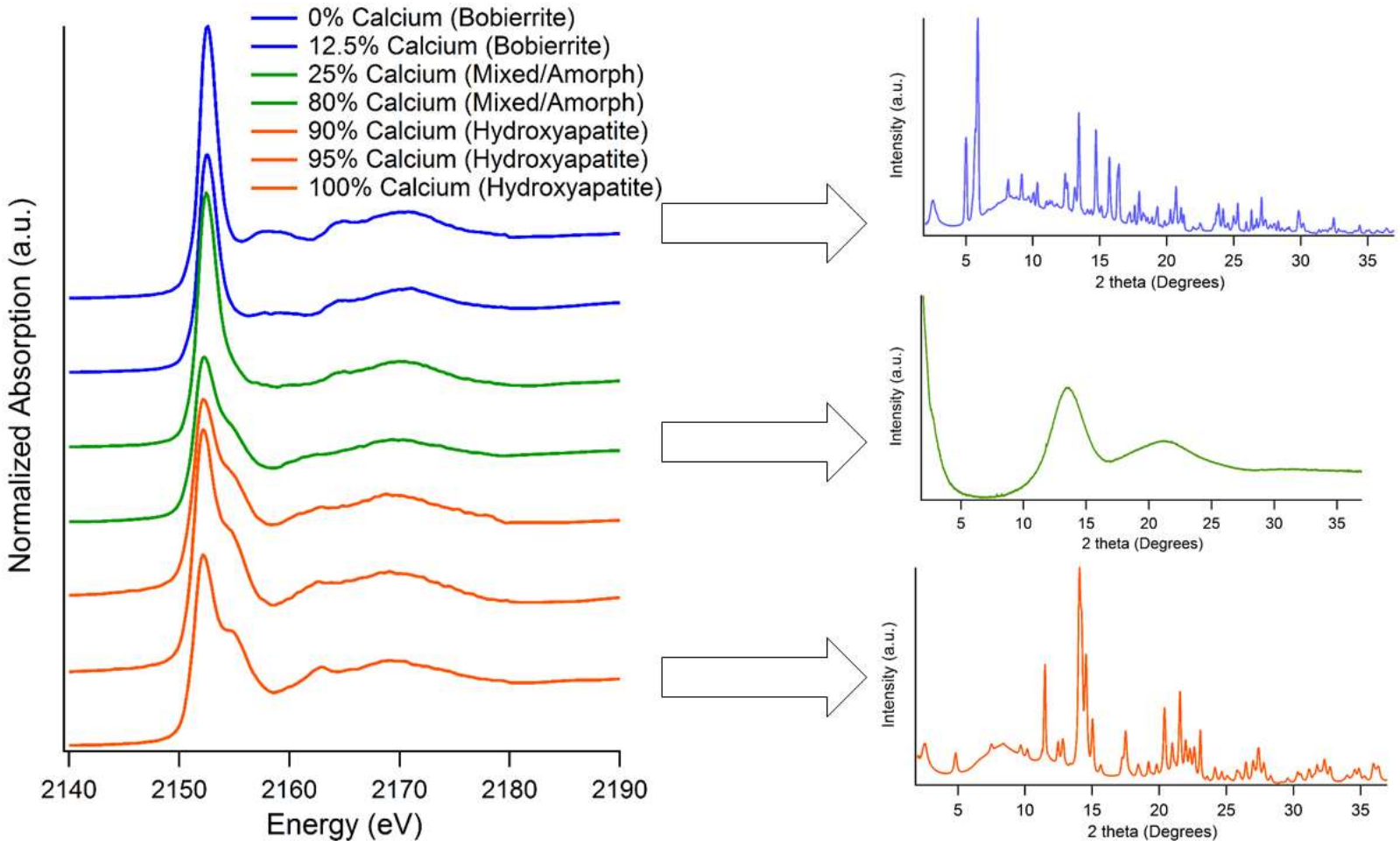

Figure 3.4: Hydroxyapatite/amorphous calcium phosphate/bobierrite P K-edge XANES and XRD, Blue spectra/patterns indicate magnesium phosphates, green spectra indicate minerals formed in mixed cation solutions with unique characteristics (i.e., ACP), and orange spectra are crystalline calcium phosphates.

Precipitates formed in solutions comprising of 10 to 50 % Mg are similar to HAP in regard to local bonding environment but are indistinct structurally. (Table 3.1) The Ca:P ratio of these minerals falls within the range of what is considered ACP: 1.41 in the 5:1 mineral to 1.34 in 1:1 mineral (Dorhzkin, 2011). There is not a corresponding increase in Mg that would preclude significant cationic substitution as the 5:1 mineral is composed of only 1.8% Mg. The XRD patterns of these phases are amorphous, with no defined peaks and only two broad, low-intensity features located at 14 and 22º 2-theta (Figure 3.4). The P K-edge XANES of these "amorphous" substituted phases are consistent with slightly altered hydroxyapatite spectra, where the post edge shoulder and 2162 eV oscillations are less defined. Similarly, the ATR-FTIR spectra are altered, with the intensity of the peak at 1027 cm^{-1} (ν_3 PO with carbonate) being decreased, the band at 962 cm^{-1} (ν_1 PO) becoming more prominent, and the shoulder of 1087 cm^{-1} (ν_3 PO) absent. The relative intensity of the ν OH^- stretch at 3300 cm^{-1} is of greater magnitude, though this is possibly due to a decrease in the intensity of the main PO_4 absorbance. However, these particles of these precipitates are strikingly different when examined via TEM (Figure 3.3 D,E,F). The 5:1 mineral is composed of chains of spherical/ovoid individuals with a binary size distribution. The larger crystallites within this binary distribution are approximately 125 nm in width and while the smaller particles are 30 nm in dimensions. Overall, the short-range order hydroxyapatite appears as apatite via ATR-FTIR and P K-edge XANES, but with SP-XRD and TEM the mineral(s) appear as amorphous and very small particles. Effectively, this Mg 'influenced' calcium phosphate is an amorphous calcium phosphate where the short-range order is consistent with hydroxyapatite. It is possible that much of the hydroxyapatite that

has been identified within soils with P K-edge XANES is, instead, this short-range order phase rather than pure HAP.

Magnesium rich alkaline conditions will form a mineral precipitate identifiable as bobierrite with XRD. The local bonding environment of bobierrite is not affected by the mixed cation solution. Phosphorus K-edge XANES spectra feature the diagnostic features of bobierrite: white line energy and a twin set of oxygen oscillations shifted to higher energy, relative to the XANES spectra of calcium phosphate minerals. The ATR-FTIR spectrum of concentrated Mg systems is unchanged from the pure bobierrite phase and distinct from systems which are predominantly Ca due to more prominent ν_3 PO vibrations, located at 1010, 1041, 1066 cm^{-1}. There is also a large spectral contribution in the 3500 to 3100 cm^{-1} region that are associated with the νOH^- stretches of water, which is expected since the structure of this mineral contains eight different crystallographic positions for water molecules. Synthesized 0% Ca-bobierrite is composed of particles of varying size and morphology. These particles are generally composed of straight lines and angles as opposed to being curved or ovoid in nature with a wide range of crystals from 275 × 175 nm to 630 × 430 nm. These particles are not observed in mixed cation solutions of 1:4 and 1:8; instead aggregated spherical or ovoid crystals that are under 200 nm in diameter and as small as 60 nm are found. It was found that bobierrite is able to form in solutions with a large amount of Mg without affecting the local bonding environment.

Despite direct observation of brushite and ACP in many soils using XAS, thermodynamics predicts that hydroxyapatite should be the solubility limiting mineral phase. Consider the following (1) The Ca:P ratio is often much greater than the 1.67:1 ratio that favours the formation of apatite (2) The pH of the system is often greater than 7,

where minerals such as brushite are unstable due to HPO_4^{2-} dissociation in solution. It is possible that hydroxyapatite is favoured thermodynamically though not kinetically, but given geological time of natural systems, this seems less than convincing. The findings of this paper lead to two additional explanations for the presence of poorly crystalline phosphates in the environment that have not been previously considered: (1) Mg inhibition of hydroxyapatite crystallization and propagation, and (2) inclusion of Mg into the brushite crystal lattice.

3.6 Conclusions

This study produced a library of P K-edge XANES spectra of mixed calcium-magnesium minerals that have not been previously studied or collected. Found in the appendices is a more comprehensive set of spectra from the minerals described in this chapter, with two additional synthesis series (monetite (CaHPO4) and struvite ($NH_4MgPO_4 \bullet 6H_2O$) - STVE). Mixed solutions of Ca and Mg have an identifiable effect on the crystallography and speciation of phosphate minerals. Pure Mg phases only occurred where there was an overwhelming proportion of Mg (≥1:8 Ca:Mg). Phases produced in mixed cationic solutions were observed to be less crystalline and of smaller particle size throughout the study, which can be inferred to increase in overall mineral solubility. For low to neutral pH systems containing both Ca and Mg, it is recommended that a Mg-bearing brushite is considered in P XANES fitting. This phase is more representative of what is found in soils and has a distinct XANES spectrum that may lead to underfitting of brushite if not included. In basic solutions, it was found that Mg quite effectively limits the rapid precipitation of hydroxyapatite, which may be a strong factor in the limited occurrence of HAP in calcareous soils despite being the thermodynamic end species. Any

inclusion of Mg adversely affects the crystallization of hydroxyapatite but does not alter its spectroscopic signature in XANES or ATR-FTIR. It may be possible where HAP has been identified with P XANES in natural systems that a substantial proportion is in fact ACP, a much more soluble calcium phosphate phase. Future research directions in this field should concern the long term evolution, stability and solubility constants of the minerals formed in Ca:Mg mixed cation solutions.

4. Assessment of Linear Combination Fitting of Calcium and Magnesium Phosphates

4.1 Preface

The work found in the fourth chapter is original work undertaken by the author, D.M. Hilger, in conjunction with the principal investigator Dr. Derek Peak. Aid was provided by J.G. Hamilton in the form of data collection. The increasing prevalence and desired usage of P K-edge XANES is in Linear Combination Fitting, a technique that allows for semi-quantitative *in-situ* speciation of P. Previous work on accuracy estimates of linear combination modeling has tested vastly different minerals, i.e., $FePO_4$ vs. $AlPO_4$ vs. Ca_3PO_4, which are relatively simple to discriminate among and are not representative of minerals found in calcareous soils. This chapter tests the capabilities of Linear Combination Fitting in mixtures of calcium and magnesium phosphates (and Mg-bearing brushite) which are not only spectrally similar (and thereby challenging) but also are more relevant for calcareous soils.

The contents of this chapter are under preparation for submission as "Assessment of Linear Combination Fitting of Calcium and Magnesium Phosphates, David M. Hilger, Jordan G. Hamilton, Derek Peak."

4.2 Abstract

The semi-quantitative speciation of P using P K-edge XANES is a powerful technique that is effective at revealing environmental concentrations in complex soil matrixes. The focus of evaluating the analytical robustness of this technique has been in

systems comprised of components with very different spectral features, particularly Al and Fe phosphates. There has been little to no examination of how capable Linear Combination Fitting (LCF) is for P components in calcareous soil, specifically Ca and Mg phosphates. Eight mixtures composed of calcium and magnesium phosphates were created and measured with P K-edge X-Ray Absorption Structure (XANES) spectroscopy at the SXRMB at the Canadian Light Source, Saskatoon, Saskatchewan. Six mixtures were composed of a calcium phosphate and a magnesium phosphate; the remaining two were of three components. It was found that binary Ca/Mg phosphate mixtures were fit with an average deviation of 3.2%, with a maximum of 12.5%. A ternary mixture composed of spectrally and structurally similar minerals deviated a maximum of 24% from the actual composition. Statistical measures reduced X^2 and R-factor, were not found to correspond to how semi-quantitatively accurate LC fits were relative to other spectra/LC fits. However, statistical tests were found to be useful in the process of improving an individual fit.

4.3 Introduction

Phosphorus is an essential element in biological systems for energy transfer (via ATP), information transcription (RNA/DNA), cell membranes (phospholipids), and bones (as calcium phosphates). Phosphorus chemistry in soils and sediments is limiting for biological growth in most of the Earth's ecosystems. Phosphorus availability has tremendous implications for both modern agricultural practices and environmental quality. If P is over-applied, it may be transported into waterways and cause algal blooms and eutrophication, but if it is under-applied then dramatically lower crop yields (or even crop failure) can result. Furthermore, the total amount of P in terrestrial systems often correlates weakly or not at all to biological availability. Instead, the chemical speciation (or precise

chemical form) is more useful in predicting availability, mobility, and reactivity of phosphate. Accordingly, determining the chemical speciation using spectroscopic tools is of utmost interest to researchers in agricultural, biological, and environmental systems.

Semi-quantitative speciation with X-ray Absorption Near Edge Structure (XANES) spectroscopy in environmental samples is a well-established technique, dating over 20 years (Fendorf et al., 1994, Hesterberg, 1999) for hard X-ray samples. Similarly, P K-edge XANES spectroscopy has been extensively applied in qualitative "fingerprint" speciation since the early 2000s. As a fingerprinting tool, P XANES has been able to identify inorganic P species in manures, soils, and ocean sediments (Khare et al., 2005, Toor et al., 2005, Ingall et al., 2011, Peak et al., 2012) to a degree not capable with operationally defined wet chemical extraction techniques or other spectroscopic techniques such as NMR due to matrix issues and detection limits. The number of synchrotron facilities, quality of beamlines, improvements in detector technology, and quality of X-ray absorption spectroscopy (XAS) software have all significantly improved to the point that the data quality and ease of analysis now facilitates semi-quantitative speciation using Linear Combination Fitting (LCF) at the P K-edge. The ability to determine the exact (or even approximate) proportions of the P species constituting an environmental sample has obvious advantages over a rough qualitative estimate via fingerprinting: for example, the potential to quantify changes in speciation of minor phases which are more reactive than more abundant but relatively inert phases. However, there are inherent challenges in LCF of P K-edges XANES that arise due to a relative lack of spectral features for many phosphate minerals. Unlike sulfur, there is not a diagnostic absorption edge shift among P minerals as they all occur in in the same +5 oxidation state as orthophosphate. In addition

to lack of characteristic edge shifts due to oxidation state, phosphate species variations are further depressed by the fact that there are always four oxygen molecules of the tetrahedral orthophosphate as nearest atomic neighbors that spectrally "buffer" structural resonance compared to some elements (such as transition metals) which may be in a direct bonding environment with as many as 8 different atoms that produce far more unique XANES spectral signatures.

To date, there are only two studies that have critically assessed the technique of Linear Combination Fitting of P K-edge XANES: the works of Werner and Preitzel (2015) and Abjiboye and coworkers (2007). Both studies found the range of error within P K-edge XANES LCF can be potentially significant. Ajiboye and coauthors found errors ranging from 0.8% to 41% in binary constructed mixtures composed of two of the three of the following minerals in various proportions: variscite (aluminum phosphate), hydroxyapatite (calcium phosphate), and phosphosiderite (iron phosphate). Werner and Preitzel found much lower errors in LCF by devising an automated normalization protocol. Ternary mixtures of three of the four of the following, variscite, hydroxyapatite, and phosphosiderite, and phytic acid (organic phosphate) deviated a maximum of 12% with an average of 5.5% in the entire set. These two studies identified three main issues that need to be taken under concern when linear combination fitting P K-edge XANES to prevent poor fits:

(i) *Overfitting:* The use of too many phases is known as overfitting. If unchecked, the "best" fit as determined by the program will often be composed of many phases with low contributions. LCF programs draw on small contributions from relatively featureless spectra to decrease the residual. Practically, the number of phases should

be limited to 3 to 4 (maximum) and examined for whether the proportion and identity of the phases are logical for the sample (Werner and Prietzel 2015).

(ii) *Minor phase components:* Minor phase components are troublesome as they may be under-represented in the fit (underfit). Defining spectral features of minor phase(s) are masked or overlapped by larger components, which then omits them from the fit. Errors due to this phenomenon can be as great as 40% (Abjiboye et al., 2007).

(iii) *Reliance on fitting statistics:* Fitting statistics are largely irrelevant when comparing between samples and quality of fit that requires visual assessment. Statistical measures such as X^2 and R-factor are useful to a degree in the iterative process of refining an individual fit. But as Werner and Prietzel (2015) found, improved R factor does not correlate to an improved fit as it is overtly influenced by regions that are of less importance in semi-quantitative accuracy such as absorption edge area and intensity. For this reason, the values of these statistics are largely meaningless when comparing unique spectra.

Although the above findings are useful in guiding LCF analysis, they focused on standards with very different features. In environmental systems, the major challenge of applying LCF to P XANES is that there may be similar fits arising from either a model including (a) crystalline apatite phase plus adsorbed phosphate and (b) a single poorly crystalline calcium phosphate such as dicalcium phosphate. There has not been a systematic study as to whether different (but similar) phosphate mineral phases can be readily distinguished using LCF, which leads to uncertainties in interpretations of P XANES in soil samples. Therefore, the objective of this study was to conduct LCF analysis on a suite of constructed mixtures of Ca and Mg phosphate minerals with only subtle

differences in their XANES spectra. This study will establish the limits to applying LCF analysis to phosphate minerals in the environment.

4.4 Materials and Methods

4.4.1 Constructed mixtures

Eight constructed mixtures were created to test the capabilities of linear combination fitting of P K-edge XANES for magnesium and calcium phosphates. Calcium and magnesium phosphate mixtures are the focus of this study opposed to Iron/Aluminum/Calcium phosphates (in Ajiboye et al. 2007 and Werner and Prietzel, 2015), as this study was done in conjunction with Hilger et al., 2017, Siciliano et al., 2016, Hamilton et. al., 2017 (a,b) where these minerals were either purchased or synthesized to investigate Ca/Mg/PO_4 solid solutions or were subsequently used as reference phases in a soil petroleum hydrocarbon remediation study. Binary mixtures of hydroxyapatite (Ca)-bobierrite (Mg) and brushite (Ca)-newberyite (Mg) were produced, as these combinations of minerals are known to form at similar pH ranges. Ternary mixtures of brushite-struvite-newberyite (DCPD/STVE/NBTE) and brushite-Mg-bearing brushite-newberyite (DCPD/50-50 DCPD/NBTE) were created to reflect the complexity of soil environments which can contain multiple inorganic P minerals. The constructed mixtures were created in proportions of (as wt% that was later adjusted to wt% P) 75/25, 50/50, and 25/75 for binary mixtures and 33/33/33 for ternary mixtures. Minerals were commercially purchased (Sigma-Aldrich, Fischer Scientific) except for Mg-bearing brushite which was synthesized as per Lee and Kumta (2010) and diluted to 2% P with boron nitride (BN) to minimize self-absorption effects.

4.4.2 P K-edge XANES data collection

Prior to XANES analysis, minerals were all diluted with BN to obtain a P concentration of 2% by wt% to limit self-absorption or at least minimize variability in saturation effects. Powders were ground with an agate mortar and pestle, thinly spread on double-sided carbon tape, and mounted on a copper plate. Phosphorus K-edge XANES were collected at 06B1-1, Soft X-Ray Microcharacterization Beamline (SXRMB) at the Canadian Light Source (CLS). The CLS storage ring operates at an energy of 2.96 GeV and a stored current between 250-150 mA. Beam size for all samples was 3 mm width by 1 mm height; spectra were collected using an InSb (111) monochromator and a four-element Si-drift fluorescence detector (Bruker). The minerals were analyzed from 2110 eV to 2220 eV with the highest sampling density occurring in the P K-edge XANES region: 2110 to 2143.0 eV was collected with a 2.0 eV step size, 2143.0 to 2180.0 eV was collected with a 0.15 eV step size (reported beamline resolution), and 2180.0 to 2220 eV was collected with a 1.0 eV step size. A check of beamline resolution and stability was performed after every storage ring injection by measuring a boron nitride (BN) diluted $ZnPO_4$ standard. Two spectra were collected for each mineral sample in partial fluorescence mode, which was then averaged.

4.4.3 Linear Combination Fitting methodology

Data processing and Linear Combination Fitting was performed with ATHENA, part of the DEMETER software package (Ravel and Newville, 2005). The DEMETER/ATHENA package is open-source software that is commonly used in XAS deconvolution and processing. Samples were loaded in a normal (μ) scale and normalized to an edge step of one. Normalization range was not fixed and was manually adjusted for

each spectrum. The aim of normalization was to achieve a consistent background by having a parallel relationship between the pre-edge and post-edge normalization ranges. The pre-edge range was approximately 2120-2140 eV, and the post-edge normalization range was approximately 2175-2215 eV. All spectra were subjected to a three-point smooth in two iterations, mostly to improve aesthetics. Linear Combination Fitting was performed with the following parameters: The fit range was -20 to 30 eV in relation to E_0 as this range encompasses the diagnostic region of the spectra. Constructed mixtures were fitted in normal μ space. Finally, weights of the fit were not forced to equal one. Instead values are manually adjusted to equal one after fitting was completed. This was to resolve a software issue: when values are forced to sum to one, the XANES region 2153-2180 eV is poorly fit which produced poor fitting statistics (reduced X^2 and R-factors) compared to applying the correction after fitting.

4.5 Results and Discussion

Upon close inspection, the newberyite (NBTE) and brushite (DCPD) constructed mixture series has a visible transition in features based on the proportion of the components (Figure 4.1 A). All three mixture spectra visually appear to be a muted brushite spectra composed of a decreased post-edge shoulder and a 2160-2162 eV and 2170 eV oscillation; increasing proportion of newberyite in the constructed mixture dampens these features to a larger degree. The lack of structural features in the newberyite spectrum results in visual identification/LCF prediction between constructed mixtures of similar proportions difficult. This is an issue because speciation results rely *a priori* on LCF outputs for samples that have mineral components that have low structure spectra.

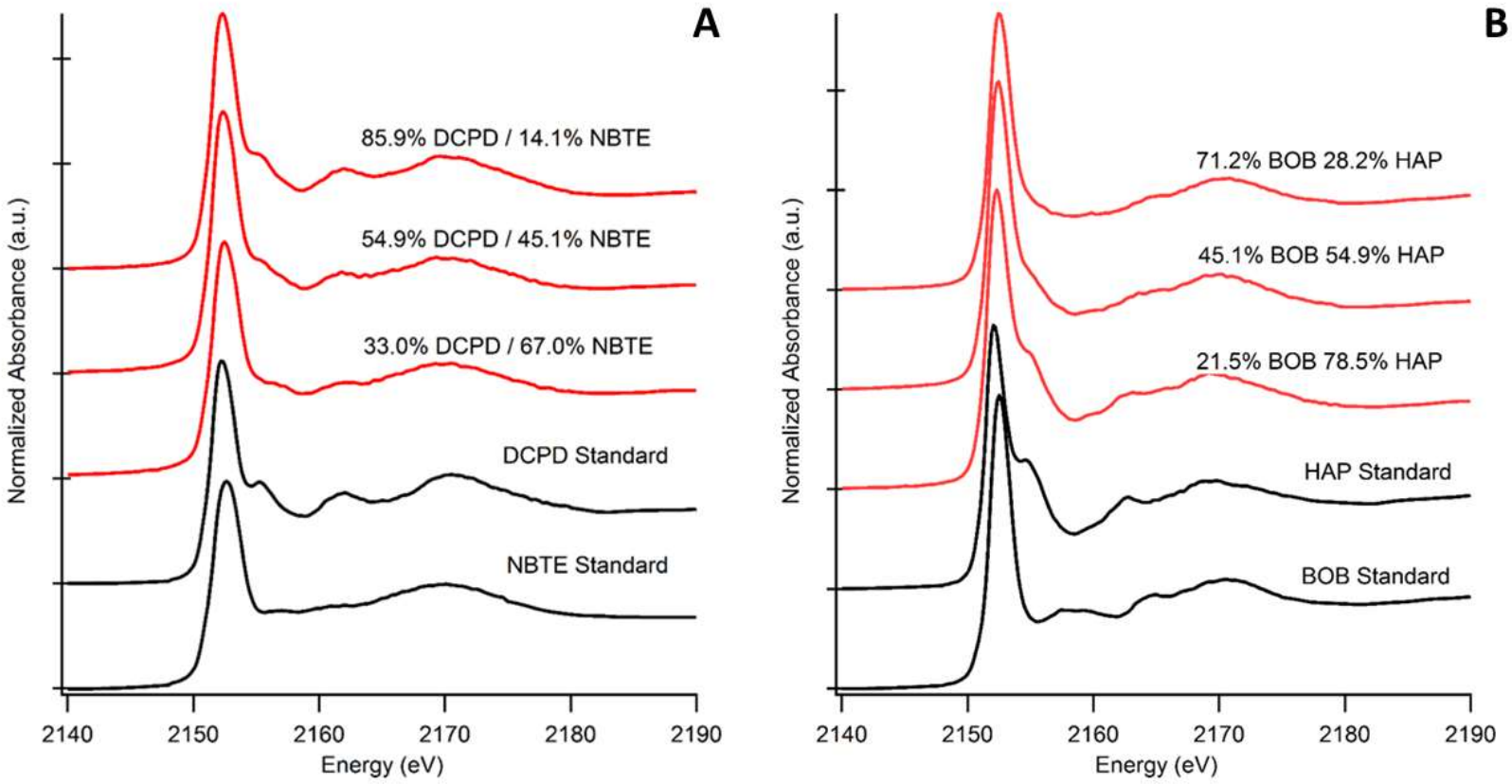

Figure 4.1: Binary Constructed Mixtures: (A) of brushite and newberyite with standards of the same; (B) of hydroxyapatite and bobierrite with standards of the same. Mineral abbreviations are as follows: DCPD = brushite, NBTE = newberyite, BOB = bobierrite, HAP = hydroxyapatite.

Visually, the bobierrite (BOB) and hydroxyapatite (HAP) series is consistent with a blending of features with intensity based on the proportion (Figure 4.1 B). The 78.5% HAP / 21.5% BOB appears as a "muted" hydroxyapatite spectra with a slight white line shift to higher energy: there is a post-edge shoulder and a 2162 eV feature, but they are less defined as they are absent in BOB. The "trough" and "dip" of HAP, located at 2159-2160 and 2165-2166 eV respectively, are partially filled by positive intensity features present in BOB at these energies. The 28.2% HAP and 71.2% BOB spectra is similar to the pure bobierrite spectra except for the feature located at 2159-2160 eV that is not observed in the mixed spectrum. There is no post-edge shoulder, the white line energy and the first oscillation located after the absorption edge are both also shifted upwards energy positions that are more consistent with bobierrite than with HAP.

The brushite/newberyite LCFs did not produce ideal reproductions of the constructed mixture spectra but are nearly perfect proportionally. The LCF has an issue in fitting the high energy tail and the 2170 eV oscillation in all three constructed mixtures as well as the intensity of the absorption edge in CM1 and CM2. This is apparent in the fit itself and the residual (Figures 4.2). The inability to fill the absorption edge intensity leads to much poorer statistical measures of these two fits relative to CM3. The statistical fits are accurate measures of how closely the fit visually reproduces the data. The binary series of NBTE and DCPD has a maximum error of 3.1% and an average error of 2.4% (Table 4.1), which is much lower than the only comparable study by Ajiboye et al., 2007. The accuracy of these fits is well beyond what is needed for inferences in natural samples, meaning in samples that are primarily composed of these two minerals, spectroscopists can report their findings with confidence if they have quality data.

Table 4.1: Accuracy and statistical parameters of Linear Combination Fitting for binary constructed mixtures.

	Mixture Composition†				Fit Percentages ‡				Statistical Measures		
	HAP§	BOB¶	DCPD#	NBTE††	HAP	BOB	DCPD	NBTE	Deviation	Reduced X^2	R-Factor
CM 1	0	0	40.3	59.7	0	0	37.2	62.8	3.1	0.0059	0.016
CM 2	0	0	67.0	33.0	0	0	68.8	31.2	1.8	0.0044	0.015
CM 3	0	0	85.9	14.1	0	0	83.7	16.3	2.2	0.0015	0.0057
CM 4	28.8	71.2	0	0	38.0	62.0	0	0	9.2	0.00032	0.00056
CM 5	54.9	45.1	0	0	56.5	43.5	0	0	1.6	0.00047	0.00096
CM 6	78.5	21.5	0	0	79.6	20.4	0	0	1.1	0.0011	0.0018

† Composition of the constructed mixture expressed as a percentage of P in the mixture. Samples are 25/75 (CM 1), 50/50 (CM 2), and 75/25 (CM 3) brushite/newberyite, and 25/75 (CM 4), 50/50 (CM 5), and 75/25 (CM 6) hydroxyapatite/bobierrite as a percentage of weight.
‡ The contribution of each component as determined by LCF adjusted to be reported as a percentage of the P total
§ HAP = hydroxyapatite
¶ BOB = bobierrite
 # DCPD = brushite
†† NBTE = newberyite

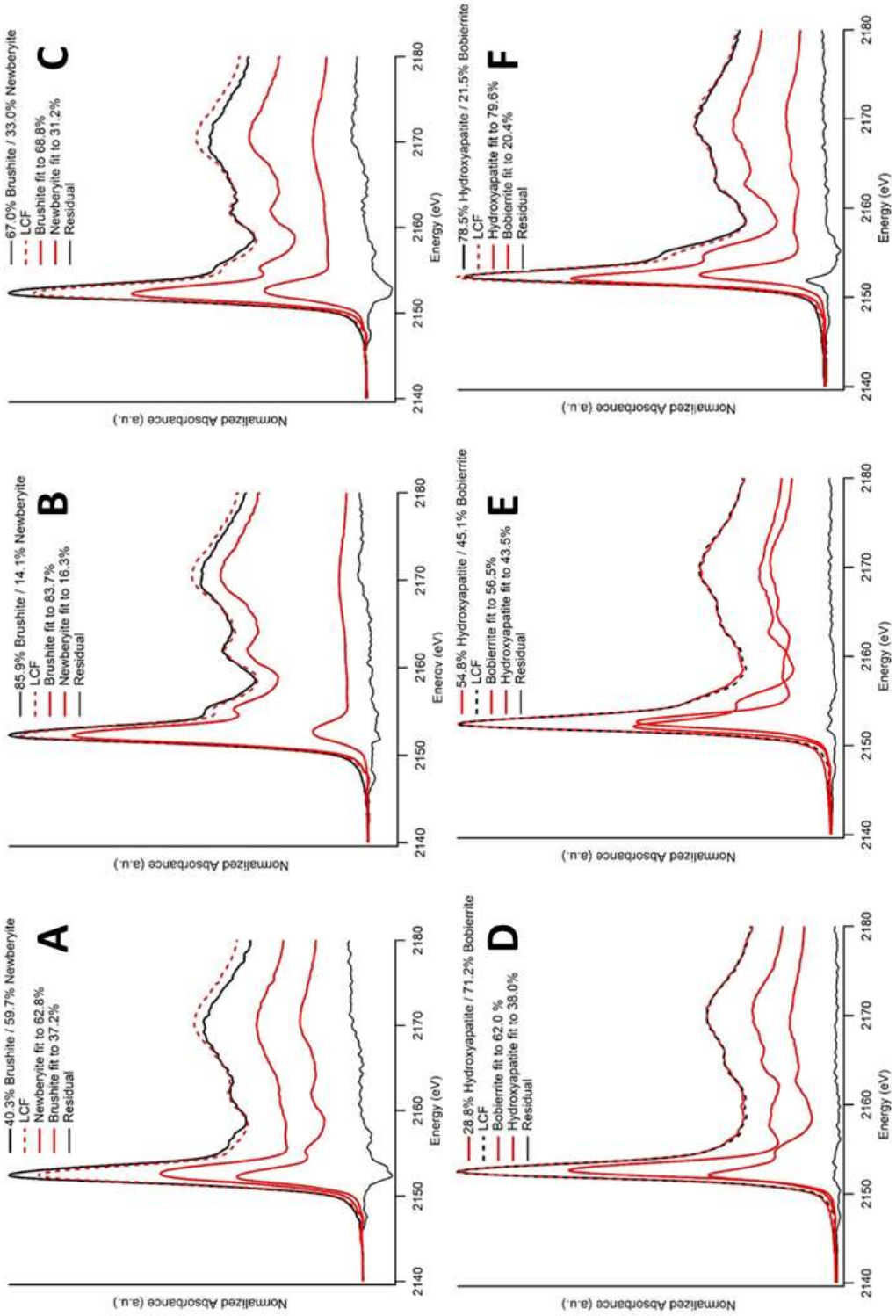

Figure 4.2: Binary constructed mixtures and Linear Combination Fits: (A) CM 1, equal percent weight brushite: newberyite; (B) CM 2, low brushite: high newberyite; (C) CM 3, high brushite: low newberyite (D) CM 4, low hydroxyapatite: high bobierrite; (E) CM 5, equal percent weight hydroxyapatite: bobierrite; (F) CM 6, high hydroxyapatite: low bobierrite.

Constructed mixtures CM4, CM5, and CM6, composed of hydroxyapatite and bobierrite produced LCF fits very close to the actual proportions of the mixtures. (Table 4.1) Statistical measures of reduced X^2 and R-factor would indicate that CM4 is the most accurate fit, but based on actual composition CM4 is overfitted with respect to HAP by 9.2%, whereas CM5 and CM6 are fit to within 1.6% of the actual composition.. The LCF of the constructed mixtures is very close to reproducing the spectra for all three constructed mixtures, CM4/CM5/CM6 based on both statistical parameters and visual comparison (Figure 4.2). The intensity of the absorption edge is fit almost perfectly, an issue in CM1 and 2 for NBTE/DCPD, which results in better statistical metrics for the HAP-bearing mixtures. More importantly, the fits very closely match the post-edge structure, with essentially no structure in the residual present for all the unique features of the spectra. The quality of the fits can be attributed to the distinctiveness of the spectra for the individual components, as the P K-edge XANES spectra of hydroxyapatite and bobierrite have sharp spectral features such as the HAP post edge shoulder at 2154 eV and BOB distinctive spectral feature at 2160 eV. Additionally, shared features such as the post-edge double oscillations (~2162-2170 eV) and the P-IV K-edge are significantly shifted relative to one another to provide measures to which reach a semi-quantitatively accurate fit.

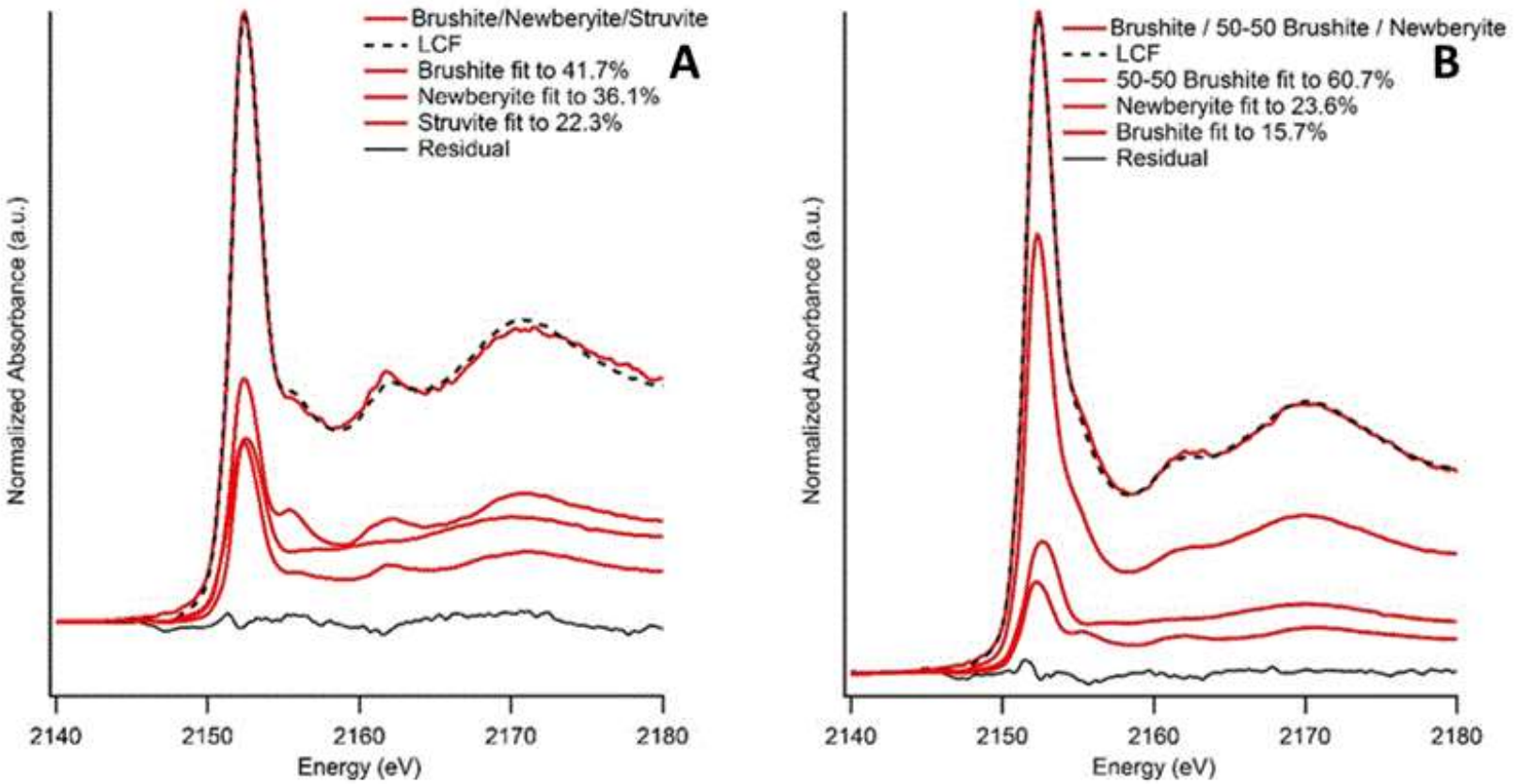

Figure 4.3: Constructed mixtures of three components of equal wt%: (A) CM 7, brushite, struvite, newberyite; (B) CM 8, brushite, 50-50 brushite, newberyite.

The LCF of CM7 is acceptable for both its proportional accuracy and in simulating the original spectra (Figure 4.3 A). The component weightings vary from the actual composition by a maximum of 12.5% and a minimum of 3.3% (Table 4.2) which is comparable to Werner and Prietzel (2015), in which there was an extensive normalization procedure to minimize error. This margin of error is likely to be acceptable for most P soil studies. These three minerals have enough differences within their structure to provide quality fits using LCF. There is no issue in the absorption edge intensity, but the fit has a degree of difficulty in matching the magnitude of the 2162 eV and 2170 eV spectral features. As a result, CM7 is statistically a much poorer fit than the other ternary constructed mixture, CM8, which is drastically off on its component weights compared to the actual values.

Table 4.2: Accuracy and statistical parameters of Linear Combination Fitting for Ternary constructed mixtures.

	Mixture Composition†				Fit Percentages ‡				Statistical Measures		
	DCPD§	STVE¶	NBTE#	50-50 DCPD††	DCPD	STVE	NBTE	50-50 DCPD	Deviation	Reduced X^2	R-Factor
CM 7	54.2	19.0	26.8	0	41.7	22.3	36.1	0	-12.5/+9.3/+3.3 ‡‡	0.0059	0.016
CM 8	39.7	0	19.6	40.7	15.7	0	23.6	60.7	-24.0/+4.0/+20.0 §§	0.0044	0.015

† Composition of the constructed mixture expressed as a percentage of P in the mixture. CM7 is 33/33/33 (brushite/struvite/newberyite), and CM8 is 33/33/33 (brushite/50-50 brushite/newberyite) as a percentage of weight.
‡ The contribution of each component as determined by LCF adjusted to be reported as a percentage of the P total
§ DCPD = brushite
¶ STVE = struvite
 # NBTE = newberyite
†† 50-50 DCPD = Mg-bearing brushite
‡‡ LC fit deviation from actual mixture composition as a percentage of P, in the order of (DCPD/STVE/NBTE)
§§ LC fit deviation from actual mixture composition as a percentage of P, in the order of (DCPD/NBTE/50-50 DCPD)

The semi-quantitative fit of CM8 is weak (Figure 4.3 B), due to the 50-50 brushite (a 1:1 Ca/Mg brushite phase) component being overfit by 24.0%; pure (Ca-only) brushite is underfit by 20.0%. However, the visual quality of the fit appears to be nearly perfect with much of the residual arising from data noise. Most error in the LCF stems from the similarity between the spectrum of the constructed mixture and the spectrum of the Mg-bearing brushite. There are only slight differences with the post-edge shoulder, and 2160 eV features being of slightly greater intensity than Mg-bearing brushite. (Table 4.1) The values of Reduced X^2 and R-factor are comparable to the well fit CM1 and CM2 mixtures despite CM8 being very far off actual proportions.

4.6 Conclusions

This constructed mixture study has aided in identifying the limitations of LCF analysis for mixed calcium and magnesium phosphate systems. Phosphorus K-edge XANES LCF for binary mixtures was excellent, with mixtures fit to a minimum of 1.1% and a maximum of 9.2% error. The choice of compounds in the ternary mixture was intended to challenge the technique, and as a result was not quite as robust as the binary mixtures. The brushite-struvite-newberyite constructed mixture (CM7) has an acceptable level of error (12%), but the brushite – Mg-bearing brushite – newberyite (CM8) system was out as much as 24%. The magnitude of this error is not altogether surprising considering the Mg substituted, and pure brushite have very similar crystal lattices, and there is little XANES structure in the newberyite component. It is difficult to construct a more challenging ternary mixture of phosphate minerals to test the technique. Nonetheless, this margin of error warrants further study in the ability of LCF to discriminate when Mg-bearing brushite is present, as this model may produce non-unique solutions. Rather than

the margin of error of 10% (Ajiboye et al., 2007, Werner and Prietzel, 2015) for LCF analysis of P XANES, an error margin of 20% is perhaps a more accurate in environmental systems composed of low structural feature P species such as absorbed PO_4, newberyite, or Mg-bearing brushite.

5. CONCLUSIONS, IMPLICATIONS, AND FUTURE RESEARCH

5.1 Summary of findings

The first hypothesis proposed "changes in calcium phosphate crystal structure upon magnesium substitution will result in identifiable changes to P K-edge XANES spectra". By systematically measuring how Mg affects the precipitation of calcium phosphates as a function of pH and Mg concentration, the hypothesis was validated at both neutral and basic pH; mixed cation solutions adversely affect the crystallinity of calcium phosphate minerals. The effect of Mg on acidic/neutral calcium phosphate minerals is less pronounced than minerals formed in basic solutions. Brushite incorporated up to 20% Mg without any change to the crystal structure or the local bonding environment. Equimolar solutions composed of 25% to 75% Mg formed a slightly altered brushite, designated as Mg-bearing brushite. X-ray diffraction characterized these minerals as brushite with a small amorphous component while XANES spectra appear as brushite with dampened features, i.e., post edge shoulder and oxygen oscillations. In contrast to brushite, hydroxyapatite formation was heavily inhibited when only 10% of the reactant solution was composed of Mg. Elemental analysis indicated very little Mg was incorporated into hydroxyapatite. The mineral was no longer identifiable via XRD, appearing entirely amorphous. The local bonding environment did not appear altered as evidenced by ATR-FTIR and XANES spectroscopy, but TEM showed decreased particle size. From this data, it was concluded that ACP is spectroscopically analogous to nano-sized/short-range order hydroxyapatite.

With the goal of testing the second hypothesis, the capabilities of Linear Combination Fitting for semi-quantitative analysis of calcium and magnesium phosphate mixtures was assessed. The study found the technique works exceptionally well for systems composed of two Ca/Mg P phases but can be inaccurate in discerning ternary mixtures composed of phases that are structurally similar. In binary systems, the average level of accuracy is 3.2% (from six mixtures), with the least accurate having a deviation of 9%. These values are comparable to those found in previous studies composed of Al/Fe/Ca phosphates. The sample size in this study consisting of ternary systems was considerably smaller, being composed of only two mixtures. One mixture, composed of struvite, newberyite, and brushite, was comparable to the binary mixtures with a maximum deviation of 12.5%. The other ternary mixture composed of Mg-bearing brushite, brushite, and newberyite was considerably worse, with a maximum deviation of 24% from the actual composition. The entirety of this error derives from the overfitting of Mg-bearing brushite at the expense of brushite. The source of this error is clear as the spectral similarities between the mixture (CM8) and the Mg-bearing brushite "standard" are striking. The results of this study indicate that the confidence level of LCF in binary systems and ternary systems composed of "spectrally distinctive" minerals, is in the region of 10%. In low structure systems, the tentative limits of calcium-magnesium phosphate LCF analysis is 25%. A tertiary goal of the study was to examine the use of statistical measures in LCF analysis. It was found that statistical measures such as reduced X^2 and R-factor were not great indicators of how well the constructed mixtures were fit proportionally. Instead, statistical values were only useful in the fitting process to improve the quality of fit within the individually constructed mixtures.

5.2 Research implications and recommendations

Overall, the result of this study is an improved understanding of calcium-magnesium phosphates and a stronger confidence in being able to identify them within soil systems. The study has shown that there are "intermediate" minerals formed where there are Mg - Ca mixed solutions, namely Mg-bearing brushite formed in acidic solutions and an amorphous calcium phosphate / short-range order hydroxyapatite in basic solutions. This has important implications in speciation of P in calcareous soil systems, which are also mixed cation systems.

Characterizing Mg-bearing brushite as a specific phase identifiable by P XANES has two broad implications. 1) Where brushite has been identified in calcareous soils, there is a strong possibility that the mineral is instead Mg-bearing brushite, which is not only more soluble but also prohibits the formation of HAP. 2) In P XANES fitting, brushite has been under identified at the expense of some combination of apatite and adsorbed species which have different chemistries. Mg-bearing brushite is almost assuredly more soluble and thereby potentially more bioavailable than pure brushite (Wadu et al., 2012) as it is smaller particle size/larger surface area and the bonds are less ordered. If misidentified as "pure" brushite, the estimated bioavailability would be incorrect and may not react to amendments or manipulations as a predicted from solubility. Brushite has the potential to be under-fitted in XAS; if not provided a Mg-bearing brushite reference, LCF routines instead chose a mixture of a relatively featureless P XANES spectra such as adsorbed phosphate and a crystalline calcium phosphate. Adsorbed species may have an entirely different fate and availability within the soils and it is important to accurately estimate this relatively labile fraction and differentiate it from inorganic minerals. Additionally, Mg-

bearing brushite presence is significant as research has indicated that Mg-bearing brushite does not evolve to hydroxyapatite (Salimi et al., 1985). The Mg-bearing brushite phase is potentially quite significant and is now possible to identify within soil.

The prevalence of ACP formation in the laboratory means it is also likely very common in soils. As P K-edge XANES spectra of HAP is hard to distinguish from ACP due to a near identical short-range order, unless both were included in an LCF analysis process, a researcher would not realize there would be a possible misfit or missing phase. ACP is on the order of four times as soluble as HAP (Dorohzkin, 2011)

Consistent with the significance of Mg-bearing brushite in laboratory conditions, this phase has been used to successfully perform solid-state P speciation in two recent manuscripts (Siciliano et al., 2016, and Kar et al., 2017) and it is anticipated that that the XANES reference spectra available with this thesis will be useful for many other future studies. The struvite and brushite series were an important component in the study by Kar et al., 2017 "Direct chemical speciation of soil P in a Saskatchewan Chernozem after long and short-term manure amendments." Kar and co-authors examined the evolution of liquid hog manure (LHM) and solid cattle manure (SCM) in a cropped calcareous soil over six months, two years, and ten years. By using the study of struvite (Appendix A) and Mg-bearing brushite (Ch 3) formed in varying Ca/Mg ratios, the authors could significantly improve the speciation of P in their samples compared to previous models. Kar and coauthors found that P within LHM, composed initially of struvite and organic phosphate, quickly solubilizes and persists as adsorbed phosphate and Mg-bearing. Solid cattle manure, initially composed primarily of organic phosphate and brushite, evolves to consist of Mg-bearing with a small component of apatite. As both systems contain a significant

proportion of organic acids, which are known to inhibit P mineral precipitation and crystallization (Grossl and Innskeep, 1991), an argument can be made that the difference between these two evolutions is at least in part due to Mg content in LHM.

The research in this study has also been used in the manuscript by Siciliano et al., (2016) titled "Total Phosphate Influences the Rate of Hydrocarbon Degradation but Phosphate Mineralogy Shapes Microbial Community Composition in Cold-Region Calcareous Soils." As the title would indicate, this study was an examination of the effect on microbial populations and biodegradation of hydrocarbons from P amendments. The library generated in this thesis was instrumental in LCF analysis of P K-edge XANES in this calcareous subsurface system that was amended with $MgSO_4$ and H_2PO_4. Major components of newberyite and Mg-bearing were found after 3 months of amendment in the field. This is significant as the former mineral is often overlooked, and the latter having never been measured with XAS before this thesis. The authors could determine that there was a relationship between microbial composition and P speciation, i.e., different microbe communities were more abundant if the system was dominated by adsorbed phosphate or Mg-bearing brushite. Degradation rates were determined to be entirely controlled by total P with no link to speciation.

5.3 Future research considerations

It is the recommendation of this thesis that any research utilizing P K-edge XANES in an environmental study needs to consider the implications of mixed cation systems. If it is possible, the best option is to build a robust library of the specific system if it has not been previously studied or the spectra are not available. Without mixed cation reference spectra, LCF software may draw upon a new, incorrect component such as phytic acid or

absorbed P in an attempt to account for the difference between the pure phase and the mixed phase. Beamtime at a tender X-ray beamline is very valuable, but this recommendation can be accomplished with 4-6 samples carefully selected based upon mineralogy.

There are several interesting research projects that could stem from this study. First, a complete study of the relative solubilities of mixed cation phases is needed. Semi-quantitative values derived from a technique such as thermogravimetric analysis is useful for researchers seeking to estimate solubilities, for example. Next, octacalcium phosphate (OCP) is a mineral that should be studied and was conspicuously absent from this study. There were multiple efforts to synthesize this mineral based on several different references, but the product formed was always either brushite or hydroxyapatite. Finally, research could examine the findings of this study within a soil matrix by spiking a very well characterized "known soil" with solutions of PO_4 and varying Ca:Mg ratios. This would be a useful exercise to determine what minerals are produced at varying reaction conditions and reaction times and to test further the capabilities of the P XANES spectroscopic technique.

6. REFERENCES

Abbona, F. & Baronnet, A., 1996. A XRD and TEM study on the transformation of amorphous calcium phosphate in the presence of magnesium. Journal of Crystal Growth, 165, pp.98–105.

Ajiboye, B., O. O. Akinremi, and A. Jürgensen. 2007. Experimental Validation of Quantitative XANES Analysis for Phosphorus Speciation Soil Sci. Soc. Am. J. 71:1288-1291.

Alvarez, R., Evans, L.A., Milham, P.J. and Wilson, M.A., 2004. Effects of humic material on the precipitation of calcium phosphate. Geoderma, 118(3), pp.245-260.

Arai, Y. and Sparks, D.L., 2001. ATR–FTIR spectroscopic investigation on phosphate adsorption mechanisms at the ferrihydrite–water interface. Journal of Colloid and Interface Science, 241(2), pp.317-326.

Aramendia, M.A., V. Borau, C. Jimenez, J.M. Marinas, and F.J. Romero. 1999. Synthesis and Characterization of Magnesium Phosphates and Their Catalytic Properties in the Conversion of 2-Hexanol. Journal of Colloid and Interface Science 217: 288–298.

Arellano-Jiménez, M.J., R. García-García, and J. Reyes-Gasga. 2009. Synthesis and Hydrolysis of Octacalcium Phosphate and Its Characterization by Electron Microscopy and X-Ray Diffraction. Journal of Physics and Chemistry of Solids 70 (2) (February): 390–395.

Ball, MC, and MJ Casson. 1973. Dehydration of Calcium Hydrogen Phosphate Dihydrate. Journal of Chemical Society, Dalton Trans. (34): 34–37.

Beauchemin, S., D. Hesterberg, and M. Beauchemin. 2002. Principal component analysis approach for modeling sulfur K-XANES spectra of humic acids. Soil Sci. Soc. Am. J. 66:83–91.

Beauchemin, S., Hesterberg, D., Chou, J., Beauchemin, M., Simard, R.R. and Sayers, D.E., 2003. Speciation of phosphorus in phosphorus-enriched agricultural soils using X-ray absorption near-edge structure spectroscopy and chemical fractionation. Journal of Environmental Quality, 32(5), pp.1809-1819.

Ben-Nissan, B. ed., 2014. Advances in Calcium Phosphate Biomaterials.

Cao, X., W.G. Harris, M.S. Josan, and V.D. Nair. 2007. Inhibition of Calcium Phosphate Precipitation under Environmentally-Relevant Conditions. The Science of the Total Environment 383 (1-3): 205–15.

Cao, Xinde, and Willie Harris. 2008. Carbonate and Magnesium Interactive Effect on Calcium Phosphate Precipitation. Environmental Science and Technology 42 (2): 436–42.

Carpenter, S. R., and V. H. Smith N. F. Caraco, D. L. Correll, R. W. Howarth, A. N. Sharpley. 1998. Nonpoint Pollution of Surface Waters with Phosphorus and Nitrogen. Ecological Applications 8 (1998): 559–68.

Carter, C Barry, and David B Williams. 2016. Transmission Electron Microscopy Diffraction, Imaging, and Spectrometry. Springer.

Catalano, J.G., McKinley, J.P., Zachara, J.M., Heald, S.M., Smith, S.C. and Brown, G.E., 2006. Changes in uranium speciation through a depth sequence of contaminated Hanford sediments. Environmental science & technology, 40(8), pp.2517-2524.

Cooper, James, Rachel Lombardi, David Boardman, and Cynthia Carliell-Marquet. 2011. The Future Distribution and Production of Global Phosphate Rock Reserves. Resources, Conservation and Recycling 57 (January). Elsevier B.V.: 78–86.

Cordell, Dana, Jan Olof Drangert, and Stuart White. 2009. The Story of Phosphorus: Global Food Security and Food for Thought. Global Environmental Change 19 (2): 292–305.

Darr, J A, A A Chaudhry, J Goodall, M Vickers, J K Cockcroft, I Rehman, and J C Knowles. 2008. Synthesis and Characterisation of Magnesium Substituted Calcium Phosphate Bioceramic Nanoparticles Made via Continuous Hydrothermal Flow Synthesis. Journal of Materials Chemistry 18 (48): 5900–5908.

Degen, T., M. Sadki, E. Bron, U. König, and G. Nénert. 2014. The HighScore suite. Powder Diffraction 29 (S2): S13-S18.

Diallo-Garcia, Sarah, Danielle Laurencin, Jean Marc Krafft, Sandra Casale, Mark E. Smith, Hélène Lauron-Pernot, and Guylène Costentin. 2011. Influence of Magnesium Substitution on the Basic Properties of Hydroxyapatites. Journal of Physical Chemistry C 115 (49): 24317–27.

Dixon, J.B. 1982. Minerals in soil environments. Soil Science Society of America, Madison, Wisc.

Dorozhkin, S.V. 2011. Calcium orthophosphates: Occurrence, properties, biomineralization, pathological, calcification and biomimetic applications. Biomatter 1(2): 121-164.

Dorozhkin, S. V. 2012. Biphasic, triphasic and multiphasic calcium orthophosphates. Acta Biomaterialia, 8(3), 963–77.

Dosen, A., and R. F. Giese. 2011. Thermal Decomposition of Brushite, CaHPO4-2H2O to Monetite CaHPO4 and the Formation of an Amorphous Phase. American Mineralogist 96 (2-3) (February 11): 368–373.

Driessens, F.C.M. and Verbeeck, R.M.H. 1990. Biominerals. CRC Press, Boca Raton, Florida, USA

Elliot, J.C. 1994. Structure and Chemistry of the Apatites and Other Calcium Orthophosphates. (The London Hospital Medical College). Elsevier: Amsterdam.

Elser, James J., Matthew E S Bracken, Elsa E. Cleland, Daniel S. Gruner, W. Stanley Harpole, Helmut Hillebrand, Jacqueline T. Ngai, Eric W. Seabloom, Jonathan B. Shurin, and Jennifer E. Smith. 2007. Global Analysis of Nitrogen and Phosphorus Limitation of Primary Producers in Freshwater, Marine and Terrestrial Ecosystems. Ecology Letters 10 (12): 1135–42.

Elzinga, E.J. & Sparks, D.L. 2007. Phosphate adsorption onto hematite: An in situ ATR-FTIR investigation of the effects of pH and loading level on the mode of phosphate surface complexation. Journal of Colloid and Interface Science, 308(1), pp.53–70.

Farmer, V.C., 1974. Infrared spectra of minerals. Mineralogical society.

Fendorf, S.E., Sparks, D.L., Lamble, G.M. and Kelley, M.J., 1994. Applications of X-ray absorption fine structure spectroscopy to soils. Soil Science Society of America Journal, 58(6), pp.1583-1595.

Grossl, P.R. and Inskeep, W.P., 1991. Precipitation of dicalcium phosphate dihydrate in the presence of organic acids. Soil Science Society of America Journal, 55(3), pp.670-675.

Güngör, K., Jürgensen, A. and Karthikeyan, K.G., 2007. Determination of phosphorus speciation in dairy manure using XRD and XANES spectroscopy. Journal of environmental quality, 36(6), pp.1856-1863.

Hamilton, JG., Hilger, D., D. Peak. 2017. Mechanisms of tripolyphosphate adsorption and hydrolysis on goethite. Journal of Colloid and Interface Science. 491 (1): 190-198.

Hesterberg, D., Zhou, W., Hutchison, K.J., Beauchemin, S. and Sayers, D.E., 1999. XAFS study of adsorbed and mineral forms of phosphate. Journal of Synchrotron Radiation, 6(3), pp.636-638.

Hedley, M. J., J. W. B. Stewart, and B. S. Chauhan. 1982. Changes in Inorganic and Organic Soil Phosphorus Fractions Induced by Cultivation Practices and by Laboratory Incubations. Soil Science Society of America Journal. 46: 970-976.

Hong, K. S., Nam, K.T., Jang, H.L., Ryu, H.S., Jin, K.S., 2014. “Whitlockite and Method from Manufacturing the Same.” United States Application Publication, Application Number 13/645,508.

Ingall, E. D., Brandes, J. A., Diaz, J. M., de Jonge, M. D., Paterson, D., McNulty, I., Crawford Elliot, W., Northrup, P. 2011. Phosphorus K-edge XANES spectroscopy of mineral standards. Journal of Synchrotron Radiation, 18(Pt 2), 189–197.

Johnsson, M.S. & Nancollas, G.H., 1992. The Role of Brushite and Octacalcium Phosphate in Apatite Formation. Critical reviews in oral biology and medicine, 3(1–2), pp.61–82.

Kar, G. Hundal, L.S., Schoenau, J.J., and Peak, D. 2011. Direct chemical speciation of P in sequential chemical extraction residues using P K-Edge X-Ray absorption near-edge structure spectroscopy. Soil Science, 176(11), p.589–595.

Kar, G., Peak, D. & Schoenau, J.J., 2012. Spatial Distribution and Chemical Speciation of Soil Phosphorus in a Band Application. Soil Science Society of America Journal, 76(6), p.2297.

Kar, G., Schoenau, J., Hilger, D. and Peak, D. 2017. Direct chemical speciation of soil phosphorus in a Saskatchewan Chernozem after long and short-term manure amendments. Canadian Journal of Soil Science.

Khare, Nidhi, Dean Hesterberg, and James D. Martin., 2005. XANES Investigation of Phosphate Sorption in Single and Binary Systems of Iron and Aluminum Oxide Minerals. Environmental Science and Technology 39 (7): 2152–60.

Khasawneh, F.E., Sample, E.C. and Kamprath, E.J. 1980. The role of phosphorus in agriculture. American Society of Agronomy, Crop Science Society of America, Soil Science Society of America.

Kizewski, Fiona, Yu-Ting Liu, Amanda Morris, and Dean Hesterberg. 2011. Spectroscopic Approaches for Phosphorus Speciation in Soils and Other Environmental Systems. Journal of Environmental Quality 40 (3): 751.

Kolmas, J., A. Jaklewicz, A. Zima, M. Bućko, Z. Paszkiewicz, J. Lis, A. Ślósarczyk, and W. Kolodziejski. 2011. Incorporation of Carbonate and Magnesium Ions into Synthetic Hydroxyapatite: The Effect on Physicochemical Properties. Journal of Molecular Structure 987 (1-3): 40–50.

Kumaragamage, D., O.O. Akinremi, D. Flaten, and J. Heard. 2007. Agronomic and Environmental Soil Test Phosphorus in Manured and Non-Manured Manitoba Soils. Canadian Journal of Soil Science 87 (1): 73–83.

Kurtulus, G., and a.C. Tas. 2011. Transformations of Neat and Heated Struvite (MgNH4PO4·6H2O). Materials Letters 65 (19-20): 2883–2886.

Larson, A.C. and R.B. Von Dreele, 2000. General Structure Analysis System (GSAS), Los Alamos National Laboratory Report LAUR 86-748.

Laurencin, D., N. Almora-Barrios, N.H. de Leeuw, C. Gervais, C. Bonhomme, F. Mauri, W. Chrzanowski. 2011. Magnesium Incorporation into Hydroxyapatite. Biomaterials 32 (7): 1826–1837.

Lee, Donghyun, and Prashant N. Kumta. 2010. Chemical Synthesis and Characterization of Magnesium Substituted Amorphous Calcium Phosphate (MG-ACP). Materials Science and Engineering C 30 (8). Elsevier B.V.: 1313–17.

Lee, D., and P.N. Kumta. 2010. Chemical Synthesis and Stabilization of Magnesium Substituted Brushite. Materials Science and Engineering: C 30 (7): 934–943.

Ler, Adeline, and Robert Stanforth. 2003. Evidence for Surface Precipitation of Phosphate on Goethite. Environmental Science and Technology 37 (12): 2694–2700.

Lindsay, W.L., 1979. Chemical equilibria in soils. John Wiley and Sons Ltd.

Liu, J., Yang, J., Cade-Menun, B.J., Liang, X., Hu, Y., Liu, C.W., Zhao, Y., Li, L. and Shi, J. 2013. Complementary Phosphorus Speciation in Agricultural Soils by Sequential Fractionation, Solution P Nuclear Magnetic Resonance, and Phosphorus K-edge X-ray Absorption Near-Edge Structure Spectroscopy. Journal of environmental quality, 42(6), pp.1763-1770.

Lu, X. & Leng, Y., 2004. TEM study of calcium phosphate precipitation on bioactive titanium surfaces. Biomaterials, 25(10), pp.1779–1786.

Makris, Konstantinos C., Willie G. Harris, George A. O'Connor, and Hassan El-Shall. 2005. Long-Term Phosphorus Effects on Evolving Physicochemical Properties of Iron and Aluminum Hydroxides. Journal of Colloid and Interface Science 287 (2): 552–60.

Manceau, A., Lanson, B., Schlegel, M.L., Harge, J.C., Musso, M., Eybert-Berard, L., Hazemann, J.L., Chateigner, D. and Lamble, G.M. 2000. Quantitative Zn speciation in smelter-contaminated soils by EXAFS spectroscopy. American Journal of Science, 300(4), pp.289-343.

Manceau, A., Marcus, M.A. and Tamura, N. 2002. Quantitative speciation of heavy metals in soils and sediments by synchrotron X-ray techniques. Reviews in Mineralogy and Geochemistry, 49(1), pp.341-428.

Mills, S. A., and W. T. Frankenberger. 1994. Evaluation of Phosphorus Sources Promoting Bioremediation of Diesel Fuel in Soil. Bulletin of Environmental Contamination and Toxicology 53 (2): 280–84.

Peak, D., G. Kar, L. Hundal, and J. Schoenau. 2012. Kinetics and Mechanisms of Phosphorus Release in a Soil Amended With Biosolids or Inorganic Fertilizer. Soil Science 177 (3):183–187.

Okude, N., Nagoshi, M., Noro, H., Baba, Y., Yamamoto, H., & Sasaki, T. 1999. P and S K-edge XANES of transition-metal phosphates and sulfates. Journal of Electron Spectroscopy and Related Phenomena, 101–103, 607–610.

Olsen, S.R., 1954. Estimation of available phosphorus in soils by extraction with sodium bicarbonate. United States Department Of Agriculture; Washington.

Ravel, B. and Newville, M.A. 2005. ATHENA, ARTEMIS, HEPHAESTUS: data analysis for X-ray absorption spectroscopy using IFEFFIT. Journal of synchrotron radiation, 12(4): 537-541.

Ressler, T., Wong, J., Roos, J. and Smith, I.L. 2000. Quantitative speciation of Mn-bearing particulates emitted from autos burning (methylcyclopentadienyl) manganese tricarbonyl-added gasolines using XANES spectroscopy. Environmental Science & Technology, 34(6), pp.950-958.

Riman, R. and C. Sever. 2012. Biomimetic hydroxyapatite synthesis US 8287914 B2.

Ryther, John H. 1971. Nitrogen, Phosphorus, and Eutrophication in the Coastal Marine Environment." Science 171: 1008–13.

Salimi, M.H., J.C. Heughebaert, G.H. Nancollas. 1985. Crystal Growth of Calcium Phosphates in the Presence of Magnesium Ions. Langmuir, 1(1): 119-122

Sato, Shinjiro, Dawit Solomon, Charles Hyland, Quirine M. Ketterings, and Johannes Lehmann. 2005. Phosphorus Speciation in Manure and Manure-Amended Soils Using XANES Spectroscopy. Environmental Science and Technology 39 (19): 7485–91.

Schindelin, J., C.T. Rueden, and M.C. Hiner. 2015. The ImageJ ecosystem: An open platform for biomedical image analysis. Molecular Reproduction and Development. PMID

Schofield, P. F.; Knight, K. S.; van der Houwen, J. A. M.; Valsami-Jones E. 2004. The role of hydrogen bonding in the thermal expansion and dehydration of brushite, di-calcium phosphate dihydrate Sample: T = 4.2 K. Physics and Chemistry of Minerals. 31: 606-624

Sherif, F.G. 1987. A process for the manufacture of highly pure trimagnesium phosphate octahydrate EP 0113153 B1

Siciliano, Steven D., Tingting Chen, Courtney Phillips, Jordan Hamilton, David Hilger, Blaine Chartrand, Jay Grosskleg, Kris Bradshaw, Trevor Carlson, and Derek Peak. 2016. "Total Phosphate Influences the Rate of Hydrocarbon Degradation but Phosphate Mineralogy Shapes Microbial Community Composition in Cold-Region Calcareous Soils." Environmental Science and Technology 50 (10): 5197–5206.

Stipniece, Liga, Kristine Salma-Ancane, Dmitrijs Jakovlevs, Natalija Borodajenko, and Liga Berzina-Cimdina. 2013. The Study of Magnesium Substitution Effect on Physicochemical Properties of Hydroxyapatite. Material Science and Applied Chemistry 28 (28): 51.

Tas, a. Cuneyt. 2009. Monetite ($CaHPO_4$) Synthesis in Ethanol at Room Temperature. Journal of the American Ceramic Society 92 (12) (December): 2907–2912

Tiessen, H. and Moir, J.O., 1993. Characterization of available P by sequential extraction. Soil sampling and methods of analysis, 7, pp.5-229.

Toby, B. H., and R.B. Von Dreele. 2013. GSAS-II: the genesis of a modern open-source all purpose crystallography software package. Journal of Applied Crystallography, 46(2): 544-549.

Toor, G.S., Hunger, S., Peak, J.D., Sims, J.T. and Sparks, D.L., 2006. Advances in the characterization of phosphorus in organic wastes: Environmental and agronomic applications. Advances in agronomy, 89: 1-72.

Van Vuuren, D. P., A. F. Bouwman, and A. H W Beusen. 2010. Phosphorus Demand for the 1970-2100 Period: A Scenario Analysis of Resource Depletion. Global Environmental Change 20 (3). Elsevier Ltd: 428–39.

Valsami-Jones, E. 2001. Mineralogical Controls on Phosphorus Recovery from Wastewaters. Mineralogical Magazine 65 (5): 611–20.

Wadu, M.C.W.M., V.K. Michaelis, S. Kroeker, and O.O. Akinremi. 2012. Exchangeable Calcium/Magnesium Ratio Affects Phosphorus Behavior in Calcareous Soils. Soil Science Society of America Journal 77 (6): 2004.

Wang, L., and G.H. Nancollas. 2008. Calcium Orthophosphates: Crystallization and Dissolution. Chemical Reviews 108 (11): 4628–69.

Waseda, Y., Matsubara, E. and Shinoda, K., 2011. X-ray diffraction crystallography: introduction, examples and solved problems. Springer Science & Business Media.
Werner, F. and Prietzel, J., 2015. Standard Protocol and Quality Assessment of Soil Phosphorus Speciation by PK-Edge XANES Spectroscopy. Environmental science & technology, 49(17): 10521-10528.

Xiong, Wenhui, Chris Mathies, Kris Bradshaw, Trevor Carlson, Kimberley Tang, and Yi Wang. 2012. Benzene Removal by a Novel Modification of Enhanced Anaerobic Biostimulation. Water Research 46 (15). Elsevier Ltd: 4721–31.

APPENDIX A: BOBIERRITE MINERAL SERIES.

Mineral synthesis and measurements of TEM, P K-edge XANES, and ATR-FTIR were taken in congruence with Materials and Methods of Chapter 3.

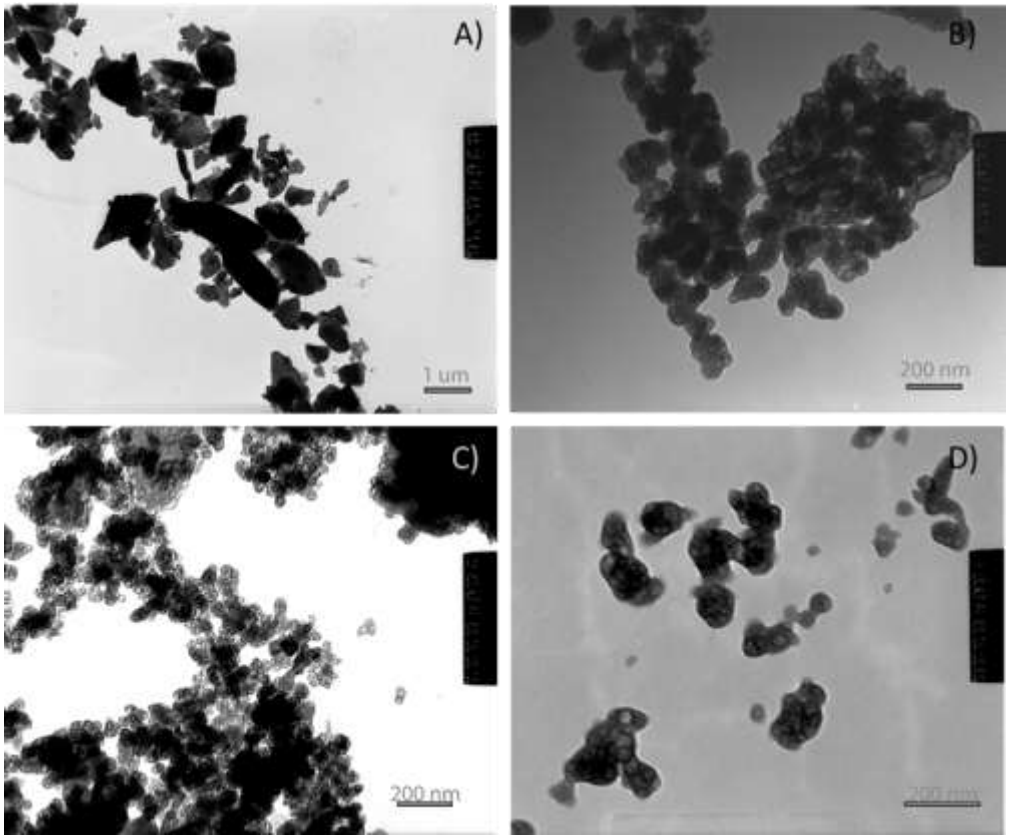

Figure A1: TEM of bobierrite mineral series where the formation solution occurred in Ca:Mg ratios of A) 0:1, B) 1:8, C) 1:3, D) 1:1.

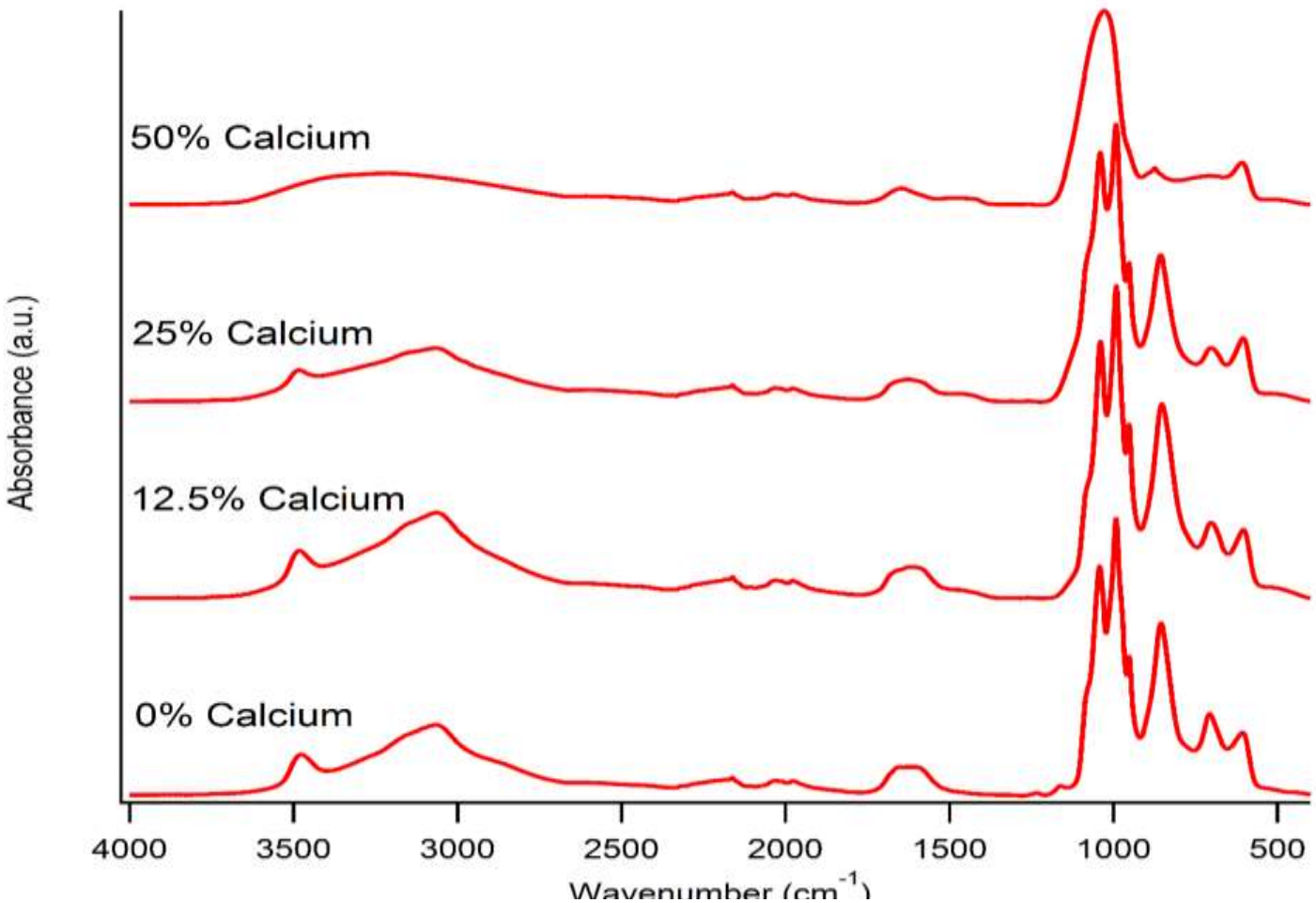

Figure A2: ATR-FTIR spectra of bobierrite mineral series

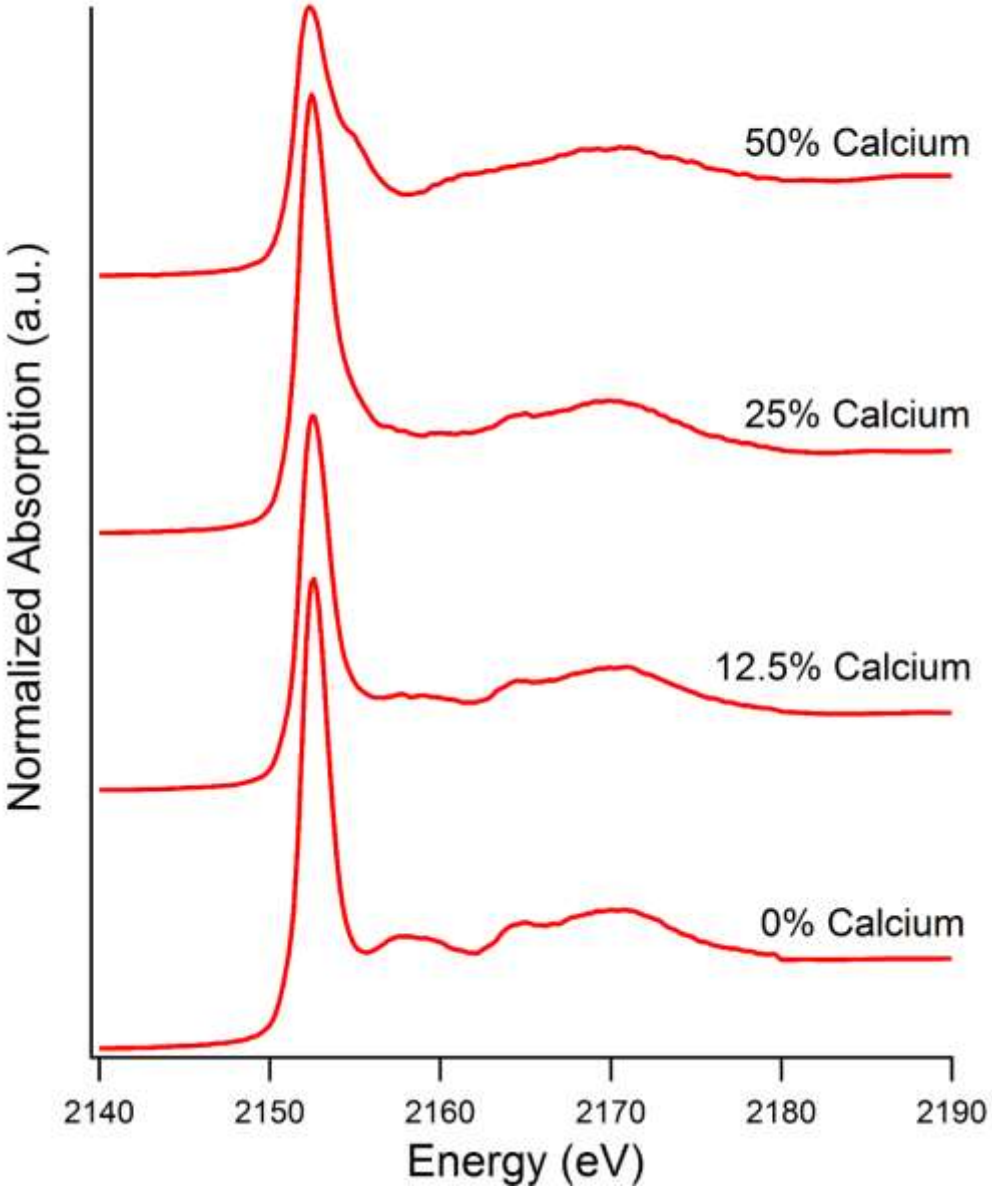

Figure A3: P K-edge XANES of bobierrite mineral series.

APPENDIX B: BRUSHITE MINERAL SERIES**.**

Mineral synthesis and measurements of TEM, P K-edge XANES, and ATR-FTIR were taken in congruence with Materials and Methods of Chapter 3.

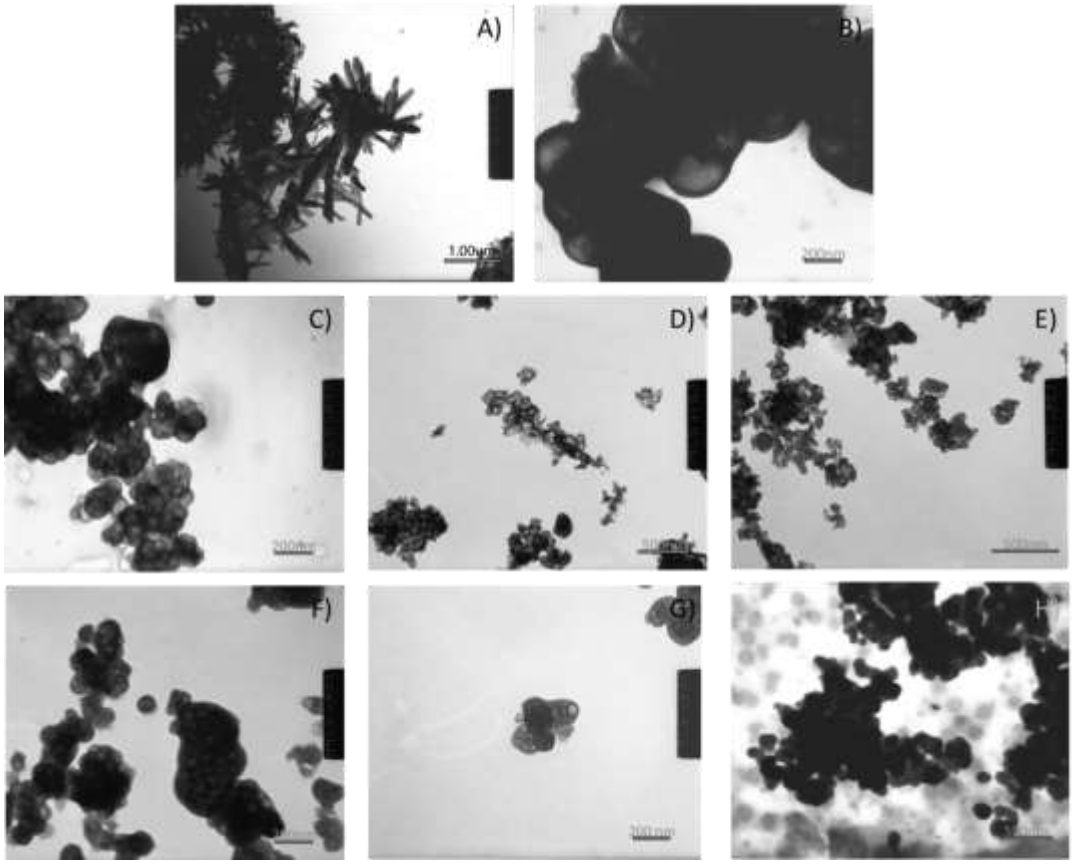

Figure B1: TEM of brushite mineral series where the formation solution occurred in Ca:Mg ratios of A) 1:0, B) 3:1, C) 11:5, D) 5:3, E) 10:7, F) 1:1, G) 1:3, H) 0:1.

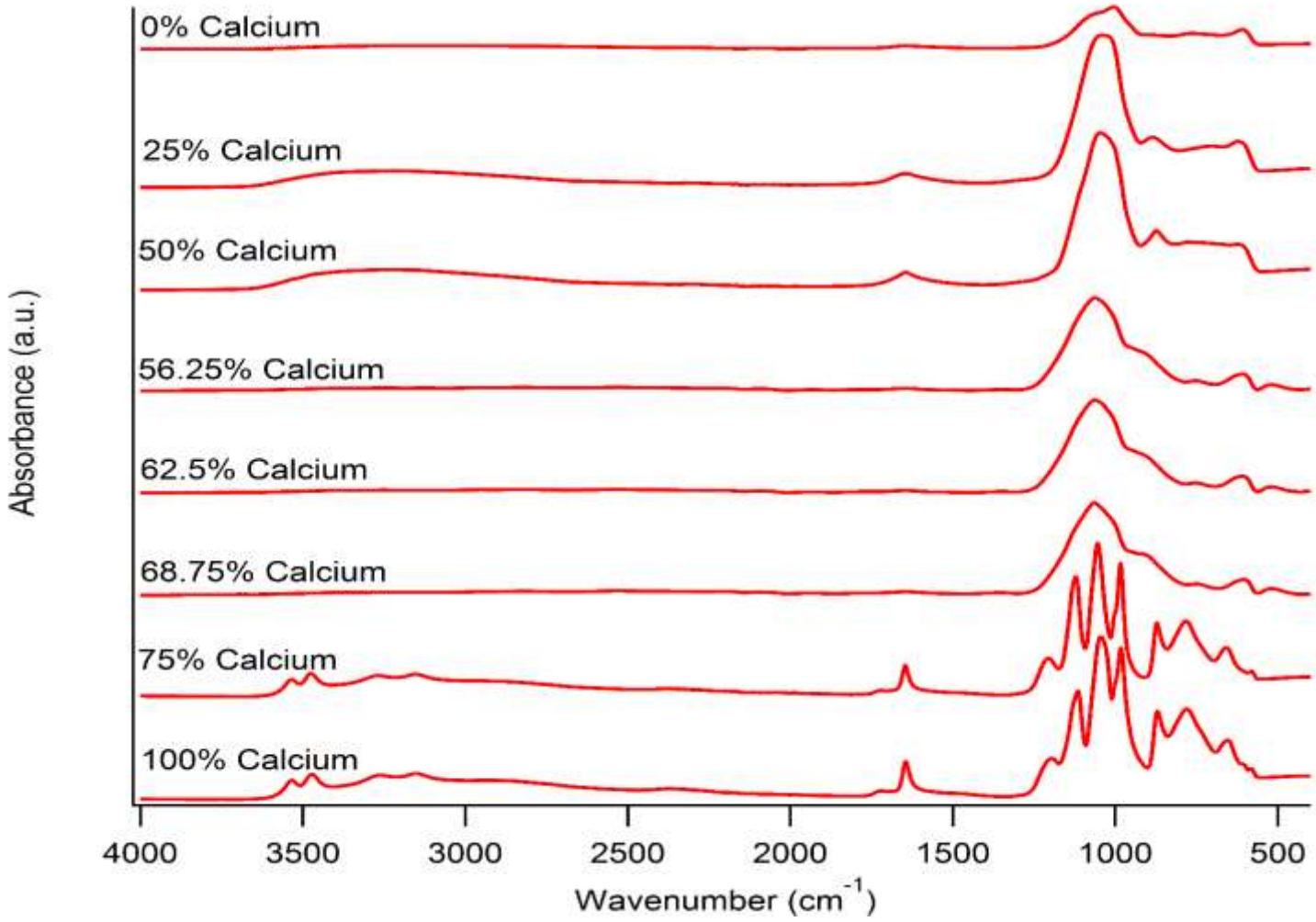

Figure B2: ATR-FTIR spectra of brushite mineral series.

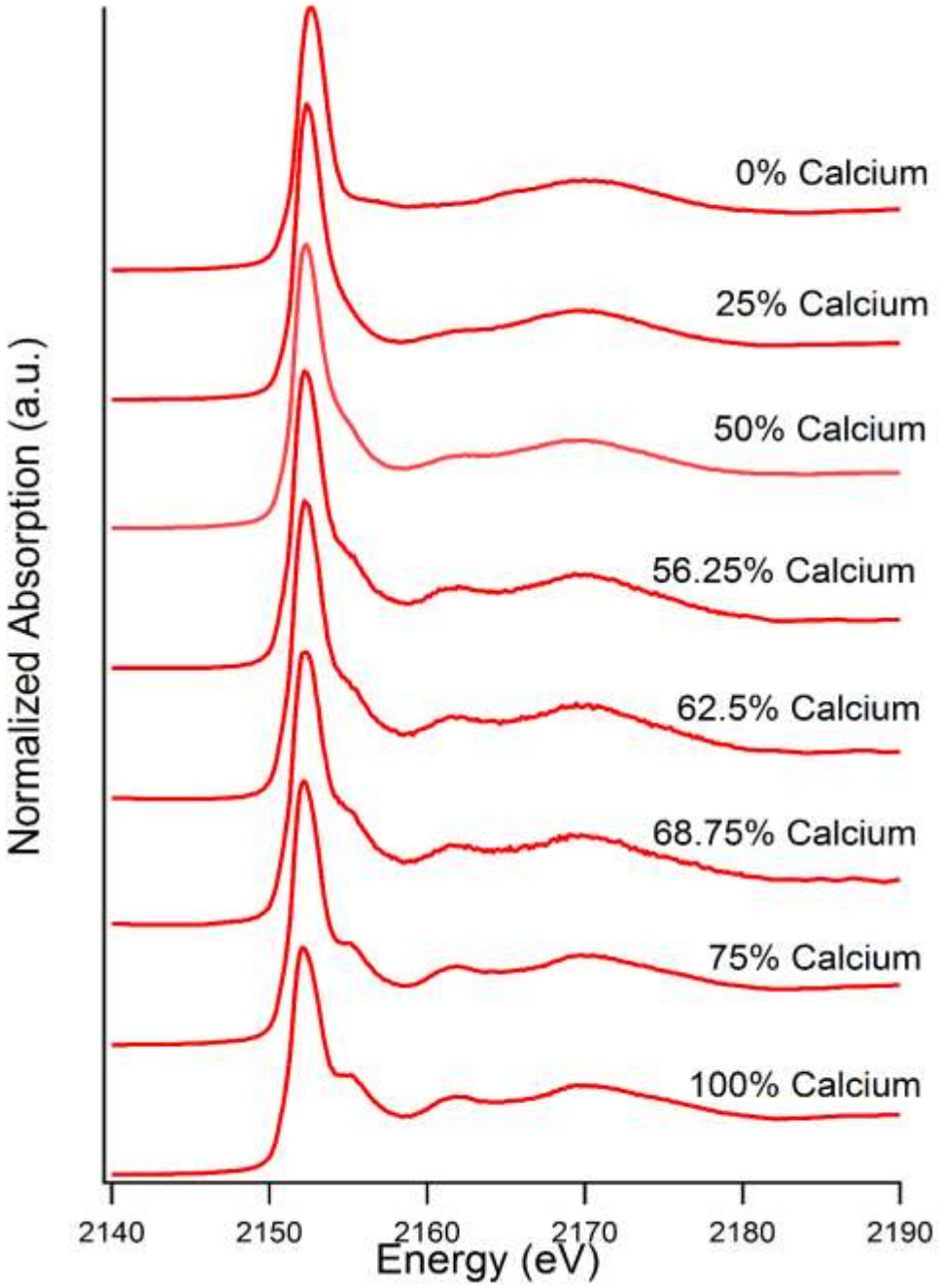

Figure B3: P K-edge XANES spectra of brushite mineral series.

APPENDIX C: HYDROXYAPATITE MINERAL SERIES.

Mineral synthesis and measurements of TEM, P K-edge XANES, and ATR-FTIR were taken in congruence with Materials and Methods of Chapter 3.

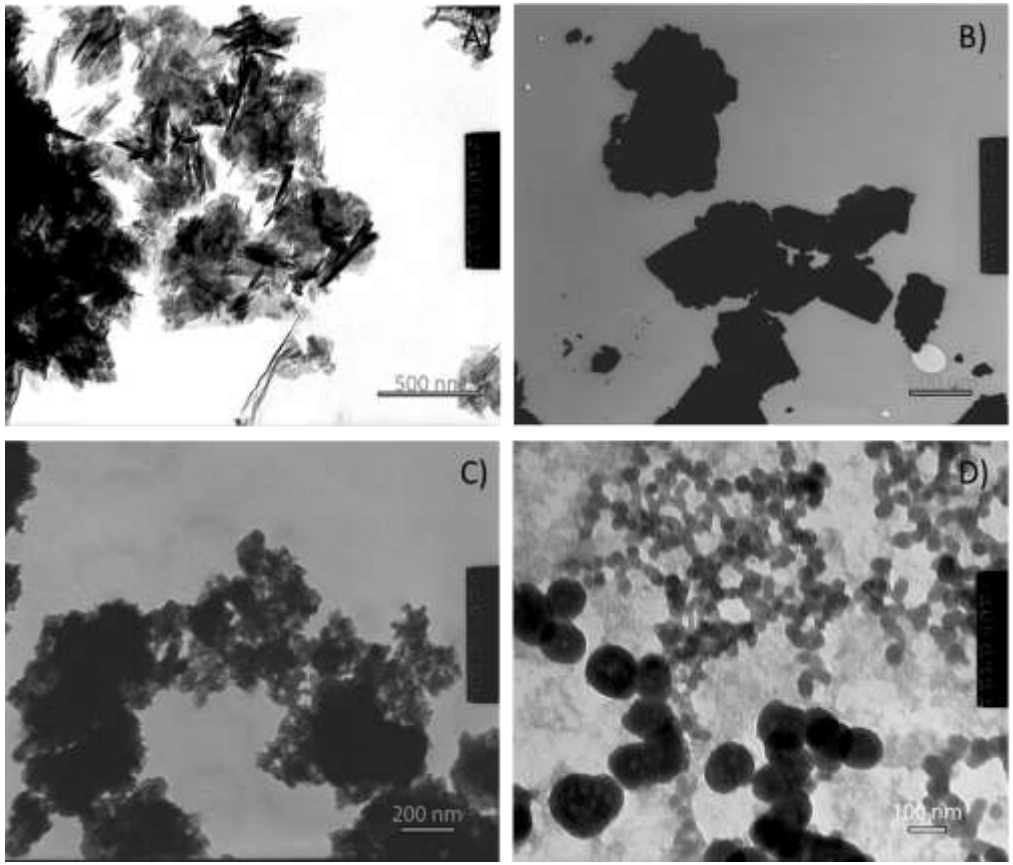

Figure C1: TEM of hydroxyapatite mineral series where the formation solution occurred in Ca:Mg ratios of A) 1:0, B) 20:1, C) 10:1, D) 5:1.

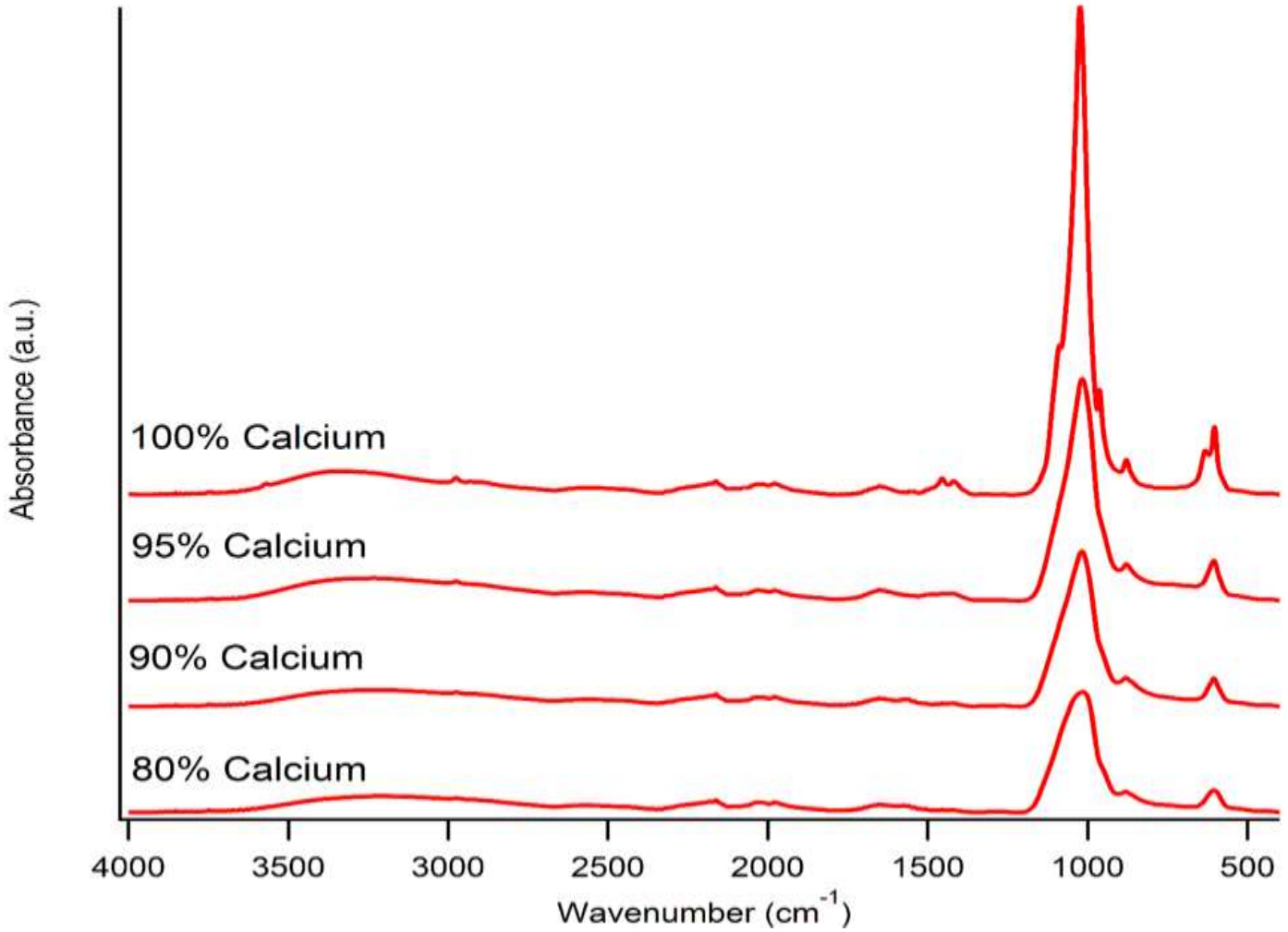

Figure C2: ATR-FTIR spectra of hydroxyapatite mineral series.

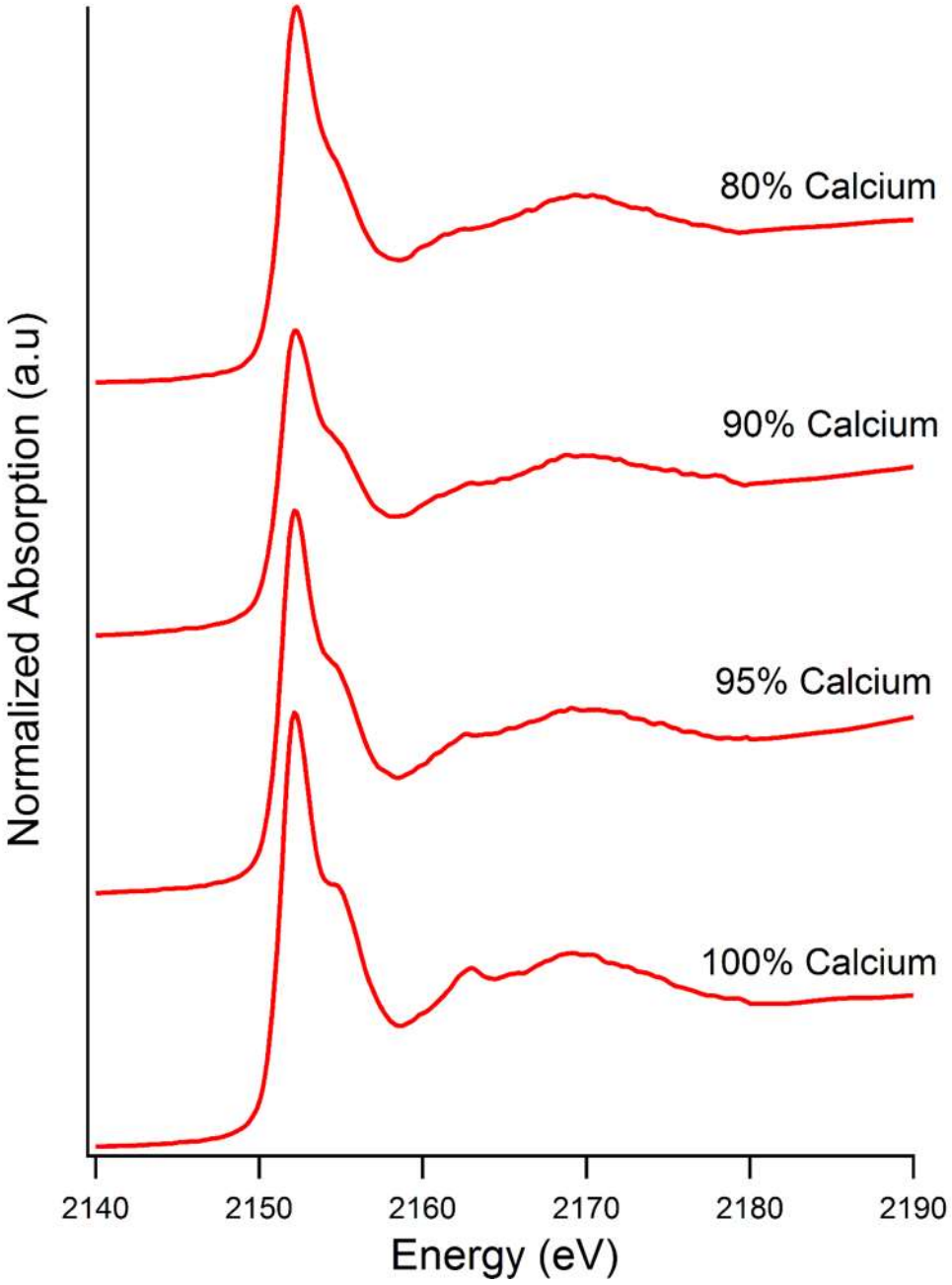

Figure C3: Phosphorus K-edge XANES of hydroxyapatite mineral series

APPENDIX D: MONETITE MINERAL SERIES.

Minerals were synthesized by the dehydration method specified in Tas (2009) and Ball and Casson (1973). Measurements of TEM, P K-edge XANES, and ATR-FTIR were taken in congruence with Materials and Methods of Chapter 3.

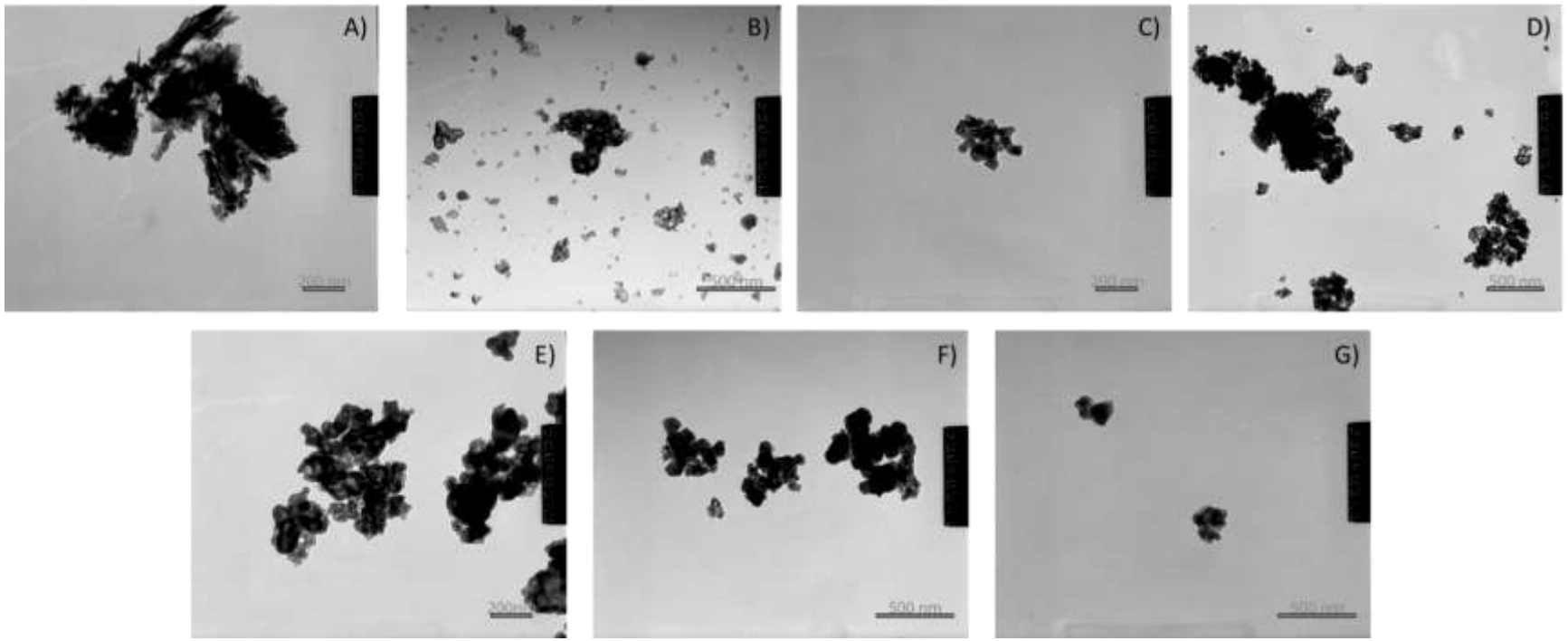

Figure D1: TEM of monetite mineral series where the formation solution occurred in Ca:Mg ratios of A) 1:0, B) 3:1, C) 5:3, D) 10:7, E) 1:1, F) 1:3, G) 0:1.

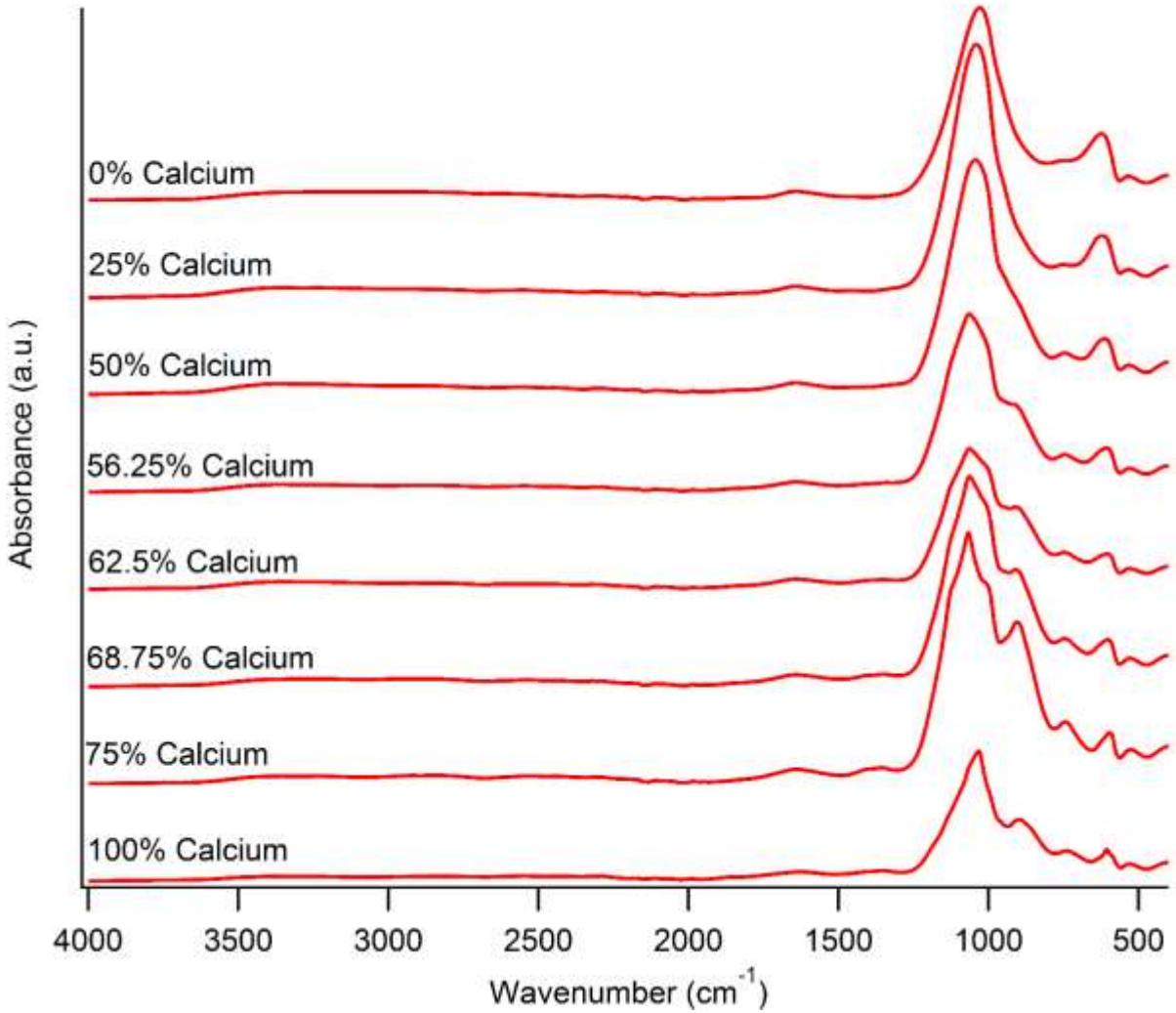

Figure D2: ATR-FTIR spectra of monetite mineral series.

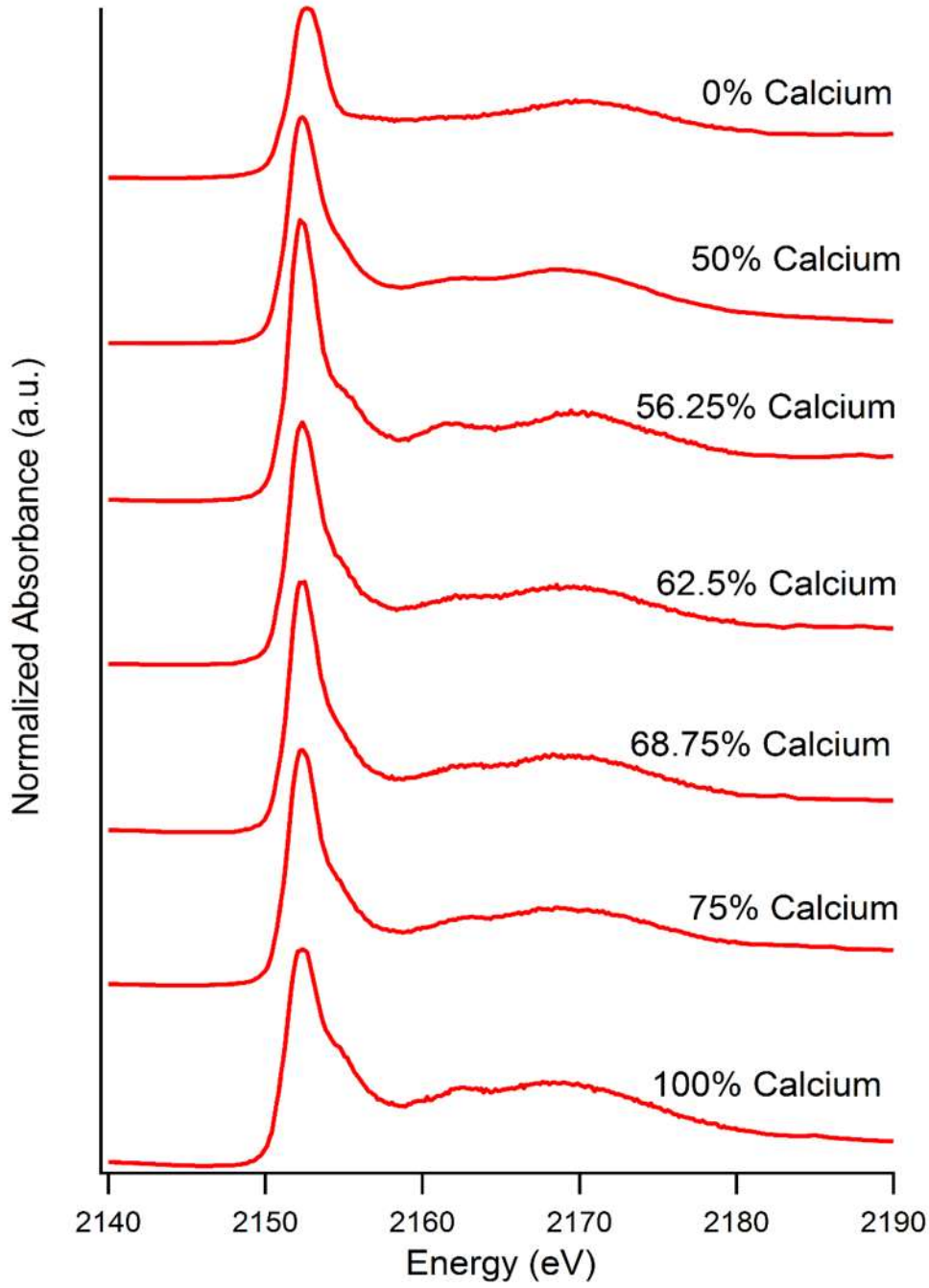

Figure D3: P K-edge XANES of monetite mineral series.

APPENDIX E: NEWBERYITE MINERAL SERIES.

Mineral synthesis and measurements of TEM, P K-edge XANES, and ATR-FTIR were taken in congruence with Materials and Methods of Chapter 3.

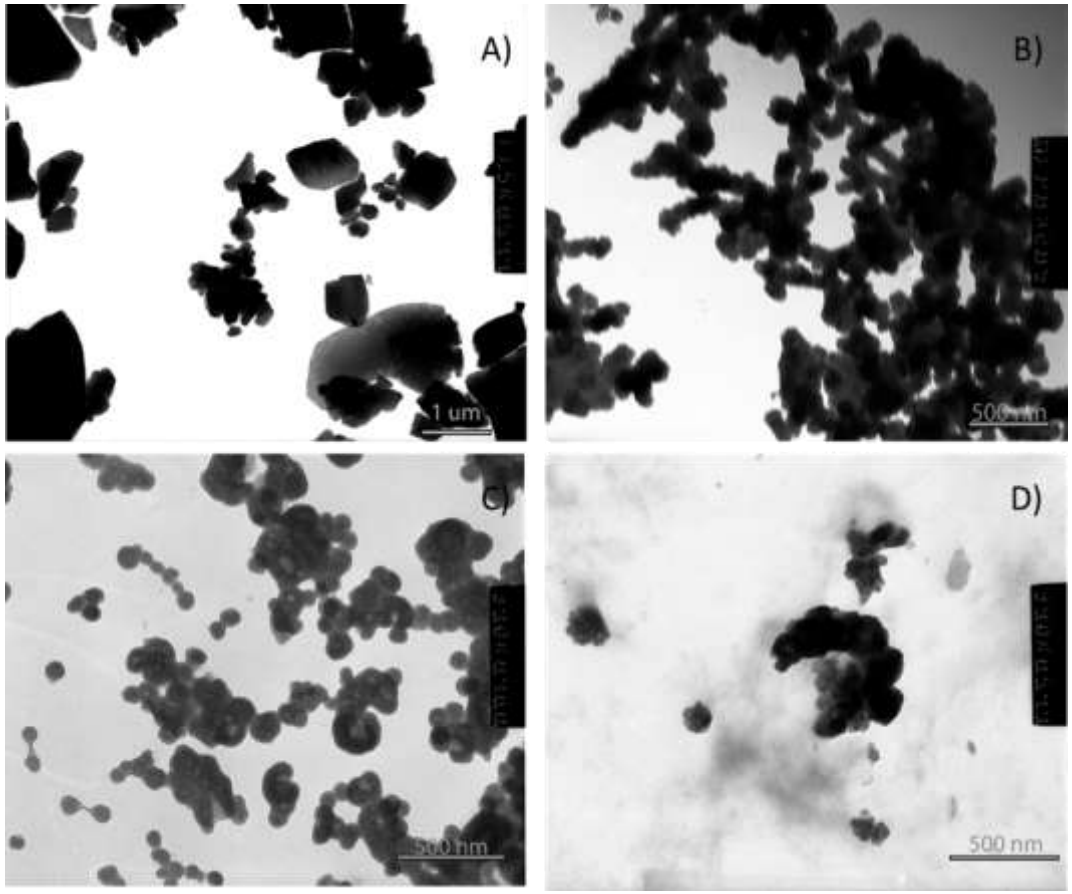

Figure E1: TEM of newberyite mineral series where the formation solution occurred in Ca:Mg ratios of A) 0:1, B) 1:8, C) 1:3, D) 1:1.

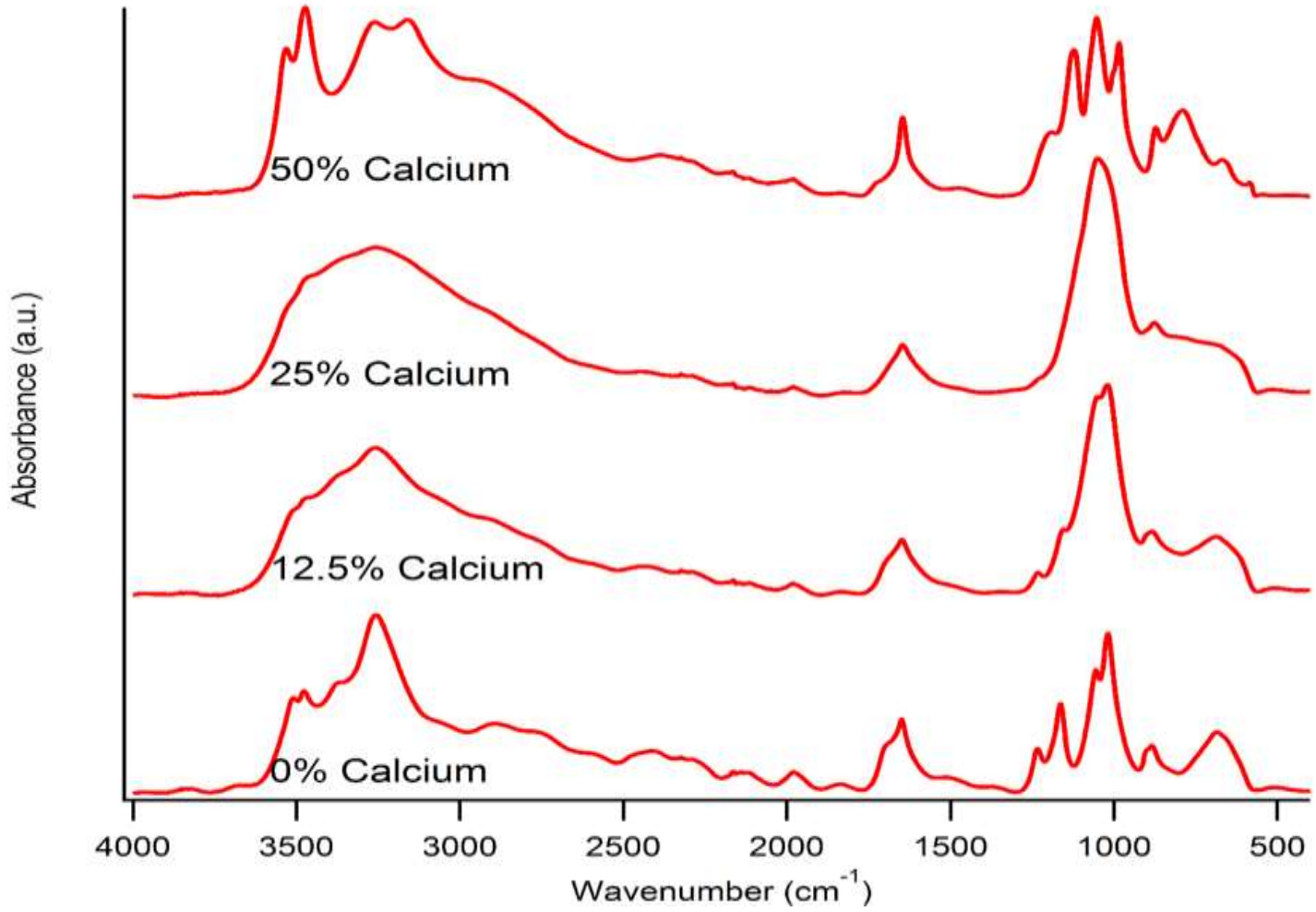

Figure E2: ATR-FTIR spectra of newberyite mineral series

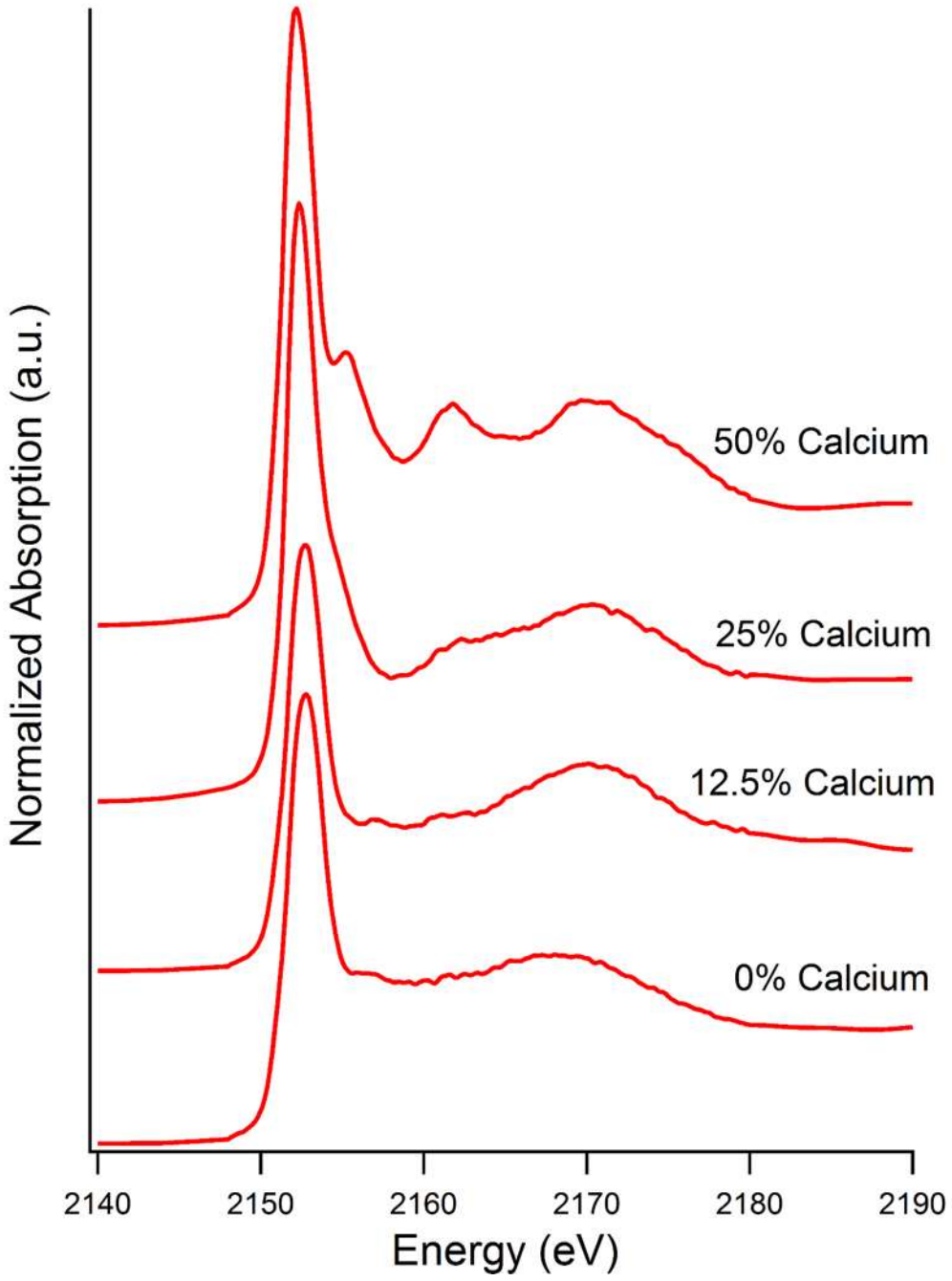

Figure E3: P K-edge XANES spectra of newberyite mineral series.

APPENDIX F: STRUVITE MINERAL SERIES.

Minerals were synthesized by the methods of Kurtulus and Tas (2011). Measurements of TEM, P K-edge XANES, and ATR-FTIR were taken in congruence with Materials and Methods of Chapter 3.

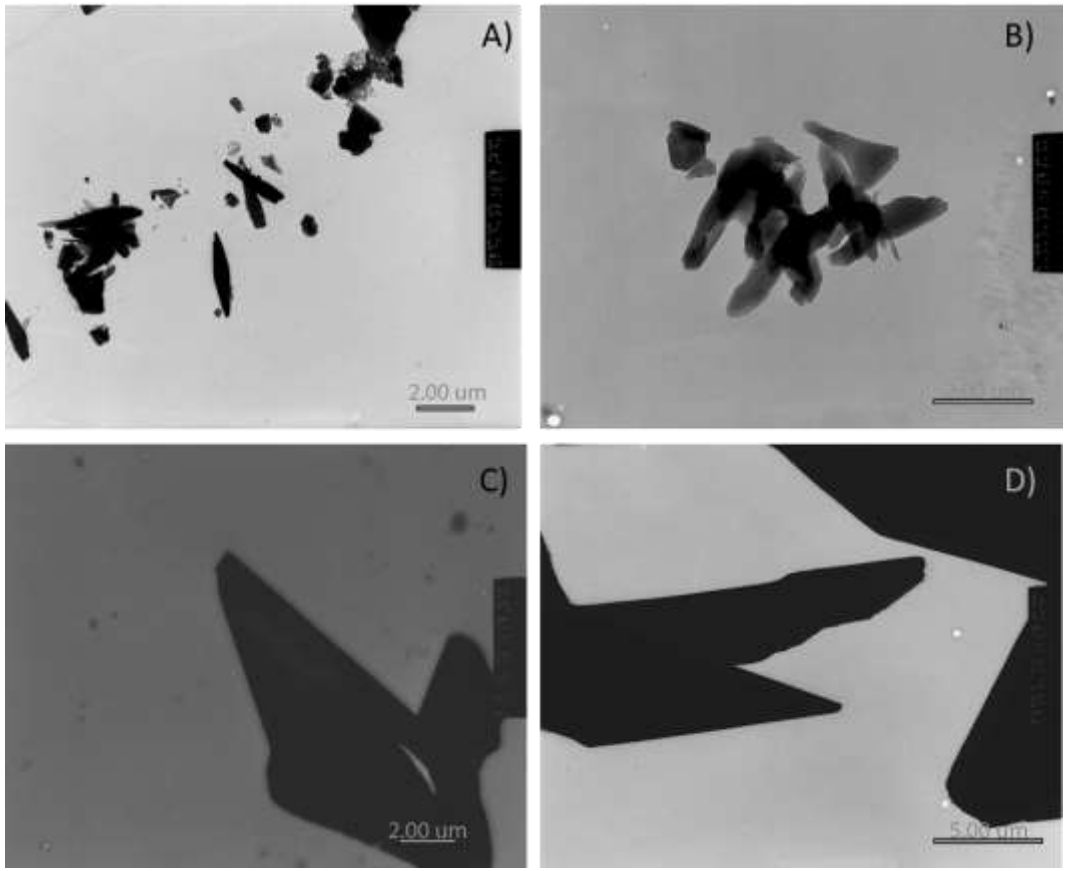

Figure F1: TEM of struvite mineral series where the formation solution occurred in Ca:Mg ratios of A) 0:1, B) 1:8, C) 1:3, D) 1:1.

92

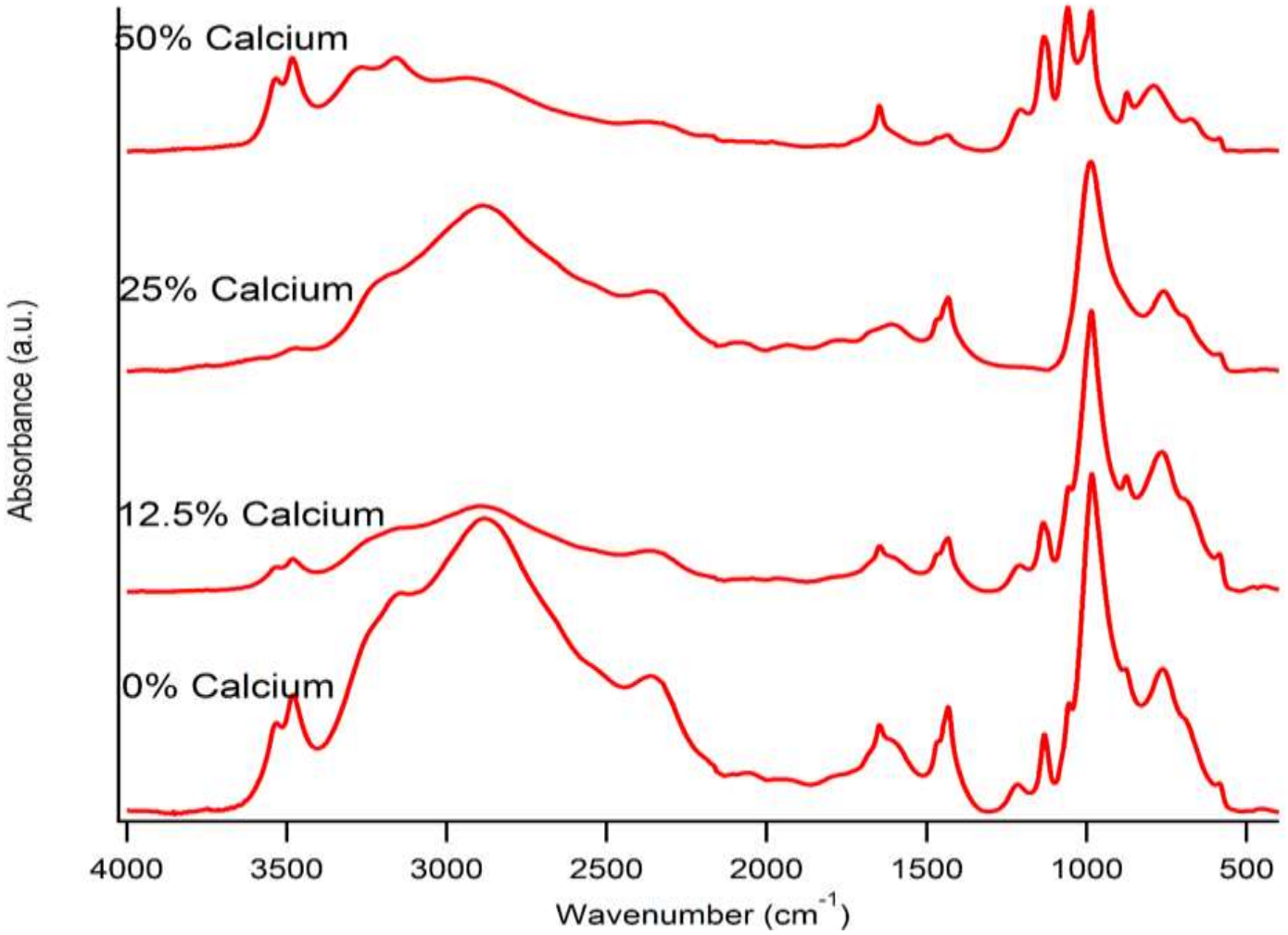

Figure F2: ATR-FTIR spectra of struvite mineral series.

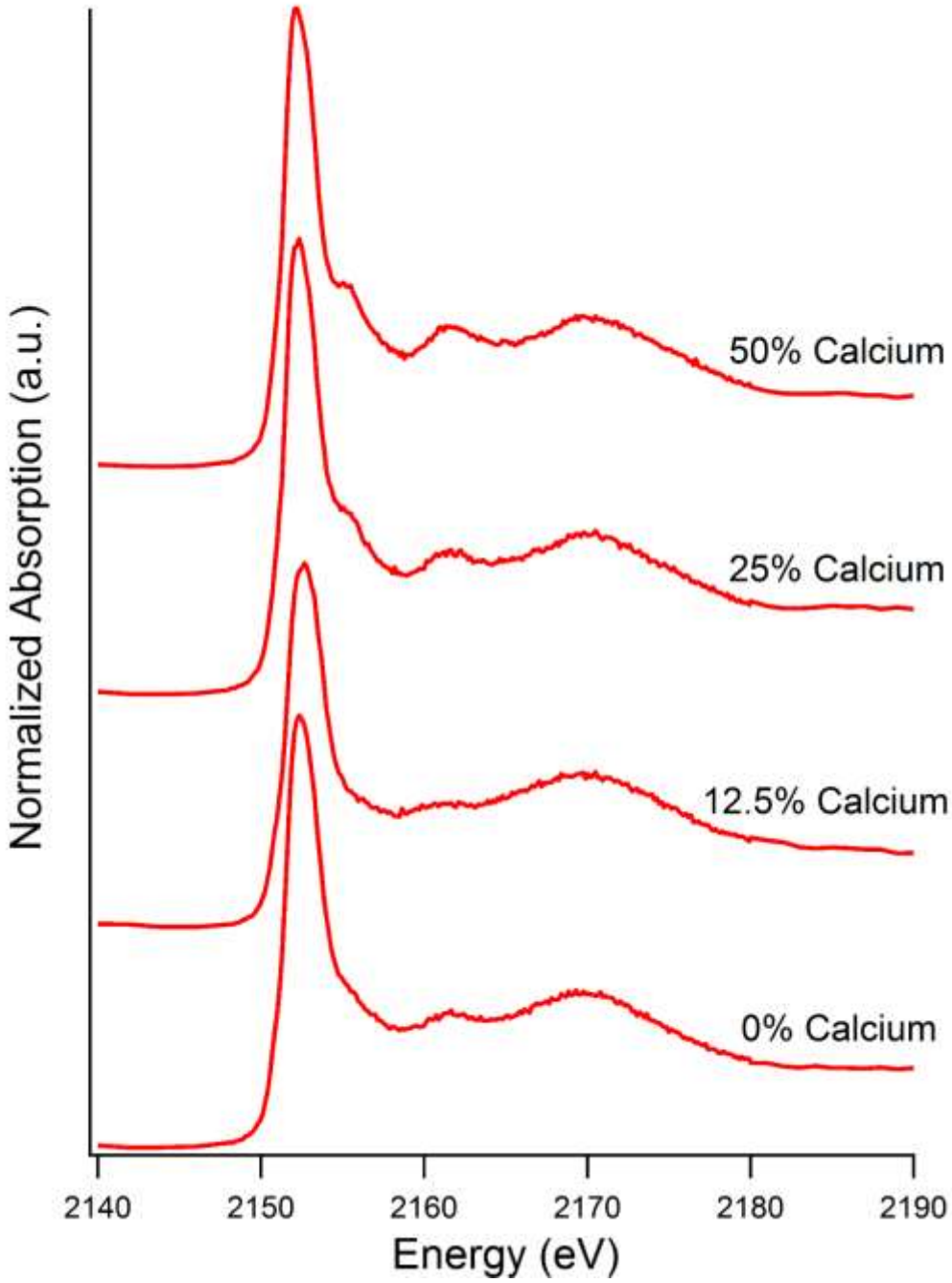

Figure F3: P K-edge XANES of struvite mineral series.